Deliverable No. 6: Project K5/2338/1

Draft Final Report

Quantification of transmission losses along the Letaba River for improved delivery of environmental water requirements (ecological reserve)

ES Riddell [1,2], S Gokool [1], Raubenheimer, R[3], T Strydom[2], JM Nel [3], C Jarmain [4], , A Swemmer [5]

With inputs from R Minnaar[3], R Lerm[5]

1 Centre for Water Resources Research, University of KwaZulu-Natal
2 South African National Parks
3 GCS Consulting, Pretoria
4 Independent Researcher, Stellenbosch
5 SAEON Ndlovu Node, Phalaborwa

Dec 2016

DRAFT

Quantification of transmission loss processes along the Letaba River

ES Riddell, S Gokool, R Raubenheimer, T Strydom, JM Nel, C Jarmain, A Swemmer

Report to the

Water Research Commission

By

South African Environmental Observation Network,

Groundwater Consulting Services,

Centre for Water Resources Research, University of KwaZulu-Natal,

South African National Parks

DRAFT

WRC Report No.

December 2016

Obtainable from

Water Research Commission

Private Bag X03

Gezina, Pretoria

0031 SOUTH AFRICA

orders@wrc.org.za

This report emanates from a project entitled: *Quantification of transmission losses along the Letaba River for improved delivery of environmental water requirements (ecological reserve)* (WRC Project No K5/2338)

DISCLAIMER

This report has been reviewed by the Water Research Commission (WRC) and approved for publication. Approval does not signify that the contents necessarily reflect the views and policies of the WRC, nor does mention of trade names or commercial products constitute endorsement or recommendation for use.

ISBN

©Water Research Commission

EXECUTIVE SUMMARY

The Letaba River system in north-eastern South Africa is an example of a fully allocated catchment which requires efficient management of all water resources demands in a semi-arid setting. Whilst most of available water resources in this system have already been exploited, progress is being made to implement the *ecological reserve* or Environmental Water Requirements (EWR) in the catchment, as required under the National Water Act (Act 36 of 1998). This has important bearing for the provision of ecosystem goods and services in the lower Groot Letaba River and the Kruger National Park (KNP). This progress stems from the implementation of an adaptive operational water resources management system, using a hydrological model to inform catchment managers how and when to make releases from upstream dams. However one of the challenges with this system has been to account for suspected losses of water from upstream storage to downstream EWR target gauges. These losses may be described as *Transmission Losses*.

The aim of this study was to provide a detailed hydrological processes definition of groundwater-surface water interaction and energy-balance processes contributing to total evaporation along the riparian zone. This focused on a 10km reach at the lower end of the Groot Letaba river close to an EWR target gauge upstream of the KNP. This reach traverses agricultural land being developed by emerging farmers before entering small protected areas upstream of the KNP.

The timing of the project also coincided with a large El Nino induced drought period which has allowed insights into interactions between river flow and geohydrological and atmospheric drivers during periods of extremely low flow.

The ground-water surface water interaction component of the study developed a piezometric borehole monitoring network on the northern and southern banks of the river under both land-uses, in order to determine the groundwater hydraulic gradient toward the perennial river system. Through continuous monitoring of the groundwater phreatic surface and hydraulic characterisation of aquifer properties calculations of losses and gains to the river were determined. This has allowed the development of a conceptual model of complex and high-spatial variability of interactions between the river with the surrounding aquifer. Western most reaches of the river within the study site show a through system of the regional aquifer to the river from the south to the north, which then reverses further downstream. At the most eastern part of the study site, within a protected area, the river sees increasing gains from the regional aquifer. However, this is complicated by the rivers interactions with the shallow/unconsolidated aquifer which appears to have a predominantly negative gradient away from the river during low flows. This was further supported through bank-full recharge events during peak flows. The lower Letaba River is therefore both a geohydrologically losing and gaining river depending of the spatial scale of analysis. Initial estimates suggest that the deeper hard rock granite/gneiss of the landscape contributes up to 14m^3/day of sustained baseflow to the reach studied, with a potential loss to aquifer of 25m^3/day.

DRAFT

In terms of water use in the riparian zone, stable isotope analysis of xylem water of riparian trees and shrubs was generally more depleted relative to samples originating from the groundwater and surface water (river flow). This indicates that riparian vegetation is predominantly utilising soil water rather than groundwater or river water. Total evaporation (ET) within the riparian zone was estimated using a combination of in-situ point surface energy balance measurements, and the SEBS model based on satellite imagery. Daily ET measured within the protected areas was shown to be higher than the western upstream area which is subject to high levels of cattle grazing. This was clear in both 2015 and 2016. While the intra-annual variability for 2016 ET follows a similar seasonal trend to the 2015 ET there was significant increase in ET for 2016. While rainfall for both 2015 and 2016 was similar, and well below average, the greater ET in 2016 was due to an isolated rainfall event in March 2016, which appeared to enhance ET well into the dry season. Overall, losses of the river flow via ET resulting from both evaporation of river water and transpiration of riparian vegetation, were negligible relative to river flows.

DRAFT

ACKNOWLEDGEMENTS

The research in this non-solicited project was initiated, managed and funded by the Water Research Commission, for whose assistance we are sincerely grateful. The project would also not have been possible had it not been for the funding and services by members of the Department of Water Affairs Limpopo drilling division for the borehole drilling campaigns during 2015. Special thanks go to the staff of SAEON: Mr Rion Lerm, GCS: Mr Raymond Minnaar, SANParks: Mr Annoit Mashale and IWR Water Resources: Mr Stephen Mallory & Dr Tendai Sawunyama.

Members of the Reference Group (below) are thanked for their time and invaluable expertise:

Dr Brilliant Petja (Chairperson)	Water Research Commission
Dr Chris Moseki (Chairperson former)	Water Research Commission
Ms Celiwe Ntuli	Department of Water & Sanitation
Mr Isaac Nyatlo	Department of Water & Sanitation
Dr Alistair Clulow	University of KwaZulu-Natal
Ms Kershani Chetty	University of KwaZulu-Natal
Dr Bill Pitman	Independent Researcher
Miss S Tjaden	Water Research Commission

The following people provided valuable assistance in the field:

Environmental Monitors: Andile Ndzamba, Masana Htimani, Salvation Shikwambani, Peska Nkuna, Dipuo Ramalepe, Mosa Mokgalaka, Ponisiwani Mathebula, Hlanganani Mabunda, Evidence Shikwambani, Queen Malatji, Solani Maswanganyi, Rahab Mohale, Peace Nkuna, Elma Mashale, Raina Ramoshaba, Lassie Mokgalaka, Elijah Masango, Sharon Ngobeni, Ntsako Makhubele, Jako Lombard, Gladness Khosa

Students: Kgetho Mashile, Kinsley Manyama, Angel Mavasa, Delina Chipape, Rinaldar Mochemi, Oliver Stirzaker

DRAFT

TABLE OF CONTENTS

DRAFT

DRAFT

LIST OF FIGURES

DRAFT

LIST OF TABLES

DRAFT

DRAFT

ACRONYMS

BBM	Building Block Method
CSR	Coarse spatial resolution
DWA	Department of Water Affairs
EC	Electrical Conductivity
EC_{ET}	Eddy covariance ET
ERT	Electrical Resistivity Tomography
EWR	Environmental Water Requirements
FDC	Flow Duration Curve
FL	Borehole Fluid Logging
GLeWaP	Groot Letaba Water Development Project
HTR	High Temporal Resolution
K	Hydraulic Conductivity
IFR	In-stream Flow Requirements
KNP	Kruger National Park
LWUA	Letaba Water User Association
LMWL	Local Meteoric Water Line
MAP	Mean Annual Precipitation
MAR	Mean Annual Runoff
MSR	Moderate spatial resolution
NDVI	Normalized Difference Vegetation Index
OWRM	Operational Water Resources Management
NWA	South Africa's National Water Act
SC	Specific Conductance
SEBS	Surface Energy Balance System
TL	Transmission Losses
T	Transmissivity
UAV	Unmanned Aerial Vehicle
VSMOW	Vienna Standard Mean Oceanic Water
WRCS	Water Resources Classification System

DRAFT

1. INTRODUCTION

This deliverable report stems from the non-solicited Water Research Commission (WRC) research project K5/2338 titled:

Quantification of transmission processes along the Letaba River for improved delivery of environmental water requirements (Ecological Reserve)

This report provides a detailed hydrological processes definition of groundwater-surface water interaction and energy-balance processes contributing to total evaporation along the riparian zone of a 10km reach of the lower Groot Letaba River in north-eastern South Africa.

The rationale for this study being that the perennial rivers flowing through the arid and semi-arid parts of South Africa are all said to be closing, with water abstractions exceeding, or close to exceeding supply (e.g. Molle et al., 2010). Environmental water requirements (EWR), or 'ecological reserve' flows were shown to be deteriorating in many catchments of the South African lowveld during the latter decades of the 20th century due to significant land-use changes and loose governance of water resources (Pollard & du Toit, 2011a). This despite the EWR's being the only 'right' to water, in addition to the Basic Human Needs reserve under South Africa's National Water Act (NWA, Act 36 of 1998).

Intensive management of their flows, through the efficient management of water abstraction and dam outflows, is critical to ensure that all water users continue to receive adequate allocations at a good assurance of supply, while still meeting the specified ecological reserve. Efficient management in turn requires a complete quantification of the hydrological processes that significantly affect river flows. Rainfall inputs, dam releases and water abstractions are relatively easy to quantify, and are currently being used to manage flows in river operations. Meanwhile channel losses resulting from outflows from river systems remain a key gap and have limited the effectiveness of flow management to date. The Letaba River system in north-eastern South Africa provides a good case study of this situation, with: water-use abstractions often exceeding available supply (Pollard & du Toit 2011b; DWAF, 2006). This in combination with infrastructural developments and land conversion in the catchment such as dams, have meant that flows in the Letaba no longer resemble natural flows (Katambara & Ndiritu, 2010). This situation has improved somewhat following the formalisation of consensus based operational river management (Pollard & du Toit, 2011a: Riddell et al 2014). In the Letaba catchment this resulted from the development of river operating rules linked to releases from the Tzaneen dam, where flow releases are monitored by the downstream Kruger National Park (KNP) through a Strategic Adaptive Management feedback mechanism with the dam operators (McLoughlin et al, 2011).

The Letaba system operating rules were developed by the Department of Water Affairs (DWA) in 2006 and are facilitated by the use of a real-time ecological reserve implementation model, SPATSIM (Hughes et al 2008, Sawunyama & Hughes, 2010). It was recognized within this development that any method for implementing the ecological reserve must account for different water resource development and supply situations. These can be divided up into situations where a water manager has control over the flow rates in the channel through controlled releases from reservoir storage (which is the case in Letaba system where releases are made from Tzaneen dam) and those where the manager has no control. It was agreed that the first step in implementing the SPATSIM modelling system and associated feedbacks (within an adaptive management framework) would be to

DRAFT

implement the relevant operating rules and initiate a network of communication feedbacks between the KNP and the dam operators (McLoughlin et al, 2011). The system was in operation from 2009 to 2012 until problems occurred with running the SPATSIM model. One of the identified problem areas is that of channel losses, which include potential alluvial channel, riparian and/or floodplain recharge, and evapotranspiration, hereafter we refer to these in combination as Transmission Losses (TL). On the Groot Letaba these TL's have been an area of considerable uncertainty due to their impacts on releases emanating from the Tzaneen dam, meaning that the specified reserve flows are often not met adequately at the Letaba Ranch (B8H008) monitoring weir close to the KNP (e.g. DWAF 2010) and aquatic bio-monitoring site (EWR4). In the DWA (2006) reserve determination study on the Letaba these TL's were estimated to be between 8-50% of the channel inflow.

Whilst the SPATSIM real-time ecological reserve sub-model is still being utilised on the Letaba system there have been a number of changes within the Letaba catchment since the original proposal for K5-2338 was submitted in 2013. These changes are:

- The Letaba system now forms part of the Olifants Water Management Area.
- The Letaba system has now seen a finalisation of the Water Resources Classification System (WRCS), which has seen the gazetting of the lower Groot Letaba as a Management Class II, C Recommended Ecological Category river. Importantly the EWRs have increased from those presently implement through SPATSIM.
- A concomitant part of the WRCS was the distinction of operationalising the EWR prior to and post commissioning of the new N'wamitwa dam.
- The updated national water resources availability assessment (WR2012, Bailey & Pitman) study has now been completed which reveals a significant reduction in the Mean Annual Runoff (MAR) for the Letaba system under present catchment conditions.
- Hydrometric streamflow gauging in the Letaba river has deteriorated significantly over the past few years, meaning that there is no accurate flow gauging along a >90km stretch of river between Letsitele (B8H009) and Letaba Ranch (B8H008)

To this end it is critical to improve the data inputs to any model used to operationalise the system moving forward, as it quite clear that the system is fully allocated and efficiency is key. Therefore by determining the actual rather than estimated transmission losses in a semi-arid system such as the Letaba will significantly reduce the uncertainty associated with operational decision-making. Hence it is expected that the results of this study will be used to:

1) Change and update the operating rules: There is a need to adjust the operating rules, and determine when to impose restrictions, making sure that the system is sustainable. This is necessary to provide transparent but accurate information to inform river operations decision making in a consensus driven manner. To this end, it is a pre-requisite to improve data inputs such as dam levels; river flows and rainfall.
2) Establish the reliability and integrity of the data in an on-going basis, which include the accurate determination of TLs reducing the impact of releases from the controlling dam, to determine water release 'tolerances'.

DRAFT

2. LITERATURE REVIEW

Environmental water requirements

Due to the regulation of flow by dams, excessive water abstraction, the discharge of effluent in river systems, and increasing water demands, it is critical that the Environmental Water Requirements (EWR) be determined for all major rivers (Malan and Day, 2003) and for this EWR to be an active, rather than passive component of water resources management (Poff, 2009). An EWR refers to the flow needed by a river to sustain a healthy ecosystem. Typically, this EWR is determined to mimic the components of a river's natural flow variability, taking into consideration the magnitude, frequency, timing, duration, rate of change, and predictability of flow events (Arthington *et al.* 2006). There is a global concern about the deterioration of water quality in rivers, and it has been acknowledged that the decline in river health is highly influenced by changes in river flows (O'Keeffe, 2008). EWR flows are being negatively-affected by significant changes in land-use and poor water resource governance (Pollard and du Toit, 2011b), meaning that that EWRs have been notoriously difficult to implement. In order to meet the determined EWR as well as to ensure that all water-users receive their allocated water supplies, dedicated flow management is required through the efficient management of water abstraction, effluent discharge and dam outflows. In South Africa this is termed 'Operational Water Resources Management (OWRM)'. However for OWRM to be truly effective, it is required that the hydrological processes which affect river flows is quantified. Transmission processes, i.e. losses and gains of surface water from a river channel, are key knowledge gaps which currently undermine effective water allocation and management.

Until the early 2000s the EWRs of South African rivers utilised the Building Block Method (BBM; King and Louw 1998), which at that time were called 'in-stream flow requirements' (IFRs) representing the highly variable nature of the country's rivers. The BBM process defines a set of monthly (daily average) flow blocks that should be applied during 'normal/maintenance' years as well as a set that should be applied during 'drought' years (Hughes, 2001). However, Hughes (1999) also emphasized that IFRs are not sufficient for incorporating into the type of water resource systems models that are used in South Africa. The argument was that IFRs do not provide the necessary temporally dynamic information on the frequency of occurrence, or assurance levels, of the different flows. A way to overcome this was to use flow duration curves (FDCs) instead of actual flow values which display the full range of river discharges from low flows to flood events. These now form the hydrological basis of reserve determination studies, which generate FDCs as site specific flow 'assurance rules'. These assurance rules are then typically implemented/monitored at hydrometric flow gauges (typically operated by DWS) close to EWR bio-monitoring sites. Through the national Water Resources Classification System (WRCS), as mandated in the NWA, a river will be classified through public participation process, and on that basis a class of river and associated assurance rules are gazetted as the future management and operating scenario for a river system.

Transmission Losses

DRAFT

Globally, transmission losses (TL) are also known as *channel*, *river* or *water losses*. TL can be defined as a reduction in the volume of flow in a river/stream channel system between upstream and downstream points (Lane *et al.*, 1990; Walters, 1990; Hughes and Sami, 1992; Cataldo *et al.*, 2010; Shanafield and Cook, 2014). The reduction in the flow volume between the upstream and downstream points is attributed to the loss of water through three natural processes i.e. (a) Total evaporation in the riparian zone and open water evaporation from the river channel, (b) evaporation or infiltration of water, stored in channel depressions or the flood plain and (c) the recharge of ground water as water infiltrates the stream channel, its banks or the floodplain (Cataldo *et al.*, 2010). Walters (1990) describes transmission losses as the reduction in river flow due to evaporation and infiltration to the river bed, river banks and even the adjacent floodplain. Boroto & Gorgens (2003) described transmission losses as storage recharge in alluvial channel beds or alluvial banks, and as evaporation and evapotranspiration; direct evaporation from the water body surface; deep groundwater recharge and during extreme climatic events as losses to floodplain flows. Water lost via infiltration may either percolate to recharge aquifers or will return to the river downstream and contribute to the flow (Hacker, 2005). Sharp and Saxton, 1962; cited by Hacker (2005) propose that the key factors influencing transmission losses are:

- the size and sequence of floods;
- the geology and soils of the valley;
- the gradient, depth, size, continuity, meander, and number of channels;
- riparian and phreatophytic vegetation along the channel and in the valleys;
- soil-frost conditions;
- depth to the water table;
- soil-moisture content;
- gross and gravitational pore space in the soil;
- man-made structures and alterations;
- antecedent and current rainfall; and
- the content and nature of sediment in the stream flow.

TL can be a significant contributing process to the water balance of river systems, particularly in arid and semi-arid environments (Hughes and Sami, 1992; Lange, 2005; Hughes, 2008; Costelloe *et al.*, 2003; Cataldo *et al.*, 2010; Shanafield and Cook, 2014; Huang *et al.*, 2015). Therefore to ensure effective water management and water provision in these environments, it is critical to understand transmission losses considering that it is a key component of the water balance or hydrological budget (Gu and Deutschman, 2001).

TLs have been well documented for arid and semi-arid environments around the world, but there remains a paucity of studies in southern Africa (Hughes, 2008). While transmission losses have yet to be properly quantified for any South African river, they are estimated to be high for perennial rivers flowing through arid and semi-arid areas, such as the Letaba system. According to Hacker (2005), transmission losses are amplified in arid or semi-arid regions where the water table is very deep and predominantly lower than the water level in a channel. Boroto & Gorgens (2003) predicted that up to 30% of the Limpopo River's mass balance may be allocated to transmission losses due to evapotranspiration and recharge to aquifer storage. Everson *et al.* (2001) quantified losses due to evapotranspiration between two gauged sites on the Sabie River to be 0.32 m^3/s in low flow months — a significant proportion of total available flow considering that low flows range between 0-5 m^3/s (e.g. Pollard & du Toit, 2011a). A similar figure has been noted for alluvial TL's in semi-arid regions of north-east Brazil (Costa et al., 2013). More recently, a figure of 10% has been used in the lower Olifants (DWA, 2011). In the Letaba River Reserve determination study by DWAF (2006a), TLs were estimated to be between 8-50% of the channel inflow.

Quantitative investigations of transmission losses are therefore necessary in order to calculate flows in a river and appropriately allocate water for different users (Gu and Deutschman, 2001).

Incorporating the Total Evaporation Process into Streamflow Transmission Losses Estimation Procedures

Even though there are various factors which have been identified to have an influence on the TL process, only a select few parameters have been successfully incorporated into TL estimation techniques (Hacker, 2005). Runoff volume and velocity, the river channel geometry and characteristics of the channel bed material are amongst the most commonly utilized factors for TL estimation procedures (Hacker, 2005). Ultimately, the choice of factors used for TL estimation procedures is controlled by the characteristics of the study-site and the availability of data (Cataldo *et al.*, 2004). However, one of the factors which is seldom included or adequately represented in TL estimation procedures is the total evaporation process.

It is often the case that total evaporation is ignored or inadequately represented in the TL estimation procedures, even though it has been identified as a contributing process to TL (Hacker, 2005; Cataldo *et al.*, 2010; Shanafield and Cook, 2014). Research and transmission loss estimation techniques have tended to focus more on the flow reduction in relation, to infiltration (Hacker, 2005; Cataldo *et al.*, 2010; Shanafield and Cook, 2014). This is largely due, to majority of TL in most ephemeral rivers occurring as a result of infiltration-based losses (Cataldo *et al.*, 2010).

Although infiltration-based losses may possess a relatively larger contribution to TL, the absolute losses, resulting from total evaporation cannot be discounted. This is particularly pertinent, to environments where total evaporation is a considerably large component of the water cycle (Everson, 2001; McKenzie, 2001; Hacker, 2005; Shanafield and Cook, 2014). According to Shanafield and Cook (2014), all processes which influence TL need to be quantified in order to fully understand the magnitude and effects of TL.

The accurate quantification of hydrological processes such as the role of riparian total evaporation and open water evaporation must be acknowledged and accounted for to successfully model TL.

DRAFT

3. OBJECTIVES

Hughes (2008) noted that there have been very few direct studies of channel transmission losses in southern Africa, this despite it being a significant component of river water balances in the region. Hughes (2008) also acknowledged that whilst the process of river losses into alluvial aquifers (recharge to the aquifer) is reasonably understood (e.g. Görgens and Boroto, 2003) it has often eluded the water resources modellers to quantify such losses. Furthermore it is even suspected that losses in hard rock terrains underlying many of the regions rivers (such as the Letaba) is significant due to the highly fractured nature of the material of bed-rock channels, suggesting that TLs from non-alluvial rivers can also be substantial. To this end the project had the following aims:

1. Actual quantification of transmission losses along a river reaches of the Groot Letaba River
2. Incorporation of this into real-time modelling systems providing an immediate and direct impact in improving the delivery of environmental water requirements
3. Development of a cost effective methodology using hydrometrics coupled with remote sensing technologies and integrated SW-GW interaction models to upscale the TL parameters
4. Regional parameters for transmission losses developed to allow role-out to other river systems in the South African lowveld
5. Contribute to the long-term monitoring of riparian zone hydrology, hydrogeology and river ecology in the lowveld under various land-uses and water resource management scenarios.

With the following objectives:

1. Determine EWR real-time implementation model uncertainties due to transmission loss parameterisation
2. Select river reaches under various geological/hydrogeological settings where transmission losses need to be determined
3. Select river reaches under various land management types where transmission losses need to be determined
4. Quantify abiotic mechanisms for transmission losses in these reaches through groundwater-surface water interaction determination
5. Quantify biotic mechanisms for transmission losses in these reaches through determination of actual evapotranspiration losses in the riparian zone
6. Upscale the quantified processes through extrapolation with remote sensing, geophysical, hydrochemical and modelling techniques
7. Develop accurate transmission loss parameters and incorporate in real-time reserve implementation models
8. Where possible provide added-value by transcribing the findings to other rivers in the lowveld.

DRAFT

4. STUDY SITE:THE LETABA RIVER SYSTEM

The Letaba River catchment is located in the Limpopo Province of South Africa and extends over an area of approximately 13 400 km^2 (Moon and Heritage, 2001). It is delineated by the Drakensberg Escarpment in the west extending into the low-lying Lowveld in the east (Figure 1). The catchment can be divided into the Klein Letaba sub-catchment in the north and the Groot Letaba sub-catchment in the south. Downstream of the Middle Letaba Dam, the Middle Letaba River flows into the Klein Letaba which drains into the Groot Letaba River at the KNP boundary. According to Heritage *et al.* (2001), nearly three-quarters of the catchment is underlain by granitic and gneiss geological formations whereas the east is dominated by volcanic formations derived from the Karoo sequence basalts. Due to the presence of granites, weathered zones are shallow and soils have a sandy soil texture. There are numerous diabase dykes across the catchment, with many intercepting the Letaba river upstream of KNP.

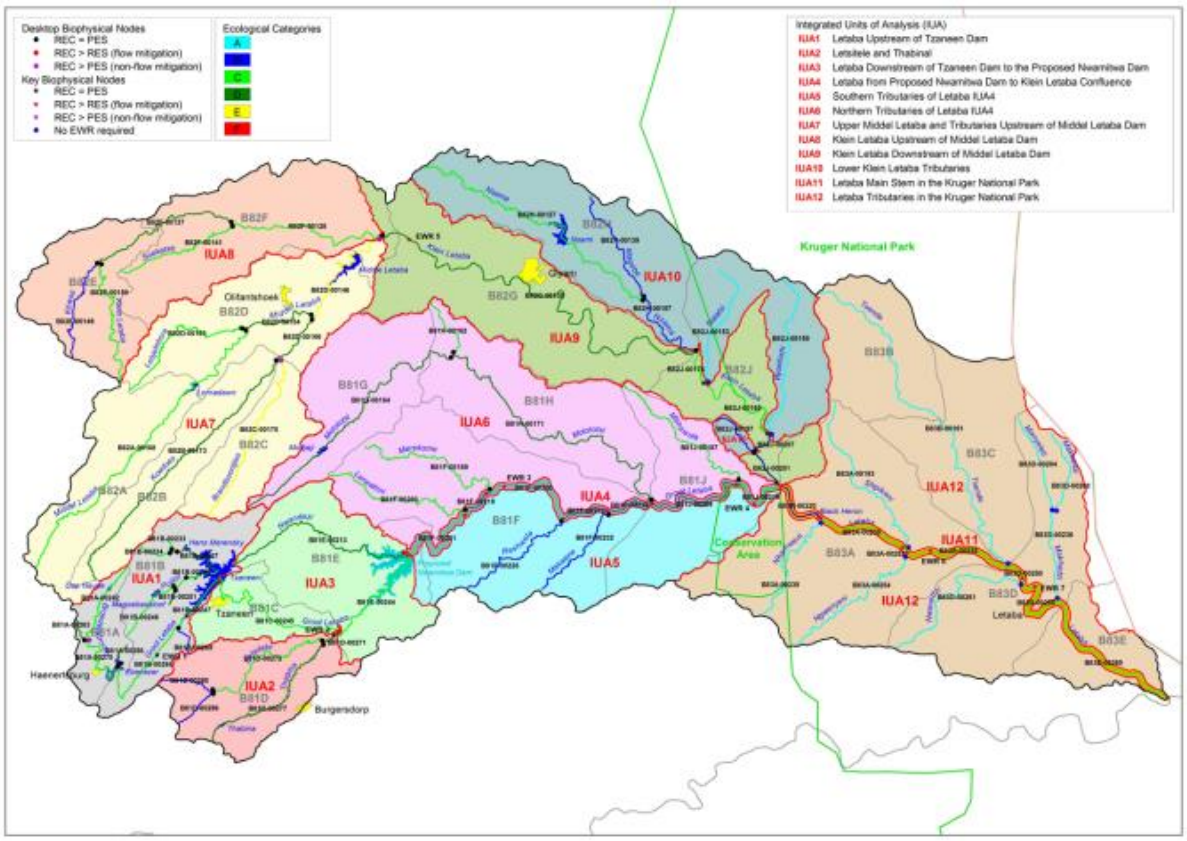

Figure 1 The Letaba catchment, with major dams and EWR sites, according the WRCS (DWA, 2013)

Climate

The climate across the catchment is considered semi-arid and varies since it extends across high altitude, mountainous areas in the west and the low-lying areas of the Lowveld in the east. Generally, summers are wet and hot whereas winter conditions are dry and mild. The

mean annual precipitation (MAP) in the catchment is approximately 612 mm, of which more than 60% is captured in only 6% of the total area, i.e. the mountainous region in the west (WRC, 2001). In particular, 500-1800 mm of rainfall falls in the western mountainous areas whereas the east receives 450-700 mm (Moon and Heritage, 2001). According to the WRC (2001), mean annual evaporation is estimated to be 1669 mm.

Hydrology and Geomorphology

There are more than 20 major dams located in the Letaba Catchment (WRC, 2001). The Letaba River is the tributary of the Olifants River just upstream of the Mozambican border. The Molototsi River and Klein Letaba are the major tributaries contributing to the Letaba River. The macro-channel of the river may be described as bedrock-bounded (van Niekerk *et al.*, 1995; cited by Heritage *et al.*, 2001). The channel is further characterized by steep bedrock including cascading boulder rapids with sporadic waterfalls (State of the Rivers Report, 2001). Further downstream in sections with gentler gradients, cobble riffles occur before changing to an alluvial channel type as it approaches KNP (WRC, 2001). Deep pools may be found all along the Letaba River. There are a number of different morphological units due to varying sediment distribution along the Letaba River (Heritage *et al.*, 2001).

Land-use Activities

Throughout the Letaba catchment, land-use is dominated by commercial agriculture, afforestation, densely-populated rural communities with informal, rain-fed agriculture and protected areas in the eastern section of the catchment (Pollard and du Toit, 2011a). The Letaba catchment is home to intense, commercial agricultural activities where citrus, tropical fruits and vegetables are the most commonly farmed produce (Pollard and du Toit, 2011a). Since the headwaters in the western section of the catchment are under commercial forestry, water resources are already under stress due to the additional demand of water supply for irrigators downstream. The upper reaches of the catchment are generally regarded as being in good condition but it deteriorates further downstream due to natural salinization and nutrient enrichment by anthropogenic influences (Pollard and du Toit, 2011a).

The water supply schemes in the catchment currently consists of numerous small to major dams for storage, bulk water pipelines as well as extensive canal networks (Pollard and du Toit, 2011a). More than a decade ago, Vlok and Engelbrecht (2000) noted that the Tzaneen Dam allocated 103.9 million m^3/a to irrigators, 8.4 million m^3/a to households and industry and 14.7 million m^3/a for environmental flows. However, the water which was allocated exceeded available supply because Tzaneen Dam could only yield 98 million m^3/a (Vlok and Engelbrecht, 2000). Situations such as these highlight the magnitude of poor water management strategies in a stressed catchment such as the Letaba.

Letaba Water Supply System – Status-quo

Katambara and Ndiritu (2010) have identified that flows in the Letaba River no longer resemble natural flows due to infrastructural developments including large dams, e.g. the Magoeboeskloof, Ebenezer and Tzaneen dams.

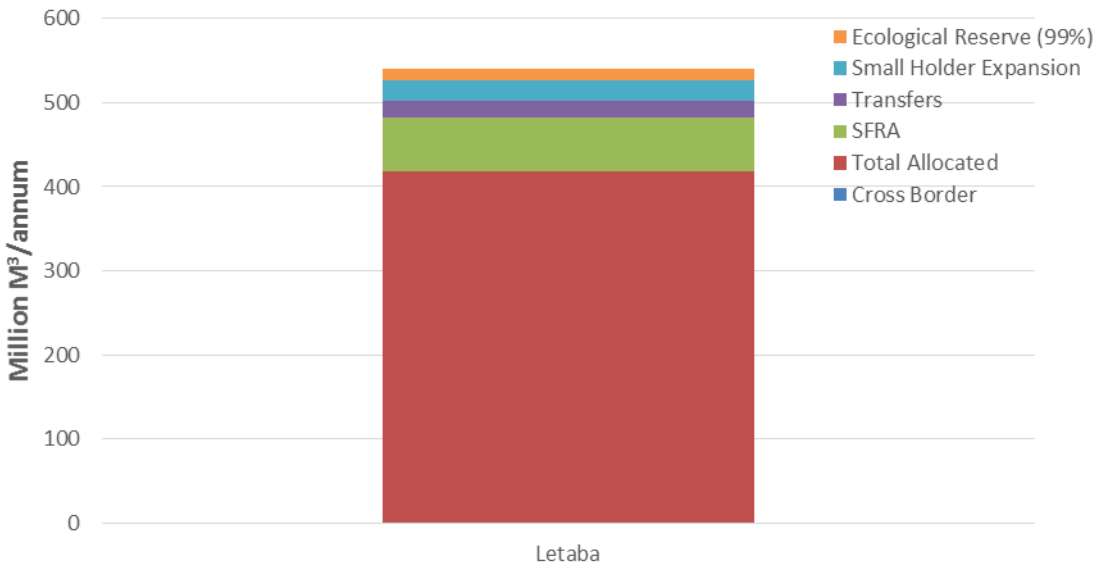

Figure 2 Status of present water allocation in the Letaba catchment, 2014 (total allocated includes commercial agriculture, industrial and domestic requirements).

In terms of water resources planning we often speak of catchments along with their associated infrastructure as *water supply systems*. The Letaba River is one such system which utilises water from the Groot, Middle and Klein Letaba rivers and their tributaries. In the Middle and Klein Letaba's there are a number of borehole supply schemes and water supply schemes using the Middle Letaba and Nsami dams. Whilst in the Groot Letaba water is supplied for bulk domestic use to towns such as Polokwane (inter-basin transfer), Tzaneen and rural communal areas. These utilise the Dap Naude, Ebenezer, Magoebaskloof, Vergelegen, Hans Merensky, Tzaneen, Thabina and Modjadji dams. However the surface water resources within the entire Letaba catchment are extensively developed (Figure 2). Faced with water shortages of increasing severity and frequency over the years, the main consumptive users of water have from time to time competed for the limited supplies and experienced significant levels of restrictions. This has resulted in the degradation of the riverine ecosystem. The water resources of the Groot Letaba are not sufficient to meet all its requirements all of the time (DWA, 2014).

The recent water resources reconciliation for the Letaba system (DWA, 2014) included amongst others the following advice to be implemented in order to achieve water resources management sustainability in this catchment up to 2040:

- Excess water from Ebenezer Dam should be allocated to users in the Groot Letaba System by augmenting the Tzaneen dam. With no further augmentation possible via inter-basin transfer to other areas (e.g. Polokwane)

– Water Conservation/Water Demand Management must be implemented in this catchment with immediate effect from both the domestic and industrial sector

- Continue with the implementation of the Groot Letaba Water Development Project (GLeWaP) which includes: raising of Tzaneen Dam by 3m to improve the assurance of supply to the users; A new major storage dam on the Groot Letaba River just downstream of the Nwanedzi River confluence, at the site known as N'wamitwa with first

water will be stored by 2019; and resulting from N'wamitwa develop a bulk water supply scheme to serve rural communities without adequate water supplies;

- Importantly (and demonstrating the added value of the WRC project K5-2338) use N'wamitwa Dam to start to deliver water according the ecological water resources requirements gazetted in the WRCS process for the Letaba.

Furthermore, large TLs were identified during the GLeWaP and other studies on the lower reaches of the Letaba. It has previously not been possible to estimate these losses as no acceptable gauging stations existed in this part of the Letaba, and because the current water resources assessment model (WRSM2000/Pitman model) only specifies transmission losses as a monthly value. Also the weir at Prieska Weir's (B8H017) sluice has been open since the 1996 floods due to a tree being stuck in the sluice gate. This already might account for the perceived losses on its own. The Prieska Weir issue should be resolved by either continuously measuring the flow from the leaking sluice or by destroying the Prieska Weir.

Pollard *et al.* (2012) through a historical (contextual) assessment of compliance with the ecological reserve showed that during the period of major water resource development (1960-94) in the Groot Letaba, meeting the present-day assurance rules close to the KNP at EWR 4 (using a 'C/D' class assurance determined prior to the WRCS process) that there was typically above 40% non-compliance with the ecological reserve, especially noticeable in the dry winter months (May-October) (Figure 3). However post 1994, the situation had begun to improve where non-compliance ranged between 20-30%. It was noted in this study that this catchment had seen continuous effort to improve water resources management since 1994 and this was attributed to close interaction between the operator of Tzaneen dam and commercial agriculture through the Letaba Water Users Association (LWUA) and then more recently with the KNP monitoring flows near the western boundary, who initially started to benchmark flows at 0.6 m^3/s in the absence of a comprehensive reserve study.

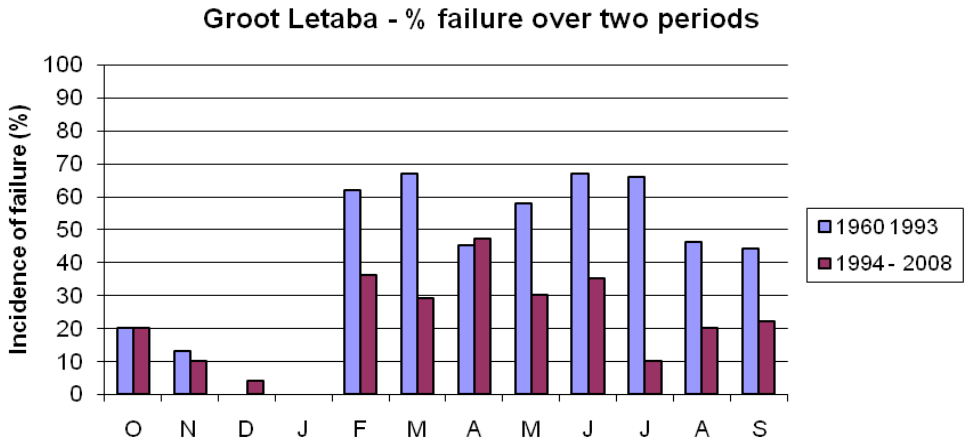

Figure 3 Compliance with the ecological reserve at Letaba EWR 4 (Pollard et al, 2012)

History and Present Operating Rules

The Tzaneen dam was completed in 1976 and by 1977 the Tzaneen Dam started to fill with an annual allocation of 130 Mm^3 whilst its full supply is 156 Mm^3 and a firm yield of 50 Mm^3.

History has demonstrated the stresses that the Tzaneen Dam is meant to endure. For instance the late 1980s and early 1990s droughts the Tzaneen dam capacity effectively dropped to below 5% and in 1995 it dried out completely. The short drought of 2004-2005 also saw its storage drop significantly. In general, approximately 14% of time dam is at 0-10% capacity, close to 20% of time dam is above 90% capacity.

Given that wet cycles in the Letaba region are about 20 years apart, it needed to be factored into the management of the dam and the history of constraints on the system meant that new operating practice had to be implemented for the sustainable utilization of the dam. This is in order to mainly provide the citrus orchards in Tzaneen area with a permanent supply of water (otherwise plants die and it takes 4-5 years before citrus can become productive again – so a significant risk for the local economy). Therefore from 2006 early restrictions were brought in to the operations (Water Years starts from 1 April to end of March) this allowed accrual of storage in the dam, which didn't occur previously.

The DWS operating rules for the Tzaneen dam plan for annual losses of 30% downstream, whilst 10-15% of the dam is reserved for domestic and industrial use. If the dam reaches the 15% level then there is a 100% curtailment to irrigators. Meanwhile, irrigators through the Letaba Water User Association (LWUA) implement their own voluntary operating rule: 95-100% capacity - then 100% assurance of supply to irrigators, below 95% then 50% curtailment on 1 April, and for each month thereafter they add a further 5% curtailment. For example, May would be 55%, until you get to 70% curtailment. These steep restrictions allow the LWUA to manage for large storage depletion in the dam.

Meanwhile it is assumed that the tributaries in the system make significant inflows that allow the reserve to be met and to meet the needs of the run-of-river users downstream. However if the tributaries are not flowing then the Tzaneen dam needs to release on average about 6 Mm^3; if they are flowing then about 2 Mm^3 is released, in order to meet requirements at Letaba Ranch (EWR4).

The comprehensive reserve determination through the WRCS process has proposed the lower reaches of the lower Groot Letaba to be a Management Class II with a C class reserve (Table 1). The implication of this is high assurance rule flows that must be implemented than the present day operating scenario (Figure 4), although it is acknowledged that this will only be fully achievable following the construction of N'wamitwa dam, wherein a new EWR rule applies.

Table 1 Management Class and Water availability in the Letaba Catchment (Drainage Region Olifants: B8), MAR data from WR2012 study.

	Management Class	REC	Catchment Area (km^2)	nMAR[1]	revised nMAR[2]		EWR Mm^3/a		
					Natural MAR	Present Day MAR	70% assurance	99% assurance	% of nMAR at 99% assurance
Letaba	II	C	13677	679.6	636	342	36	13	2

DRAFT

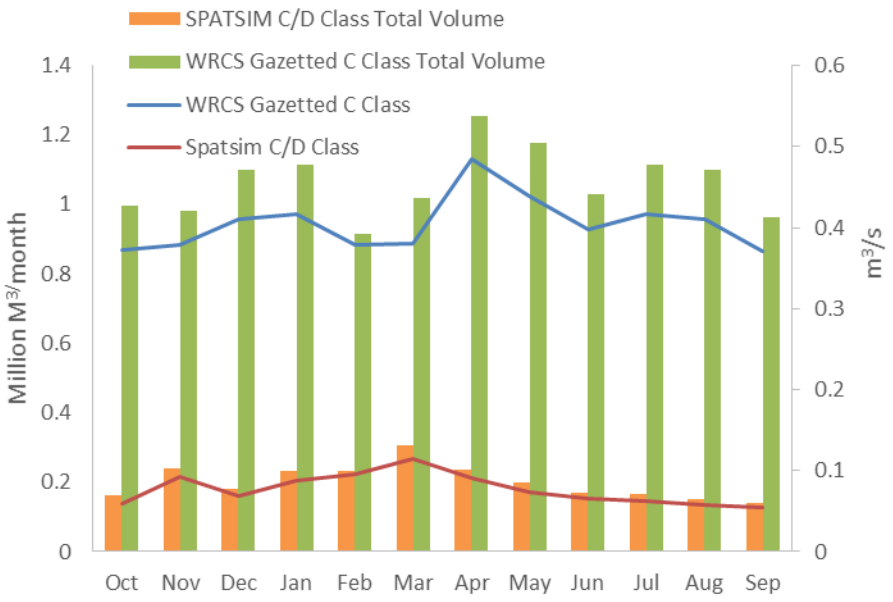

Figure 4 Operating rule for EWR4 (columns), mean daily flow (lines) for EWR4, comparing existing SPATSIM model with recently gazetted EWR requirements.

DRAFT

Transmission Loss Study Site

The Letaba River Transmission Loss study site is situated along the lower end of the Groot Letaba River just before the river enters the Kruger National Park. The site is bounded on the upstream side by the defunct Mahale weir (B8H007[1]) and on the downstream side by the Letaba Ranch weir (B8H008), Figure 5. Between these two gauges the river traverses agricultural areas under tenure by emerging farmers schemes in the west, before traversing protected areas (the community owned Mthimkhulu reserve on the northern bank, and provincial Letaba Ranch Game Reserve on the southern bank). Appendix I gives detailed site description maps on the local lithology, soils, stream networks, topography and topocadastral features. The river morphology consists of two dominant types, sandy braided alluvial system most dominant in the west, with increasing occurrence of bedrock controls (dykes) in the east (Figure 6 and Figure 7).

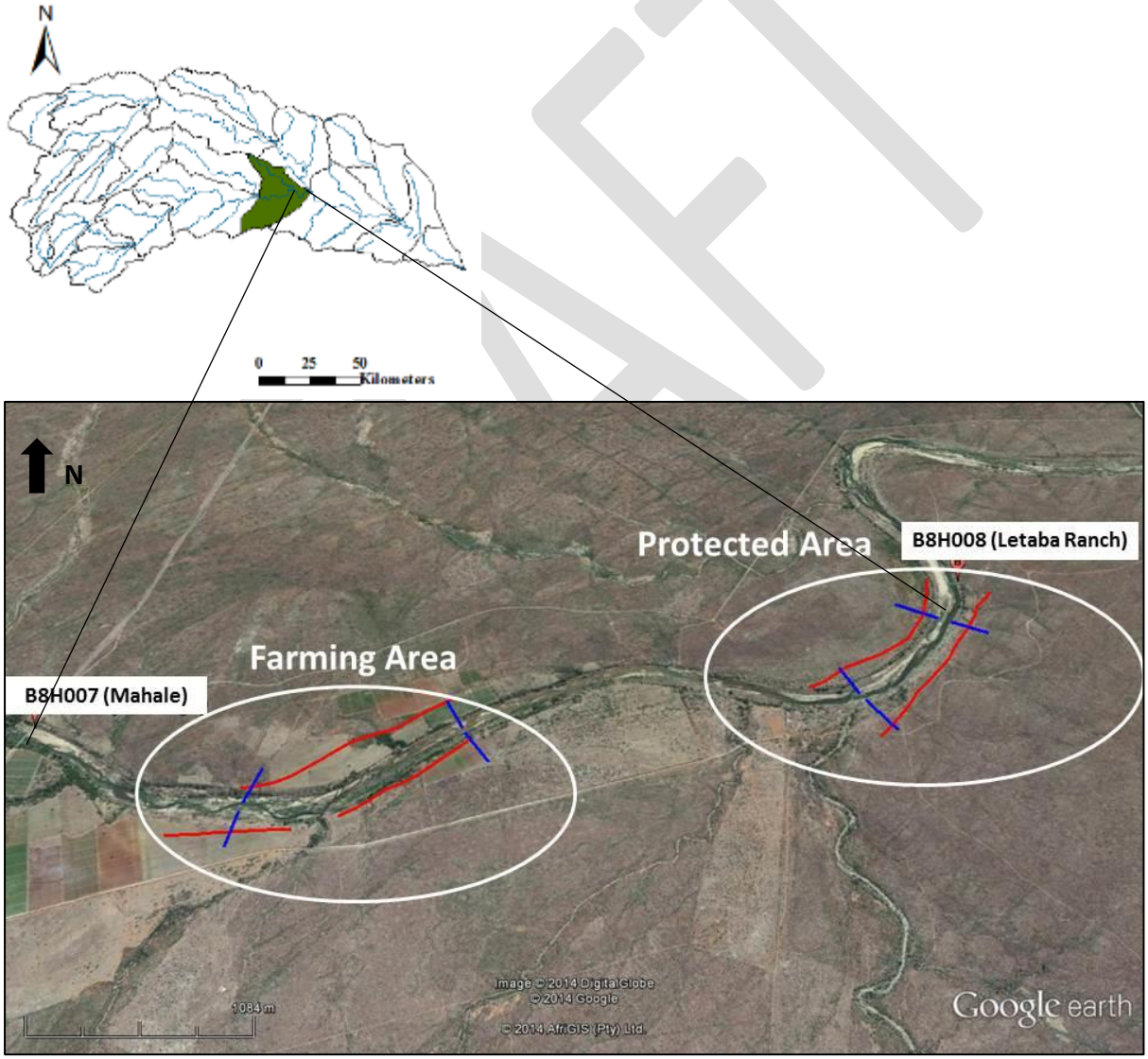

[1] This is not a gauging weir as it was constructed as a river crossing/abstraction weir although registered on the DWS hydrometry database.

Figure 5 Delineation of the study site between B8H007 (Mahale) and B8H008 and the location of geophysics transects over two different land-uses.

Figure 6 Typical river channel morphology at study site: braided alluvial channel

Figure 7 Typical river channel morphology at study site: bedrock controls

Study Site Set-up: River Hydrology and hydro-chemistry

The study made use of the two river gauges for mass-balance purposes (Figure 8). Primary flow data was available from the DWS HYDSTRA database for the downstream Letaba Ranch B8H008[2]. Meanwhile the Mahale weir (B8H007) was un-gauged, it was therefore fitted with a Solinst Levellogger to determine stage height and a rating was attempted, however the structure of the weir wall was such that it was not suitable for a full rating. This when the levellogger data showed a constant stage, this was taken to mean no overflow of the weir wall but simply continued discharge through two low flows sluices for which the following rating was determined:

Table 2 Mahale Weir low flow rating

FLOW AT WEIR PIPES (m/s)	Pipe diameter (m)	Discharge (m^3/s)	Total Discharge (m^3/s)
Pipe 1	3.4	0.3	0.24	0.50
Pipe 2	3.7	0.3	0.26	

Figure 8 Mahale weir (left) and Letaba Ranch weir (right)

Furthermore, longitudinal hydro-chemistry surveys of the river channel were conducted 3 times during the study. The first such survey in November 2014 (Figure 9) alluded to groundwater discharge into the river as the EC of the river freshened out further downstream into the protected areas. It is at the point where the river EC increases in the November 2014 survey that the river may appear to intersect the regional groundwater flow path, and it is expected that paleo-floodplain alluvium[3] is the conduit for an unconfined aquifer in this region that relinquished water to the river as accruals during the early part of the study period. However as drought conditions persisted during the study it appears that these contributions diminished hence the resulting stable EC throughout the longitudinal river profile by the April 2016 survey.

[2] https://www.dwa.gov.za/hydrology/Verified/HyDataSets.aspx?Station=B8H008&SiteDesc=RIV

[3] As suggested through the geophysics study

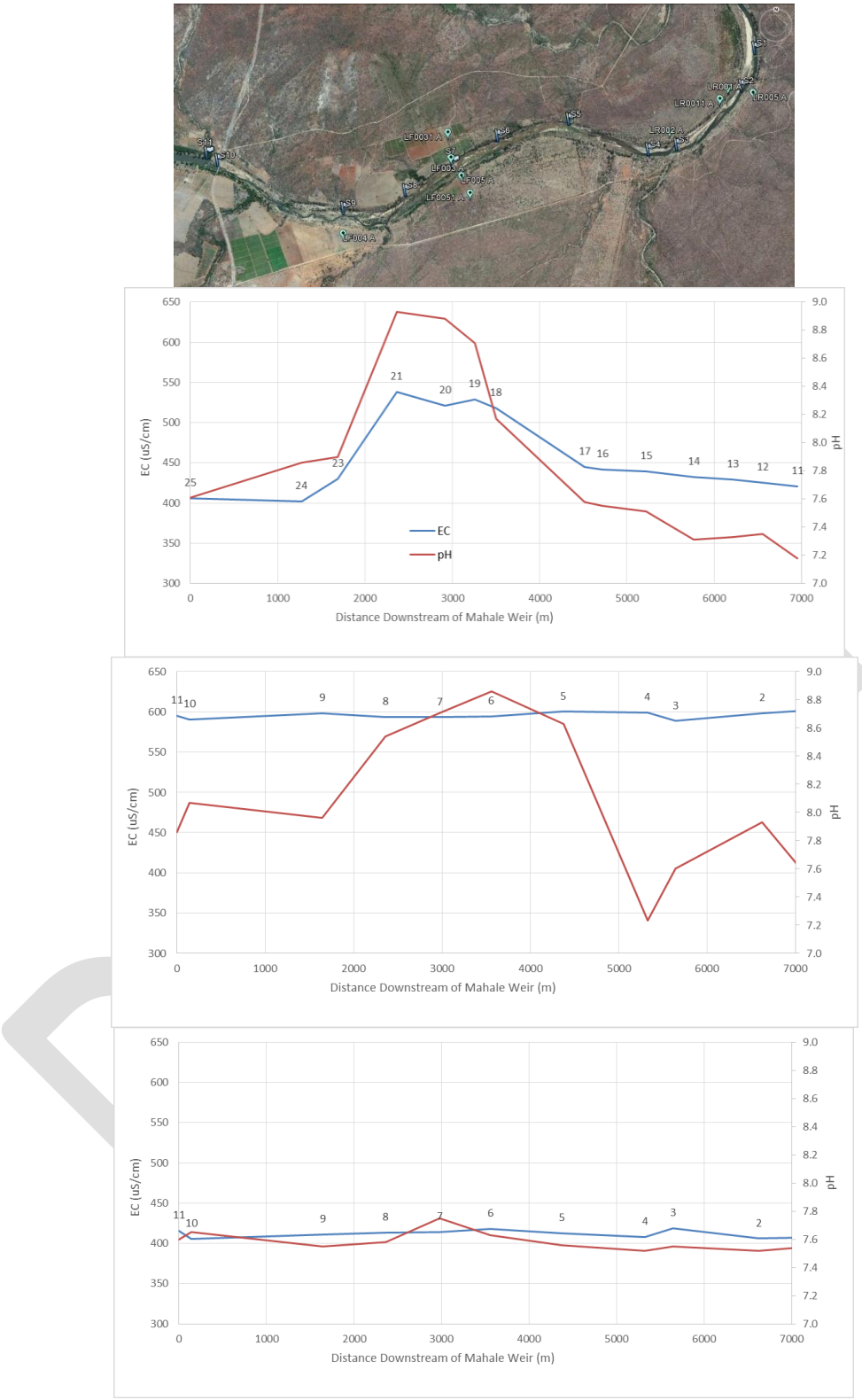

Figure 9 Longitudinal hydro-chemical surveys of the Letaba river between Mahale and Letaba Ranch on 24 November 2014 (above) using parameters measured in-situ, and both 27 October 2015 (middle) and 14 April 2016 (bottom) by the MOSA Mobile Laboratory[4].

[4] Work funded by the Middle Olifants South Africa (MOSA) project, BMBF, Germany

Study Site Set-up: Riparian Eco-Hydrology through Stable Isotopes

The study undertook to determine potential hydrological connectivity between surface water and ground water using stable isotope analysis and furthermore distinguish whether riparian zone vegetation uses either of these water sources and the temporal variation thereof.

13 individual tree species, 2 x *D. mespiliformis,* 2 x *P. violecia*, 2 x *C. Microphyllum*, 3 x *F. sycomorus*, 2 x *Z. mucronata*, 1 x *G. senegalensis* and 1 x *C. mopane*, distributed among six sampling regions across a portion of the Groot Letaba River were sampled for stable isotope analysis. These sampling regions were categorized according to their respective locations with regards to Letaba Farms (7 trees) and Letaba Ranch (6 trees). The co-ordinates and a Google Earth illustration of the sampling regions are given in Table 3 and Figure 10, respectively.

Table 3 Co-ordinates for the six sampling regions distributed across a portion of the Groot Letaba River along which 13 individual tree species were sampled

Sampling Point	Description	Latitude	Longitude
1	Letaba Farm near stream northern bank	23.669	31.017
2	Letaba Farm near stream southern bank	23.670	31.019
3	Letaba Farm near stream northern bank	23.675	31.005
4	Letaba Ranch near stream northern bank	23.662	31.047
5	Letaba Ranch within river channel	23.659	31.049
6	Letaba Ranch near stream southern bank	23.662	31.049

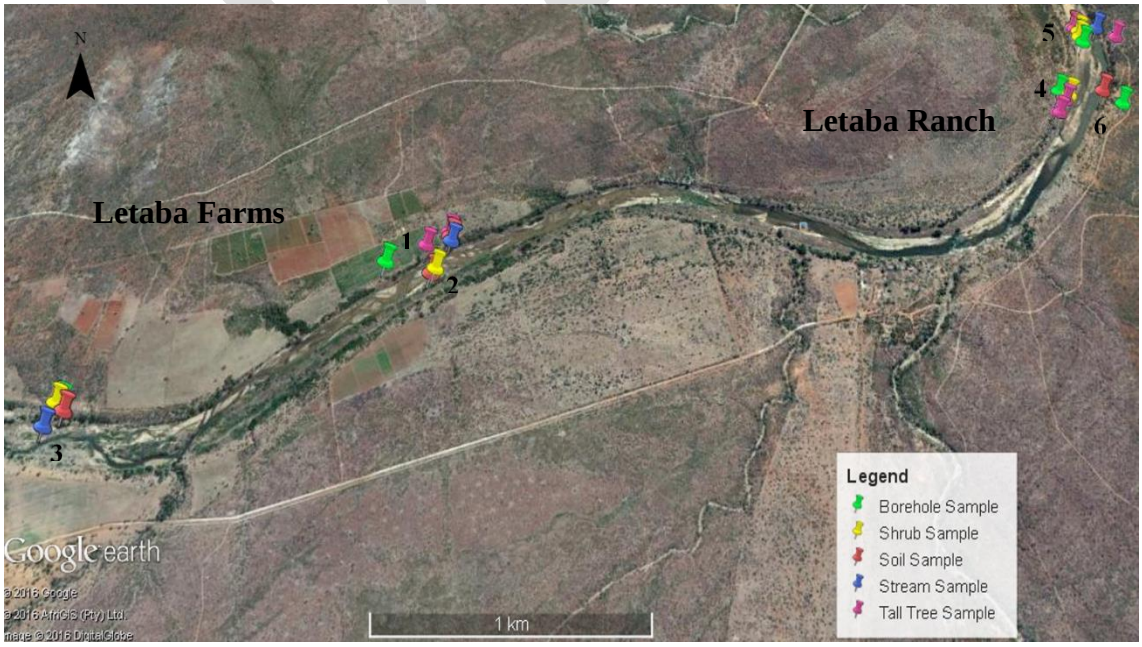

Figure 10 Location of the six sampling regions across a portion of the Groot Letaba River incorporating the 3 geomorphological zones categorized in this study

Sampling Procedure

Twig, soil, stream and groundwater samples were collected on 3 sampling occasions during the 2016 dry season (in May, August and October). Twig samples of mature wood approximately 0.3 to 1.0 cm in diameter and 4.0 to 7.0 cm in length were collected from the dominant tree species, from randomized locations. Bark was removed immediately and the underlying stem samples stored in airtight glass vials. Soil samples at depths of 30, 60 and 100 cm were collected concurrently with the twig samples. The soil samples were obtained using a hand auger and then transferred and sealed into airtight 500 ml plastic bottles. Xylem water and soil water were extracted using the Cryogenic Vacuum Distillation Method.

Stream samples from the Groot Letaba River were collected at sampling points 1, 3 and 6 and stored in airtight 500 ml plastic bottles. Ground water samples were collected from 5 boreholes situated adjacent to the active river channel at sampling points 1, 3, 4 and 5, as well as from a borehole situated within the active river channel at sampling point 6 (LWR002). These samples were then stored in airtight 500 ml plastic bottles. The stream and groundwater samples were then later transferred into small glass vials. The various samples collected in field were then stored in a fridge prior to analysis in the following days.

In addition to the abovementioned samples, 13 rainfall samples from 15th November 2015 to 19th May 2016 were collected and analysed. The δ^2H and $\delta 1^8O$ values for these precipitation events were then used to construct a local meteoric water line (LMWL) for our study site. The δ^2H and $\delta^{18}O$ values for twig, soil, stream and groundwater were then plotted and compared relative to this LMWL.

The ^2H and ^{18}O contents of rainfall, stream and groundwater samples were measured using a Los Gatos Research (LGR) DLT-100 Liquid Water Isotope Analyser at the University of KwaZulu-Natal. Water from the xylem and soil water were was extracted using an open manifold system that facilitated removal of non-condensable gases and potential organic contaminants, and the ^2H and ^{18}O contents measured using a Picarro L1102-i CRDS analyzer (Picarro, Santa Clara, California, USA). The overall analytical precision of the spectrometers was less than 2 permil (0.002‰) for ^2H and less than 0.3 permil (0.0003‰) for ^{18}O.

The ^2H and ^{18}O of the various samples (^2H and ^{18}O) were expressed in delta notation relative to the Vienna Standard Mean Oceanic Water (VSMOW), as:

Equation 1 $$\delta = (\frac{R_{sample}}{R_{standard}} - 1)1000$$

Where δ (‰) represents the deviation from the VSMOW (can be positive or negative depending if the isotopic concentration of the sample is enriched or depleted relative to the source, R_{sample} and $R_{standard}$ is the ratio of the heavy to light isotopes ($^{2H}/^{1}H$ and $^{18}O/^{16}O$) in the sample and the standard, respectively.

Study Site Set-up: Hydrocensus

An initial hydrocensus was performed during May 2014 in a local community just north of the study site. The hydrocensus was conducted in order to provide some indication of the local hydrochemistry in the surrounding area as well as how dependent local communities are on groundwater for domestic and small-scale irrigation supply. The data provided below stems from an initial hydrocensus conducted north in Mbaula and on a local reserve, Mthimkhulu (Figure 11).

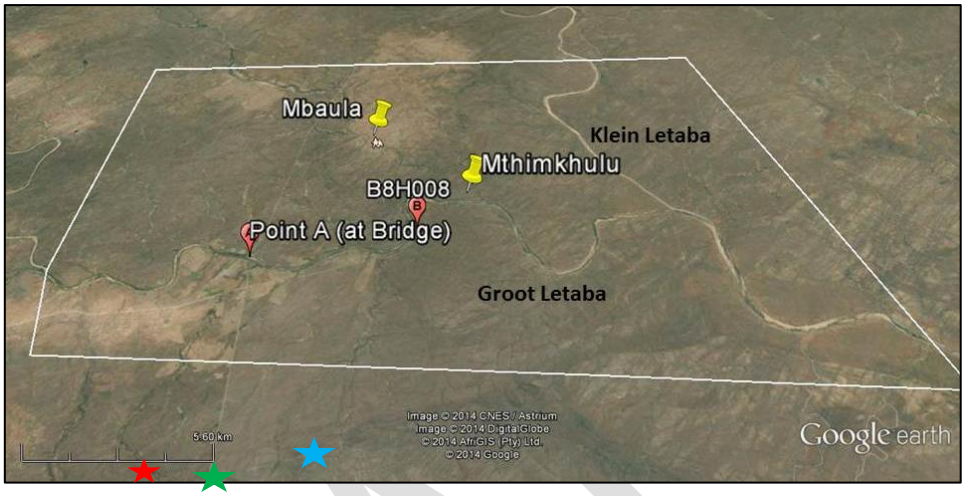

Figure 11 Mbaula Village and Mthimkhulu Reserve in relation to the study site

(i) Mbaula

A total of 37 boreholes were identified in Mbaula. However, hydrochemistry variables were only measured in 32 of these due to owners / operators not being available to switch on the pumps to obtain a water sample. Boreholes in Mbaula were drilled to an average depth of 50m. Of the 32 boreholes, the pH in Mbaula averaged at 7.19 while groundwater temperatures averaged at 24.44 °C. Groundwater measured in nine of these boreholes was extremely saline resulting in out of range EC values. In 16 of these boreholes, EC ranged between 12-19 mS/cm. In less than 22% of the boreholes measured (i.e. only 7 boreholes), groundwater was very fresh with a low EC ranging between 1-2 mS/cm. It is likely that these boreholes were drilled along dykes where preferential pathways act as conduits for fresh surface water to recharge aquifers.

(ii) Mthimkhulu

There is a total of six boreholes located throughout the Mthimkhulu Reserve, of which only five could be accessed for recording (Table 4). Not all of these boreholes are actively pumped. At these inactive boreholes, a bailer was submerged in order to collect a water sample for hydrochemistry measurements.

Table 4 Details of boreholes located on Mthimkhulu Reserve.

Borehole ID	Status	Activity (eg. Domestic, farming)	Borehole Depth (m)	Water Level (m)	pH	EC (mS/cm)	Temp (°C)	TDS (ppt)

WP 019	Active	Domestic	?	Covered				
WP 020	Not always	Domestic, Watering Hole	50	10.21	6.9	14.75	26.2	7.36
WP 021	Not active	Domestic	100	21.96	6.26	0.5	27.6	0.25
WP 022	Not active	Domestic, Watering Hole	30	2.32	6.9	13.33	25.6	6.71
WP 023	Active	Domestic, Lodge	60	10.97	7	15.5	20.2	7.64

In general, the groundwater observed on Mthimkhulu is similar to that measured around Mbaula thus providing a decent indication of the local hydrochemistry in the area. Borehole WP021, which was drilled up to 100m to supply water for a guest lodge along the Groot Letaba (just upstream of the Groot and Klein Letaba confluence), has good quality water.

(iii) Additional Hydrocensus Information

Although no formal hydrocensus was been completed on these farms, correspondence with the farmers provided additional hydrocensus information. The farm represented by the red star in Figure 11 has a total of seven boreholes on the property but only one of these are actively used to supply water for household use. Crops are irrigated directly from the Groot Letaba River. The farm represented by the green star irrigates using both groundwater as well as direct supply from the river. The exact amount of boreholes on this property is still uncertain. The farm represented by a blue star (as well as the farm directly opposite the river) does not have any boreholes drilled on the property since it irrigates daily using water directly from the Groot Letaba.

(iv) River abstraction

Direct abstractions from the river occur within the study site, especially in the farming portion. Whilst all the farms use drip irrigation and abstractions should be relatively low, the total amount needed to be quantified in order to properly understand differences in flow between the two weirs. The results of this survey suggest relatively low direct river abstraction (Figure 12 and Table 5), with an estimated mean daily abstraction of 52m^3.

DRAFT

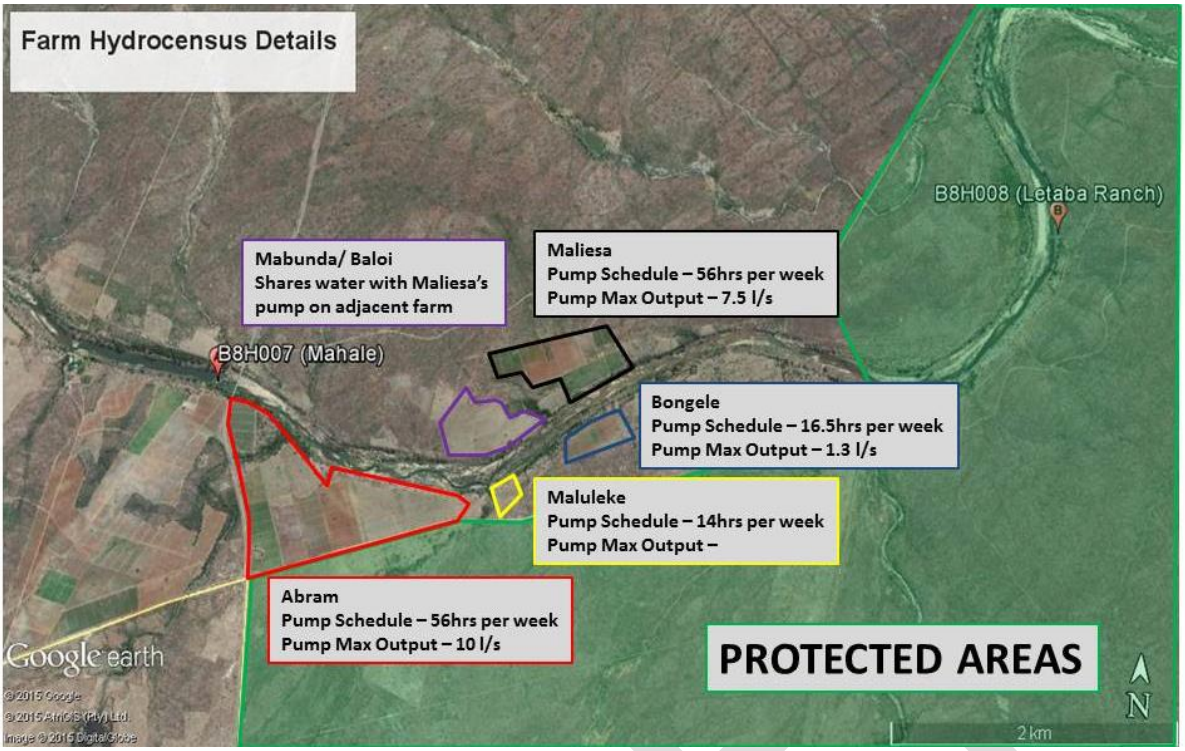

Figure 12 Agricultural water use hydrocensus at study site

Table 5 Hydrocensus information from July 2015 survey.

Farm Name	Bank	No. boreholes	Farming Scale	Pump Max. Capacity (L/S)	Pumping schedule (hours/week)	Estimated volume per day (L)
Abram	Southern	0	Commercial	10	56	28800
Maliesa	Northern	4	Commercial	7.5	56	21600
Mabunda	Northern	0	Commercial			
Bongele	Southern	5	Commercial	1.3	16.5	1103
Maluleke	Southern	0	Commercial	1	14	720
					Potential Abstractions per day (L)	52223
					m^3/day	52

Study Site Set-up: Precipitation

Rainfall data was collected during the study period from three Davis Vantage Pro weather stations situated within the study site at: Mahale farm (adjacent to Mahale weir B8H007), Mthimkulu (within the Mbaula reserve), and Phalaubeni a village 6km to the north. As can be seen in Figure 13 the study period was marked by extremely low rainfall from 1 June

DRAFT

2015 onwards, with no more than 180mm received over the study period, and a significant proportion of this being from a single event in March 2016. Up until that date, only 73mm had been recorded for the rain season.

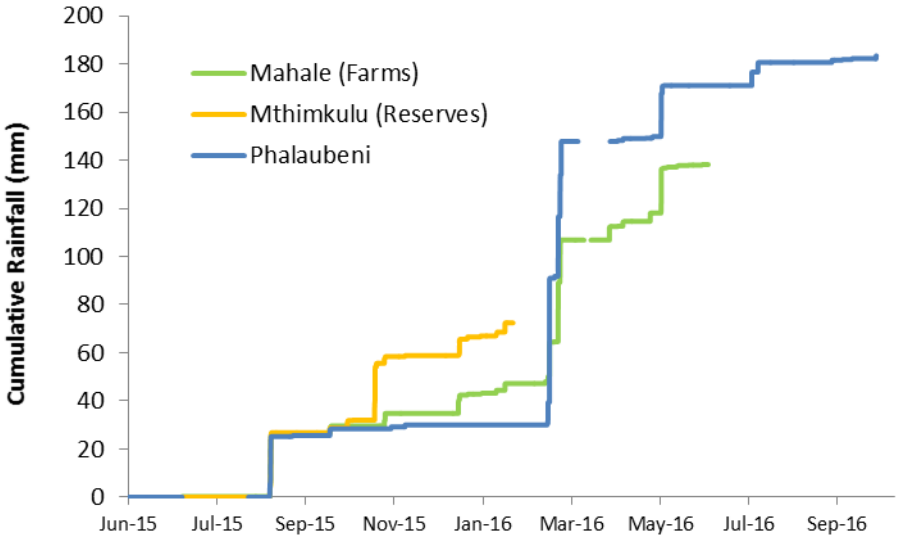

Figure 13 Rainfall measured for the 2015-16 hydrological year, within the study site (Mahale, Mthimkulu) and at nearby village north of the site (Phalaubeni)

DRAFT

Study Site Set-up: Geophysical Surveys

Geophysical survey techniques were conducted in order to obtain valuable information of the subsurface geology, using the commonly applied Electrical Resistivity Tomography (ERT). This is a common geophysics technique used in water resource and geomorphological studies (Robinson *et al*., 2008). According to Loke (1999), this technique provides a reliable account of the bedrock and lithological distribution within catchments since detailed measurements of the subsurface resistivity distribution is obtained based on known geological resistivity ranges. Resistivity values are influenced by soil/ rock properties, water content and salinity. Studies by Uhlenbrook *et al.* (2005), Kongo *et al.* (2007), Wenninger *et al.* (2008) and Riddell *et al.* (2010) have shown how the ERT method could be successfully applied in hydrological investigations in southern Africa. The purpose here was to extensively survey the subsurface resistivity distribution along the river and to identify ideal locations for drilling boreholes required for monitoring groundwater-surface water interaction. These surveys were conducted over two different land-uses, i.e. farming areas and protected areas (Figure 14), as follows:

(i) Farming Area

Two geophysics transects were surveyed on both sides of the river running in parallel, from east to west (red lines). These surveys used a minimum electrode spacing of 5m using the Schlumberger array in order to measure deep resistivity profiles (~ 70m). The blue transects represent surveys which ran perpendicular across the river. These surveys also utilsed a Schlumberger array with minimum electrode spacing of 2.5m for shallower resistivity profiles (~35m). Ideally, these perpendicular transects would have ran from one bank to the opposite bank but due to accessibility constraints, surveys had to split with each transect beginning in the river bed progressing upwards towards the river bank. The results and interpretations are depeicted in Figure 15 to Figure 20.

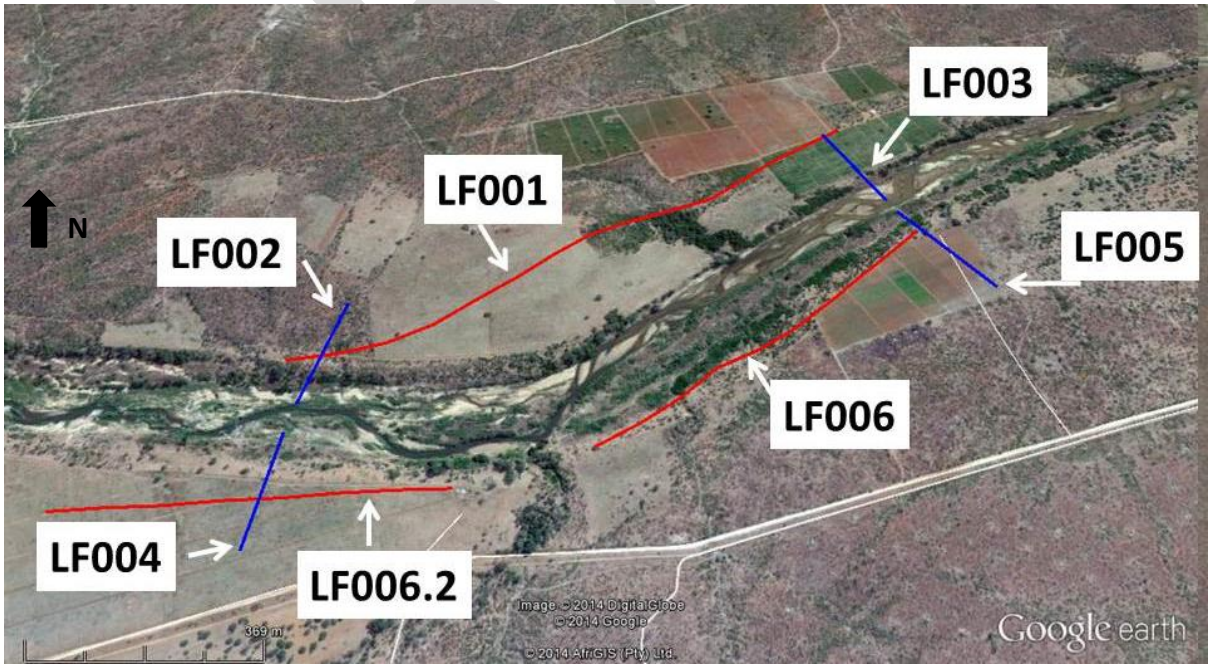

Figure 14 An illustration of the locations of geophysics transects across the farms

Letaba Farms: LF001

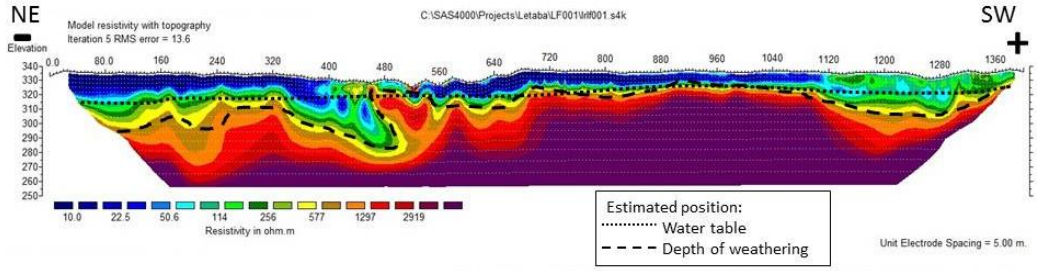

- Runs parallel to river channel (in a south-west direction)
- Evidence of tributary between 400m and 550m ~ negative weathering
- Shallow weathering 500-1100m

Figure 15

Letaba Farms: LF002

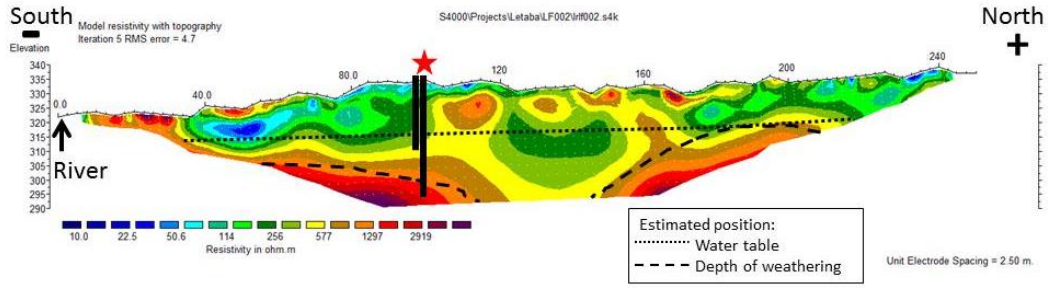

- Runs perpendicular to river channel
- A relatively flat water table
- Proposed borehole drilling location at ± 100m.

Figure 16

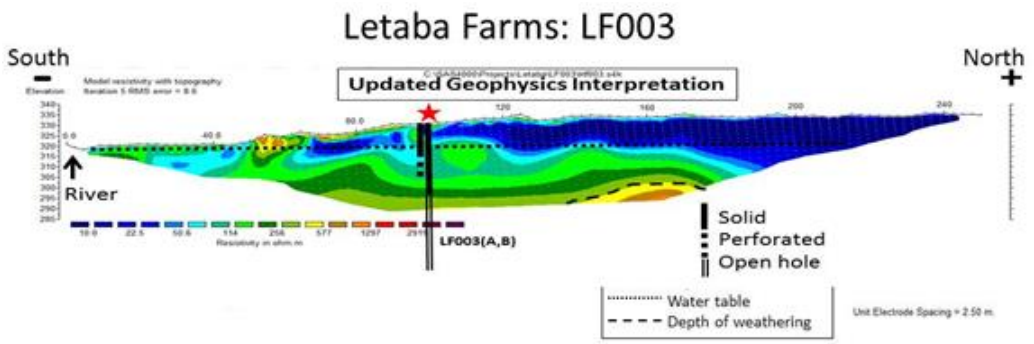

- Runs perpendicular to river channel
- Deep weathering (>25m)
- Proposed borehole drilling location at ± 100m (at edge of farm).

Initially it was assumed that there was a deep water table at around 30m. However, since the boreholes have been drilled it has been verified that it was in fact a shallow water table at around 11m which happens to be the level of the water in the adjacent Letaba River about 100m away.

Figure 17

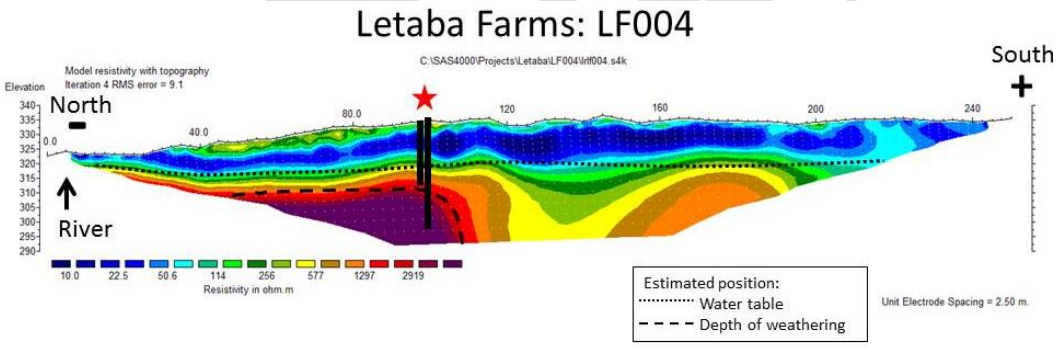

- Runs perpendicular to river channel (from north to south)
- Shallow weathering (± 10m) closer to river
- Proposed borehole drilling location at ± 100m.

Figure 18

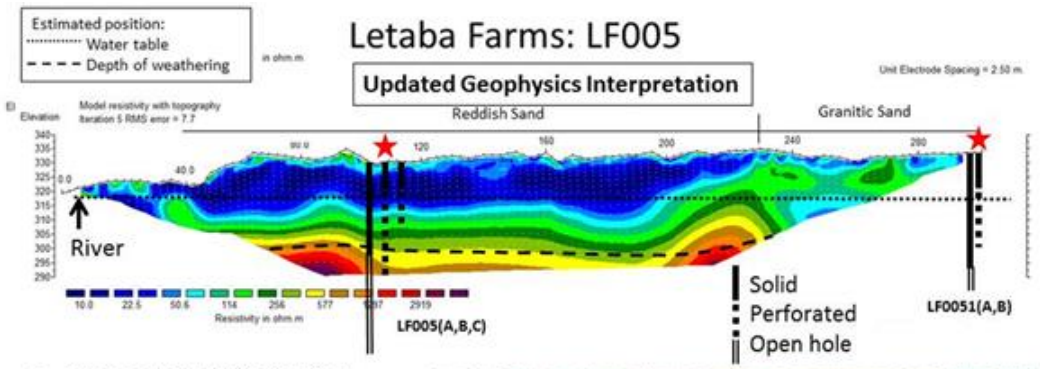

- Runs perpendicular to river channel (north to south)
- Groundwater flow direction towards the river
- Red sands up to roughly 230m; likely river deposition on floodplains.
- Typical granitic soils from 240m onwards.
- Proposed borehole drilling location at ± 110m (at edge of farm)

Initially the water table was assumed to be at a depth of about 25m. After the boreholes were installed, the water table has been verified at a depth of 12m (LF005A,B,C) and 15m (LF0051A,B). This is, however, a *flat* water table extending from the river to a distance of about 300m away. In addition, the borehole logs confirm the initial finding that the reddish sands are indeed part of historical river deposition on a floodplain up to roughly 230m with course granitic soils beyond 240m from the river. Also, the depth of weathering was slightly deeper than originally assumed.

Figure 19

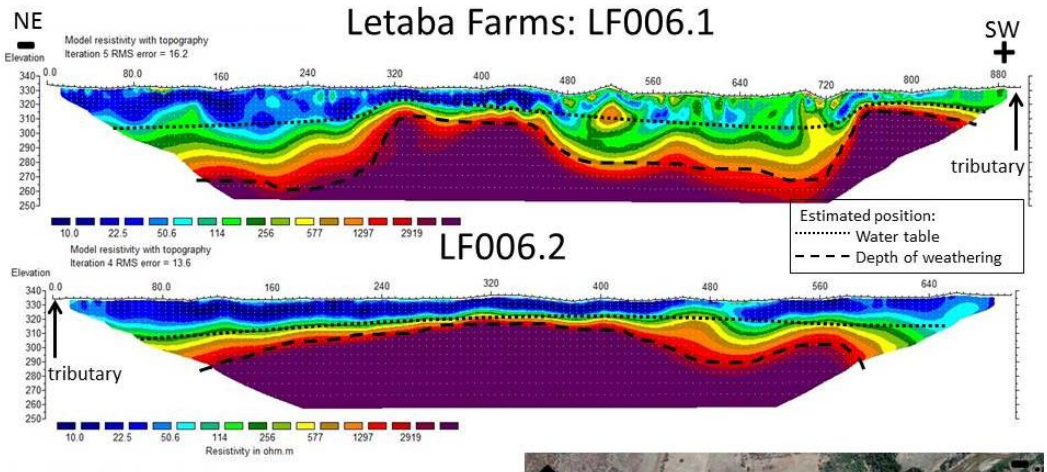

- Runs parallel to river channel (in a south-west direction)
- LF006.1- Deep sands at 0-280m and 470-750m
- LF006.2 – similar floodplain sediment with no distinct structures
- Large tributary to the Letaba intercepts between LF006.1 and LF006.2 at ± 900m

Figure 20

(ii) Protected Areas

Downstream of the farming area, geophysics surveys were set up in an identical design in the protected area. Two transects were surveyed on both sides of the river running in parallel, from east to west (red lines), Figure 21. The transect on the northern bank was spaced 2.5m short and 5m long whereas the southern bank transect was spaced 5m short and 10m long. The blue transects represent surveys which ran perpendicular to the river. These surveys were spaced 2.5m short and 5m long for shallower resistivity profiles (~35m). The results of these surveys and their interpretations are given in Figure 22 to Figure 27.

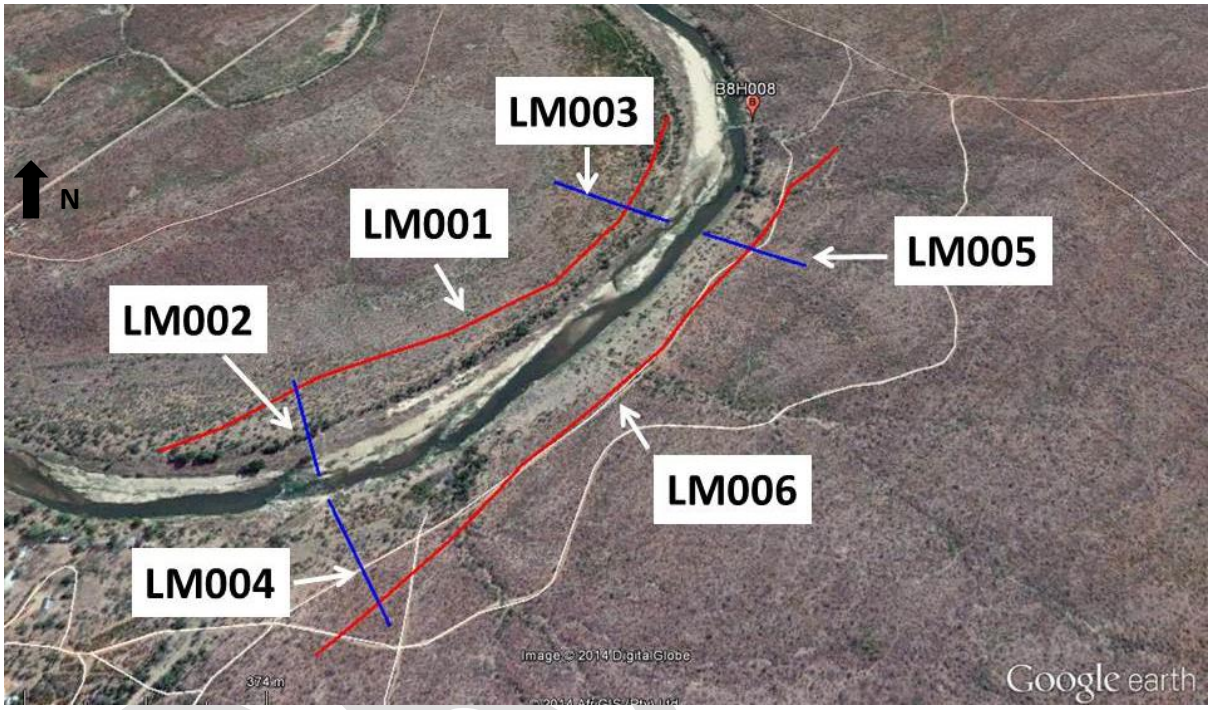

Figure 21 The locality of the geophysics surveys in the protected areas along the Groot Letaba.

Letaba Protected Areas: LM001

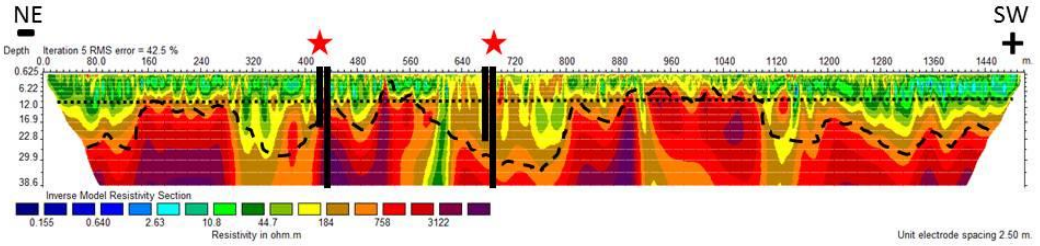

- Runs parallel to river channel (from NE to SW)
- A number of structures (dykes) possibly intercepting; i.e. 320-400m, 580-620m, ± 910m and 1100-1160m.
- Proposed boreholes drilled at 420m and 670m.
- No differential correction

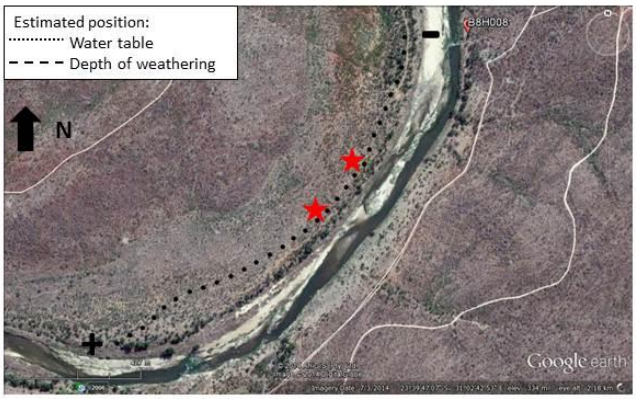

Figure 22

Letaba Protected Areas: LM002

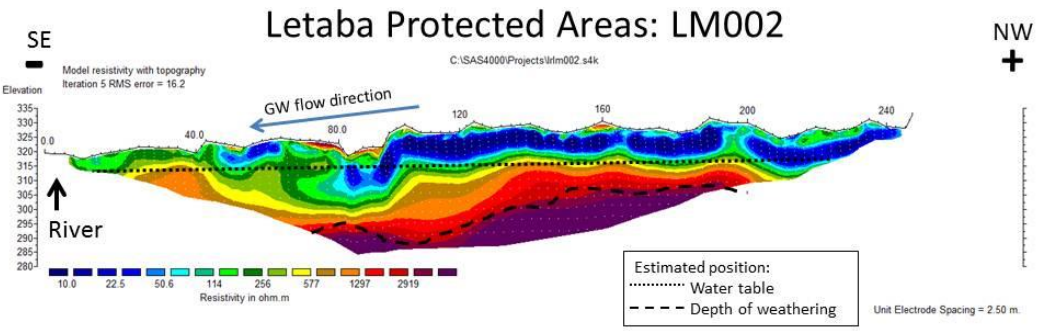

- Runs perpendicular to river channel
- Possible groundwater contribution to streamflow from bank.

Figure 23

Letaba Protected Areas: LM003

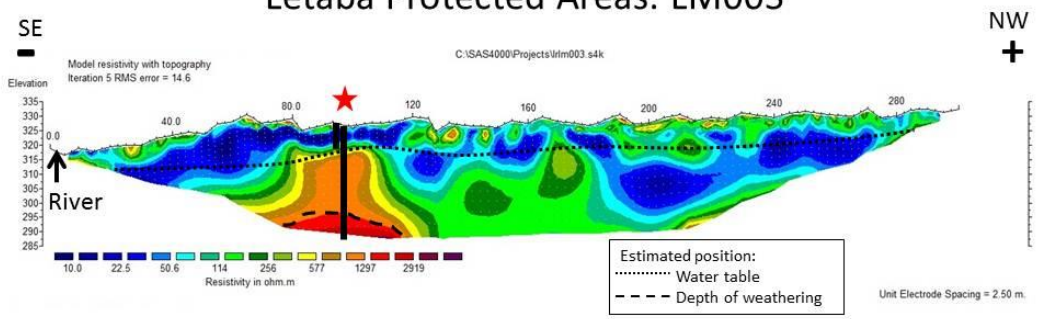

- Runs perpendicular to river channel starting in river channel
- Deep weathering after 120m to depths up (>35m)
- Proposed borehole drilling location at ± 100m

Figure 24

Letaba Protected Areas: LM004

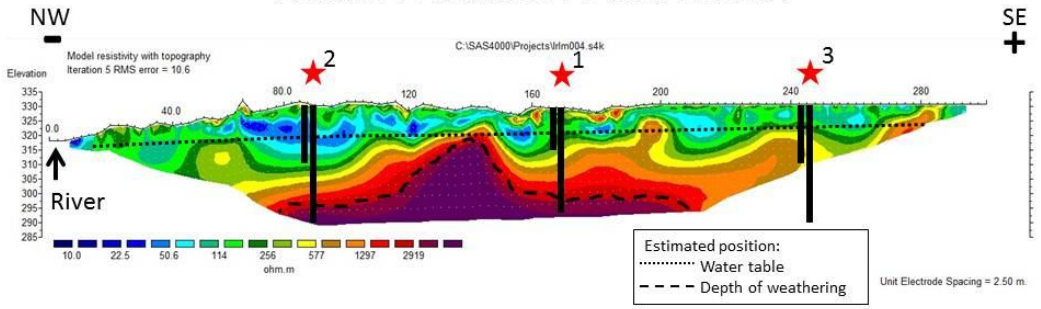

- Runs perpendicular to river channel (from north to south)
- Structure identified at ± 150m possibly having a damming effect on groundwater flow from the south towards the river.
- Proposed borehole drilling locations at ± 170m, 90m and 250m (in order of priority)

Figure 25

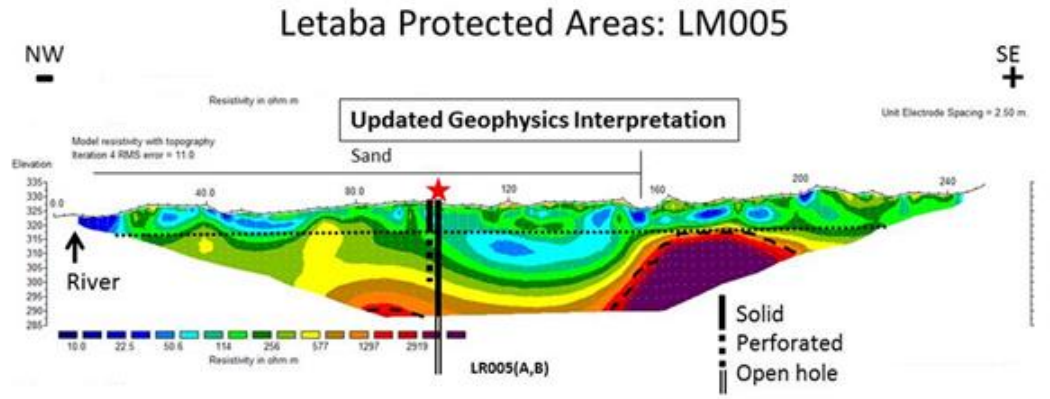

- Runs perpendicular to river channel from river in a SE direction
- Deep sands closer to river; possibly part of alluvial aquifer
- Proposed borehole drilling location at ± 100m

After drilling boreholes LR005 (A,B), the water table was confirmed to be at roughly the same depth as estimated from the initial geophysics surveys. Likewise, weathering was confirmed at a depth of around 38m where the boreholes were installed. Initial interpretation of the resistivity profiles concluded the presence of deep sands close to river which was thought to be part of an alluvial aquifer. This has been confirmed by the borehole logs with the presence of coarse sands till a depth of about 20m.

Figure 26

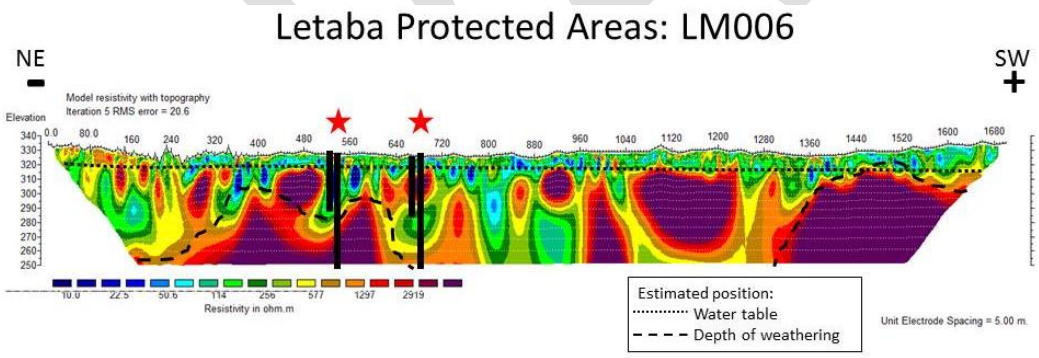

- Runs parallel to river channel in a South-westerly direction
- Shallow water table estimated
- A number of structures identified; i.e. 240m, 550m, 670m, 800m and between 1270-1350m.
- Both geophysics and aerial imagery suggests presence of more dykes on the southern side of Letaba River (i.e. Letaba Ranch).
- Proposed boreholes to be drilled at 550m and 670m.

Figure 27

In addition Magnetic surveys were conducted along the geophysics transects which can be found in (Appendix II). In summary, the results obtained from the surveys correlated well with the ERT data. In most cases the same intrusions identified during the geophysics surveys were observed in the magnetic surveys as well as additional details regarding structure width, depth, direction and dip. In general, several structures were identified that struck parallel to the Letaba River with a general strike direction of NE/SW. Initial field observations, geophysics and Google Earth imagery alluded to a higher density of dyke intrusions downstream in the protected areas compared to the farming areas. This was confirmed by the magnetic surveys which recorded at least two NE/SW striking structures running parallel to river located NW of Letaba River and at least one NE/SW striking structure running parallel to river located SE of Letaba River.

DRAFT

Study Site Set-up: Groundwater Piezometric Monitoring Network

The drilling of the piezometric borehole network by the Department of Water & Sanitation Limpopo Drilling Division at the Letaba Transmission Losses study site commenced in June 2015 with the first borehole complete on 4 June 2015. The drilling campaign focused initially on the western side of the project area within the farms, before moving east to the protected areas. In total 29 boreholes were drilled. The network which comprises paired piezometric boreholes drilled into shallow weathered material and deep fractured hard rock is depicted in Figure 28 and detailed in Table 6. This campaign used the guidance of the geophysics in order to identify suitable drilling sites within and adjacent to the riparian zone. Furthermore, two boreholes were drilled either side of the dolerite dyke, within the main river channel close to the Letaba Ranch gauging weir (B8H008), in order to characterise the longitudinal hydraulic gradient across this geological structure. The majority if these boreholes were fitted with Solinst™ Levelloggers for continuouse monitoring and routinely dip read manually.

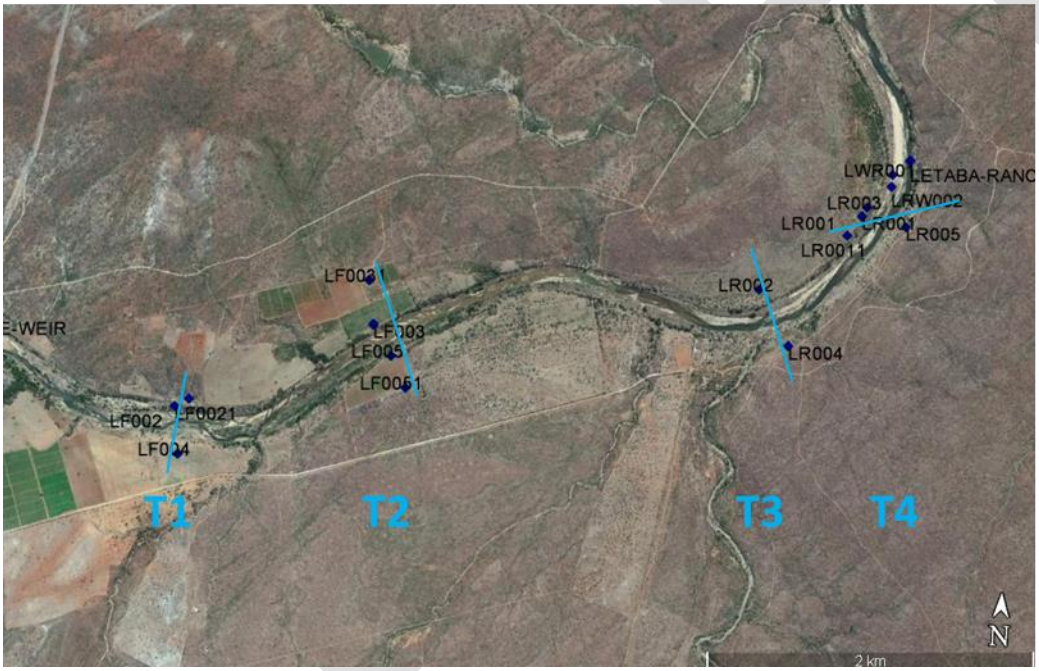

Figure 28 Groundwater peizometric monitoring network at the Letaba river Transmission Losses study site as of February 2016, with transect numbers.

Aquifer tests were performed to determine the hydraulic properties transmissivity (T) and hydraulic conductivity (K) of an aquifer. Single-borehole aquifer tests were conducted for this purpose these included pump and slug tests as described by Kruseman and De Ridder (1994).

The Cooper-Jacob (1946) equation (Equation 2) was applied for the determination of T values using a pump test. Slug tests data was analysed using the Bouwer & Rice (1976, Equation 3) method to determine T or K.

Equation 2 $$Sc(r,t) = S(r,t) - \frac{S^2(r,t)}{2D}$$

where Sc(r,t) is corrected drawdown (m); S(r,t) is observed drawdown (m); and 2D is the saturated thickness (m) prior to pumping.

Equation 3 $$K = \frac{rc^2 \ln(\frac{Re}{rw})}{2L} \frac{1}{t} \; ln \frac{y0}{yt}$$

where K is the hydraulic conductivity; r_c is inside radius of piezometer if water level is above perforated area; R_e is the effective radius over which y is dissipated; r_w is the horizontal distance from well centre to original aquifer (radius of casing plus thickness of gravel pack); the term $\frac{1}{t} \; ln \frac{y0}{yt}$ is obtained from the best fitting straight line in a plot of ln y against t.

Borehole fluid logging (FL) was used to provide undisturbed in-situ borehole parameters of specific conductance (SC), temperature and pH with depth serving as spatial baseline data across the catchment. A YSI (Yellow Spring Incorporated) Sonde multi-parameter in-situ monitoring device was used for this purpose at 2 second intervals in order to record these parameters at ~0.25m depth intervals.

DRAFT

Table 6 Letaba river Transmission Losses study site borehole drilling information

	Site Name	Site Description	Latitude	Longitude	Altitude (m)	Depth (m)	Solid Casing Depth (m)	Casing height (m)	Date completed	Initial Water Level (m)	Strike (m)	Blow Out yield (l/s)	EC (uS/cm)
Farms	LF002A	Mabunda/Baloi	-23.674299259	31.005508751	332.816	60	6	0.51	08/10/2015	11.51	11	1	
	LF002 B	Mabunda/Baloi	-23.674297937	31.005498881	332.966	15	6	0.58	10/09/2015	11.78	11	0.4	864
	LF0021	Mabunda/Baloi in river	-23.674764519	31.004662622	329.940	24	6	0.63	01/11/2015	8.26			
	LF003 A	Maliesa's Farm	-23.669515034	31.016633354	332.840	72	36	0.7	25/05/2015	10.97	15	0.3	1740
	LF003 B	Maliesa's Farm	-23.669519698	31.016568496	328.683	20	14	0.8	01/06/2015	10.76	12	<0.5	1446
	LF003C	Maliesa's Farm	-23.669494574	31.016672592	333.985			Dry					
	LF0031 A	Maliesa's Farm	-23.667002914	31.016215720	333.183	60	24	0.22	25/05/2015	12.95	21	3	1518
	LF0031 B	Maliesa's Farm	-23.667069700	31.016260718	335.904	20	6	0.255	26/06/2015	12.68	19	1	2535
	LF004 A	Abram's Farm	-23.677412130	31.005063317	337.243	72	24	0.43	22/10/2015	13.385	25	0.5	3413
	LF004 B	Abram's Farm	-23.677413088	31.005053265	338.883	15	10	0.46	23/10/2015	13.39	12	0.5	3996.00
	LF005 A	Bongele,s Farm	-23.671245070	31.017841574	328.391	72	30	0.29	04/06/2015	12.33	32	0.5	2800
	LF005 B	Bongele,s Farm	-23.671308501	31.017884338	330.151	42	6	0.305	09/06/2015	12.15	13	<0.5	3354
	LF005 C	Bongele,s Farm	-23.671222963	31.017831282	332.179	18	6	0.345	14/07/2015	10.97	13	0.5	3074
	LF0051 A	Bongele,s Farm	-23.673002919	31.018831950	328.978	54	36	0.54	11/06/2015	14.29	25/40	1.5	1446
	LF0051 B	Bongele,s Farm	-23.673047435	31.018857310	327.363	30	6	0.36	25/06/2015	14.26	16	1	1393
reserves	LR001 A	Mthimkhulu	-23.661769123	31.046823055	328.039	60	30	0.46	03/09/2015	10.35	10	0.5	5600 - 7000
	LR001 B	Mthimkhulu	-23.661764275	31.046805745	330.826	12	6	0.355	08/09/2015	11.93	10		>10 000
	LR0011 A	Mthimkhulu	-23.662934730	31.045922747	324.700	72	24	0.3	14/09/2015	10.3	10	0.1	>10 200
	LR0011 B	Mthimkhulu	-23.662913645	31.045961774	331.089	10	6	0.315	15/09/2015	10.15	10		11 100
	LR002 A	Mthimkhulu	-23.666323042	31.040506466	330.907	42	24	0.43	28/09/2015	10.59	25	0.5	2478.00
	LR002 B	Mthimkhulu	-23.666330049	31.040511463	329.536	10	6	DRY	01/10/2015				
	LR003	Mthimkhulu. Tercias BH	-23.661232653	31.047126602	326.855	10	4	0.355	26/09/2015	Initially dry	0	0	5595
	LR004 A	Letaba Ranch	-23.669463099	31.042411630	327.109	54	30	0.57	02/12/2015				
	LR004 B	Letaba Ranch	-23.669447874	31.042414074	326.388	24	0	0.505	03/12/2015				
	LR005 A	Letaba Ranch	-23.662268314	31.049551881	327.444	60	42	0.265	09/07/2015	8.95	25/38/50	5.7	1740
	LR005 B	Letaba Ranch	-23.662269810	31.049502905	328.971	24	6	0.56	13/07/2015	8.94	19	1.8	1580
	LRW001	Mthimkhulu in river	-23.659273246	31.048663193	316.063	12	0	0.35	26/11/2015	1.23	5	0.2	
	LRW002	Mthimkhulu in river	-23.659964290	31.048604409	317.902	6	0	0.52	30/11/2015	1	4	0.2	
	LR006	Mthimkhulu Near camp				75	0		24/11/2015				

The nomenclature used for these boreholes follows Letaba Farms (LF), Letaba Reserves (LR), Letaba River Water (in channel, LRW) followed by a number (e.g. 001), where two numerals are used implies the borehole was drilled away from the riparian zone (e.g. 0031. Note also that these boreholes were manually dip-read once a week and that 15 have been equipped with Solinst™ Level-loggers for continuous hourly monitoring.

DRAFT

Study Site Set-up: Vegetation Characterisation & Total Evaporation

This study proposed the implementation of the Surface Energy Balance System (SEBS) (Su, 2002) model to quantify riparian ET. Since the implementation of SEBS makes allowance for the relatively timeous and cost effective quantification of ET which can prove to be invaluable for operational water resources management.

Two of the major challenges which are limiting factors to the modelling of ET through the use of this model is:

- i) the trade-off between the spatial and temporal resolution of available imagery (Singh et al., 2014b)
- ii) the accuracy of the model and the requisite data used to capture hydrological processes (Seneviratne et al., 2010). Previous studies have proposed potential solutions to the abovementioned limitations, through the application of downscaling/disaggregation techniques and the integration of scaling factors (Hong et al., 2011; Gokmen et al., 2012; Pardo et al., 2014; Wu et al., 2014; Li et al., 2015).

While these techniques may offer feasible solutions to improve the modelling of ET in SEBS, it is essential that any uncertainty that these techniques introduce to the ET estimate is understood and quantified. For this purpose, a one-sensor Eddy covariance (EC) system was installed within the study area to validate the ET estimates acquired from implementing SEBS, as well as the proposed techniques mentioned above.

DRAFT

Micrometeorological and energy flux measurements

A measuring tower was installed within the study area in order to measure energy fluxes, as well as all meteorological variables required to describe the ecosystem of the measuring site in detail. The system was alternated between two positions within the river channel of the Groot Letaba River during the drier low flow periods of the study (June to October 2015 and May to October 2016) between Mahale (23.669 S; 30.991 E) and Letaba Ranch Weirs (23.658 S; 31.047 E), as illustrated in Figure 29.

During the 2015 field campaign the measuring tower was first installed at a point upstream of Mahale weir within the river channel (Site 1) from 17th June to 13th August 2015. The measuring tower was then moved approximately 1.2 km further upstream (Site 2) and measurements were acquired from 21st August to 22nd October 2015. The same procedure was repeated for the 2016 field. The measuring tower was first installed at Site 1 from 18th May to 25th July 2016. The measuring tower was then moved approximately 2.0 km further upstream from the 2015 Site 2 position and measurements were acquired from 27th July to 17th October 2016.

The channel morphology remained unchanged within this 3.2 km reach, therefore the Eddy covariance ET (EC_{ET}) estimates acquired at these locations were considered to be characteristic of the morphological river reach.

The measuring tower which incorporated a one sensor EC system, was equipped with a CSAT 3-D sonic anemometer (approximately 1.5 m above the *P. mauritianus*) that measures

the sonic air temperature, wind speed and direction. The anemometer was connected to a CR3000 datalogger and measurements were taken with a sampling frequency of 10 Hz. The averages of these high frequency measurements (from instantaneous data) were then used to compute a half-hourly sensible heat flux.

Meteorological instrumentation and energy balance sensors were used to provide measurements of; net radiation, a computed soil heat flux density, soil temperature, relative humidity, horizontal wind speed and wind direction, solar radiation and rainfall. Observations were made every 10 seconds and the appropriate statistical outputs were stored on a data logger (CR23 X, Campbell Scientific Inc., Logan, UT, USA) at 10 minute intervals. These values were then used to compute the daily estimates.

The instrumentation consisted of; two Kipp and Zonen NR Lite-2 net radiometers installed at approximately 1.0 m above the bare soil surface and vegetation, respectively, in order to provide representative and integrated estimates of *Rn* above these surfaces , Licor LI200X Pyranometer, RM Young wind sentry, and a Texas Tipping bucket raingauge (0.1 mm), six HFP01 HukseFlux soil heat flux plates (installed approximately 0.08 m below the soil surface), three pairs of soil temperature averaging probes (installed at 0.02 and 0.06 m below the surface) and two CS616 soil water reflectometers (approximately 0.08 m below the soil surface). The soil heat flux was determined as the weighted average of the computed soil heat flux for bare soil, vegetation and open water heat flux (Gokool et al., 2016).

The average integrated estimates of *Rn* above the bare soil and vegetation surfaces, the computed sensible heat flux and the weighted average of the computed soil heat flux were then used to determine the latent heat flux as a residual of the shortened energy balance equation, which is given as:

Equation 4 $R_n = Go + H + \lambda E$

The rationale for situating the measuring tower at these two locations was to capture the ET associated with distinctive land cover compositions and environmental conditions in a riparian environment. The dominant landcover classes present in this riparian environment within the river channel are *P. mauritianus,* bare soils and open water. Table 7 provides an approximation of the percentage cover for each of the aforementioned land cover classes within each of the sites, with the value for *P. mauritianus* representing the percentage of basal cover.

Table 7 Percentage cover of the dominant landcover classes within each of the sites in which the measuring tower was situated.

Land Cover class	**Site 1**	**Site 2**
Phragmites mauritianus	40 %	60 %
Bare Soils	40 %	20 %
Open Water	20 %	20 %

From Table 7, it can be seen that there is a higher percentage of basal cover for *P. mauritianus* at Site 2. Livestock (cattle) are allowed to graze within the river channel at site 1. While site 2 is situated within a pristine protected area where livestock are prevented from grazing, although buffalo and elephant graze this region their densities are significantly

lower than the cattle. Consequently, both the percentage of basal cover and canopy cover associated with *P. mauritianus* was different at both these locations.

The situation of the measuring tower at the 2016 Site, which is approximately 2.0 km further upstream from the position of the 2015 Site 2, was due to the removal of the electric fence which previously separated Site 2 from Site 1. Consequently, this area no longer represented a pristine protected area as livestock were no longer prevented from grazing in this region. Therefore, the system was moved to the 2016 Site 2, which had a similar characterization to the 2015 Site 2.

Changes in environmental conditions during the period of measurement, such as seasonal and climatic changes from winter to summer which influence environmental stress conditions may have also contributed the higher percentage of basal cover at site 2. While these two locations are situated within the same morphological reach, their respective evaporative surfaces are different in both their basal and canopy cover, as well as soil moisture status. Due to these differences, the situation of the measuring tower at these two locations provides the ideal platform to assess the performance of implementing SEBS for a riparian environment characterized by distinctive land cover compositions and environmental conditions, in a semi-arid region.

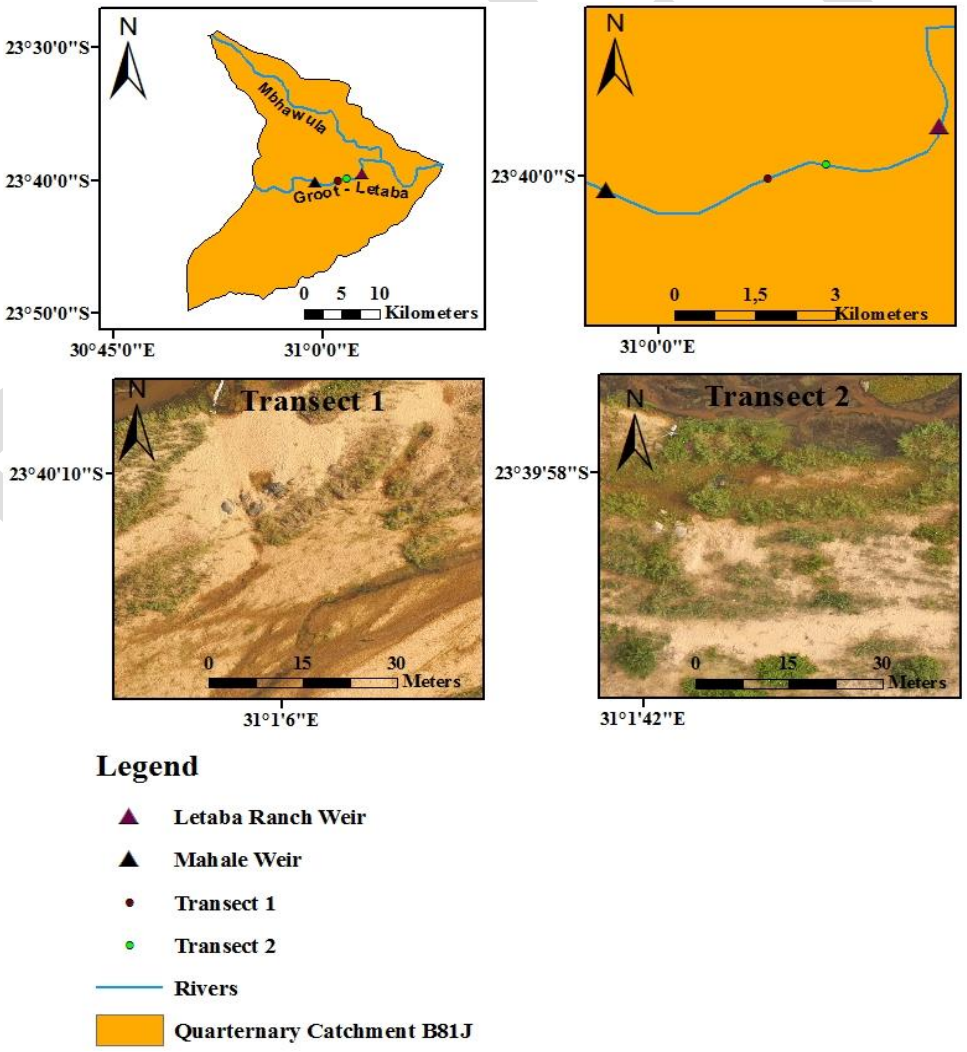

Figure 29 Location of the EC system and the general land cover distribution for transects 1 and 2.

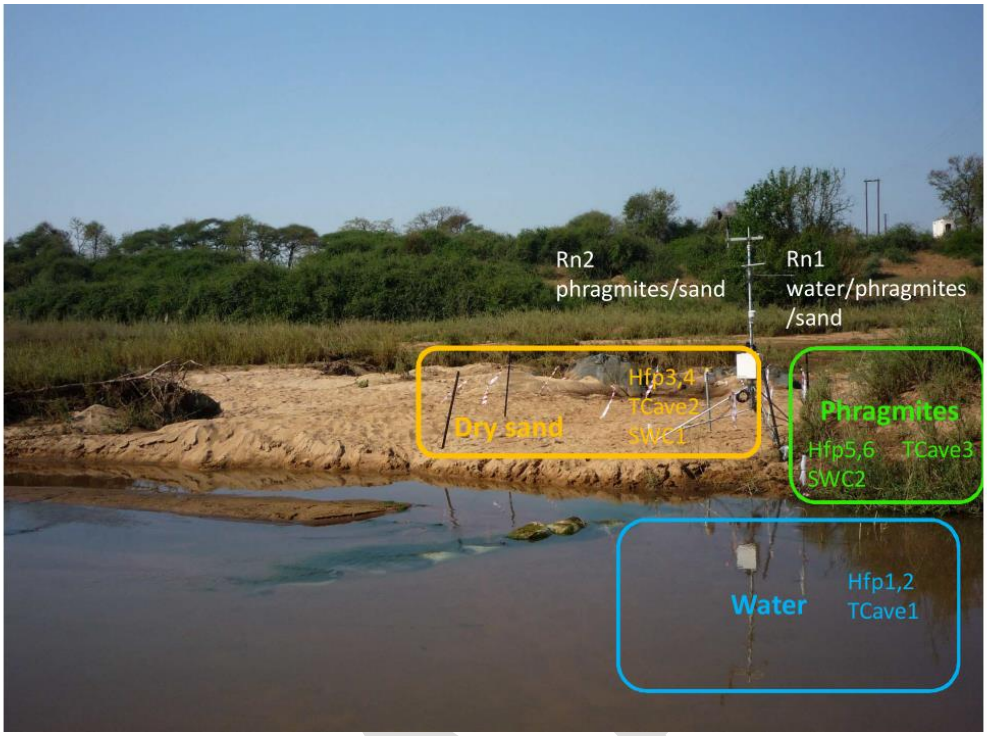

Figure 30 Installation of the Eddy Co-variance system in channel with location of sensors

The weighting of the soil heat flux density was determined as follows for transect 1; (i) 20% water contribution, (ii) 40% for bare soil and (iii) 40% for vegetation. The weighting of soil heat flux density was determined as follows for transect 2; (i) 20% water contribution, (ii) 20% for bare soil and (iii) 60% for vegetation.

The percentage contribution used for the aforementioned weighting was determined from a visual assessment of the study site through a field survey and using imagery captured from a DJI Phantom 3 Advanced Unmanned Aerial Vehicle (UAV). These images were captured at a 5 cm resolution, by an on-board 12 megapixel DJI camera at an altitude of 120 m above ground level. An orthophoto was then created using the Open Drone Map Software (https://github.com/OpenDroneMap/OpenDroneMap), Figure 31.

The EC_{ET} measurements taken during these periods were used to validate ET estimates derived from satellite earth observation data. Thirteen Clear sky Landsat (7 and 8) Level 1 Geotiff products (16 day temporal resolution), as well as 114 MODIS Level 1 B Terra images (Daily temporal resolution) from the 17th June to 22nd October 2015, were selected to estimate ET using the SEBS Model.

DRAFT

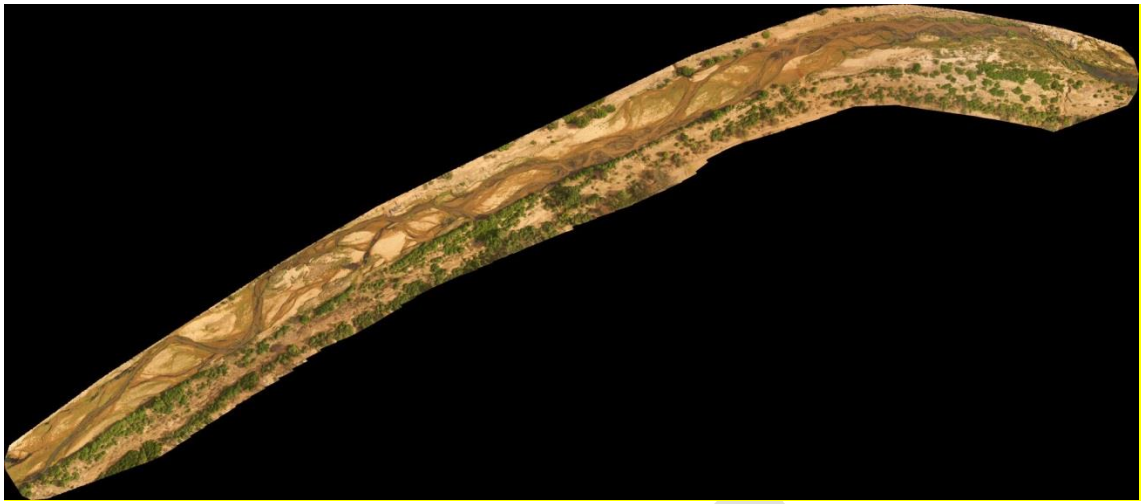

Figure 31 An Unmanned Aerial Vehicle survey conducted of the Letaba river study site around the Eddy Co-Variance installation area during November 2015.

The Simplified Surface Energy Balance System (SEBS)

The SEBS Model was selected for application in this study, as it has been extensively applied for the estimation of regional fluxes and ET and has been shown, to provide accurate estimates of ET and terrestrial heat fluxes (Jarmain et al., 2009a; Yang et al., 2010; Zhuo et al., 2014). The principle is that SEBS estimates atmospheric turbulent fluxes using both satellite earth observation and spatially representative meteorological data (Su, 2002; Liou and Kar, 2014; Pardo et al., 2014).

The model consists of a suite of tools to estimates land surface physical parameters from spectral reflectance and radiance (Su et al., 1999), a comprehensive model for the approximation of the roughness length of heat transfer (Su et al., 2001) and an innovative procedure for the estimation of the evaporative fraction on the basis of the energy balance at limiting cases (Su, 2002). The model applies the shortened surface energy balance equation to partition the available energy into sensible and latent heat flux density. The daily ET is estimated, assuming the evaporative fraction remains constant throughout the day (Su, 2002).
SEBS was therefore applied in this study, using satellite earth observation data acquired from open access imagery derived from Landsat (7&8) and MODIS, to estimate ET for the riparian zone along the Letaba River. The spatial resolution of the SEBS ET estimate is dependent on the spatial resolution of the thermal band (Su, 2002; Alidoost et al., 2015) and therefore the study was limited to the spatial resolution of these open access products.

Moderate spatial resolution (MSR) imagery acquired by Landsat (7&8) provides thermal bands at a spatial resolution of 60m and 100 m, respectively, which are resampled to 30 m and possess a temporal resolution of 16 days (USGS, 2015), however; data can be obtained with an 8 day gap between consecutive data acquisitions, if data from both Landsat 7 and 8 is available and used (USGS, 2015). Coarse spatial resolution (CSR) imagery acquired by MODIS provides thermal bands at a spatial resolution of 1 km at a daily temporal resolution.

In order to obtain a complete daily MSR ET record for the riparian zone along the Letaba River, for the measurement study period at a MSR, a combination of two approaches were followed: (a) an output downscaling with linear regression downscaling approach (Hong et al., 2011) and (b) an infilling approach using Kc_{act} (AllenSantos et al., 2008) and Penman-Monteith reference ET to infill missing data.

Spatial Downscaling of Satellite Derived Total Evaporation

The application of downscaling procedures are used to facilitate the amalgamation of the advantages of High Temporal Resolution (HTR) imagery with MSR imagery. Bierkens *et al*. (2000) and Liang (2004) define downscaling as the increase in spatial resolution resulting from the disaggregation of the original dataset. Downscaling procedures attempt to restore spatial variations at a particular scale, by assuming the values at the larger scale represent the average of the values at the smaller scale (Bierkens et al., 2000).

The procedure results in an increase of the number of pixels within an image, with the output of each pixel representing a smaller area (Hong *et al*., 2011). According to Ha *et al*. (2013) and Spiliotopolous *et al*. (2013) downscaling procedures can be broadly classified into two categories; (i) scale based traditional downscaling and (ii) pan sharpening or data fusion techniques.

In this study, a relatively simplistic downscaling procedure predicated upon a linear regression discussed in Hong *et al*. (2011) was tested to provide total evaporation estimates at a MSR with HTR, as it has been shown by Hong *et al*. (2011) and Spiliotopolous *et al*. (2013) to provide results within acceptable limits.

The regression approach disaggregates CSR imagery by applying a linear regression between two CSR images to a preceding or subsequent MSR image covering the same area of interest (Hong *et al*., 2011). It is assumed that the linear relationship between CSR imagery remains valid between MSR imagery (Hong *et al*., 2011).

In order, to create a daily continuous MSR total evaporation dataset for the period of investigation in this study, a linear regression was initially applied between two consecutive MODIS total evaporation estimates (M_1 and M_2) generated, using the SEBS Model, to obtain regression coefficients. These coefficients were then applied to the Landsat total evaporation image (L_1) generated using the SEBS Model for the same date as the first MODIS total evaporation image (M_1), in order to generate a total evaporation image (L_2) at the Landsat spatial resolution, for the same date as the subsequent MODIS total evaporation image (M_2). This procedure was repeated, however; the linear regression was then performed between the MODIS total evaporation image for day one (M_1) and the MODIS total evaporation image for day three (M_3) to obtain regression coefficients. These coefficients were then applied to the Landsat total evaporation image (L_1) obtained for the same date as the first MODIS total evaporation image (M_1), in order to generate a total evaporation image (L_3) at the Landsat spatial resolution, for the same date as the subsequent MODIS total evaporation image (M_3). This procedure was systematically repeated, until a new Landsat Level 1 Geotiff product was available. Once this product was available, the abovementioned procedure was repeated.

Figure 32 and Figure 33 provide a schematic representation of the abovementioned process to better understand how the daily continuous MSR total evaporation dataset was generated and an example of a downscaled total evaporation map generated for this study, respectively.

Bhattarai *et al*. (2015) notes that the procedures discussed in Hong *et al*. (2011) have not yet been applied to obtain a seasonal continuous MSR total evaporation dataset. Therefore, the results of the investigations conducted in this study can provide valuable insight on the suitability of applying the linear regression approach to generate continuous MSR total evaporation dataset on a daily time step.

DRAFT

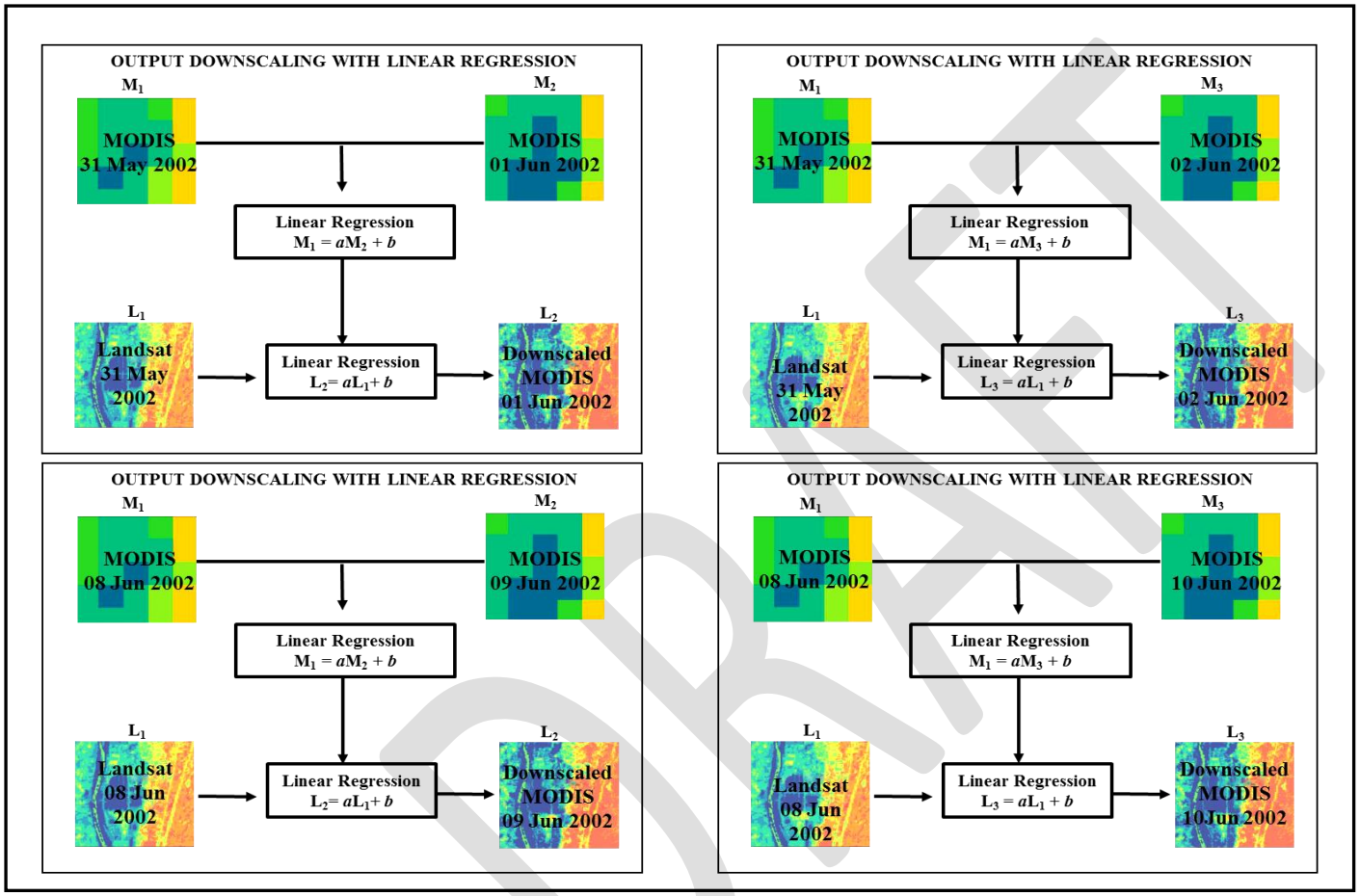

Figure 32 Schematic of the downscaling with linear regression approach methodology to create a daily continuous MSR total evaporation dataset, where *a* and *b* are the linear regression coefficients and L_2 and L_3 are the subsequent spatially downscaled total evaporation maps at the Landsat resolution (adapted from Hong *et al.*, 2011)

DRAFT

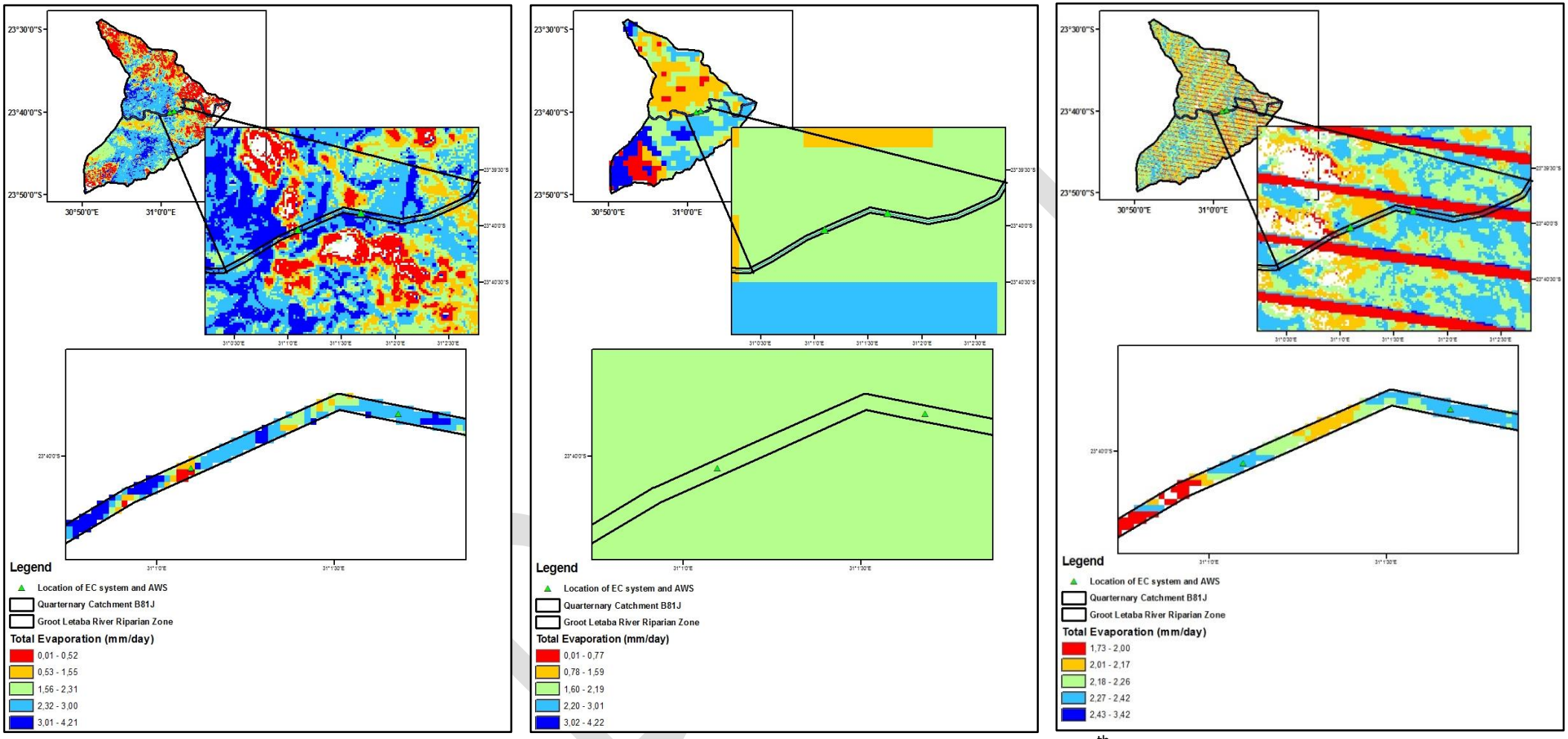

Figure 33 An illustration of SEBS total evaporation derived using MODIS and Landsat data for the 07th July 2015 a) SEBS total evaporation map derived using Landsat, b) SEBS total evaporation map derived using MODIS and c) Downscaled total evaporation derived using linear regression

Determining the Distribution of Vegetation Biomass and Identifying Land Uses

A vegetation/vegetative index can be used to quantify the biomass and/or the plant vigour within a pixel of a satellite image. The index may be computed utilizing various satellite reflectance bands, which are sensitive to biomass and plant vigour. One of the most commonly applied vegetation indices is the normalized difference vegetation index (NDVI) (Ramsey *et al.*, 2004).

The NDVI has been adopted to analyse satellite earth observation data *viz.* to assess if the region/feature which is being observed contains actively growing vegetation or not (Ghorbani *et al.*, 2012). The behaviour of plant species across the electromagnetic spectrum is fairly well understood. As a result, NDVI information can be derived from satellite earth observation data, by analysing the satellite bands which highlight the greatest responses between vegetation and radiation. The satellite bands which are most responsive to the interactions between vegetation and radiation are the red and near infra-red bands of the electromagnetic spectrum (Ghorbani *et al.*, 2012).

The reflectance of radiation in the visible portion of the electromagnetic spectrum (400-700nm) is low, due to the absorption of light energy by chlorophyll in actively growing green vegetation. Whereas, the reflectance of radiation in the NIR portion of the electromagnetic spectrum is high, due to the multiple scattering of light by plant leaf tissues (Zhang *et al.*, 2011).

The algorithm used to derive the NDVI is given in as:

Equation 5 NDVI = (NIR Band – Red Band)/(NIR Band + Red Band)

The difference between the red and NIR bands provides an indication of the amount of vegetation present in the region/feature being observed. The greater the difference between the red and NIR bands, the greater the amount of vegetation present and *vice versa* (Ghorbani *et al.*, 2012).

Numerous vegetation studies have utilized the NDVI for wide ranging applications inter alia; estimating crop yields, pasture performance, vegetation health and biomass (Petorelli *et al.*, 2005; Muskova et al., 2008). Furthermore, the NDVI technique generally allows for the identification of various features within a satellite image such as, areas which possess dense vegetation or no vegetation coverage (bare soil and rock), water bodies and ice.

The identification of a feature is based upon the NDVI value it possesses, within the range of -1 to 1 (Holme *et al.*, 1987). Table 8 provides a general representation of the features which may be identified in an image based upon their respective NDVI values.

Table 8 Identification of features within a satellite image based upon their respective NDVI values

DRAFT

NDVI Value	Feature
NDVI < 0	Water Body
0.1 < NDVI < 0.2	Bare Soil
0.2 < NDVI < 0.3	Sparse vegetation cover
0.3 < NDVI < 0.5	Moderate vegetation Cover
NDVI > 0.6	Dense vegetation cover

The NDVI was calculated for the region between Mahale and Letaba Ranch Weirs utilizing the red and NIR bands of a Landsat 8 image obtained for the 21st June 2015. These values were then used in conjunction with knowledge of the study area, to identify the density distribution of vegetation and to broadly classify land use. These are represented in Figure 34. It should be noted that this classification is a very simplistic representation of the land uses which are present in the study area.

Although Landsat 8 data is provided at a spatial resolution of 30m, classifying land use and land cover at this resolution may be too broad, as it can be difficult to determine the distribution of individual species without detailed *a priori* knowledge on the location and distribution of individual plant species, observed in the satellite image. Furthermore the presence of cloud within Figure 34 may have contributed to an incorrect identification of features.

The land uses represented in Figure 34 were broadly classified into five categories, these include; (i) Water Bodies, (ii) Bare soil, (iii) Sparse vegetation cover consisting of shrubs, thicket, reeds and grassland, (iv) Moderate vegetation cover consisting of shrubs, thicket, reeds, croplands, grassland and trees and (v) Dense vegetation cover consisting of shrubs, thicket, reeds, croplands, grassland and trees.

Each component of the total evaporation process i.e. evaporation of intercepted water, soil water evaporation and transpiration is either directly or indirectly affected by the type, distribution and density of vegetation in a specified area. Therefore, the classification of vegetation species and distribution facilitates an improved understanding of total evaporation estimates and may hold added significance when other factors which influence total evaporation are relatively stable.

DRAFT

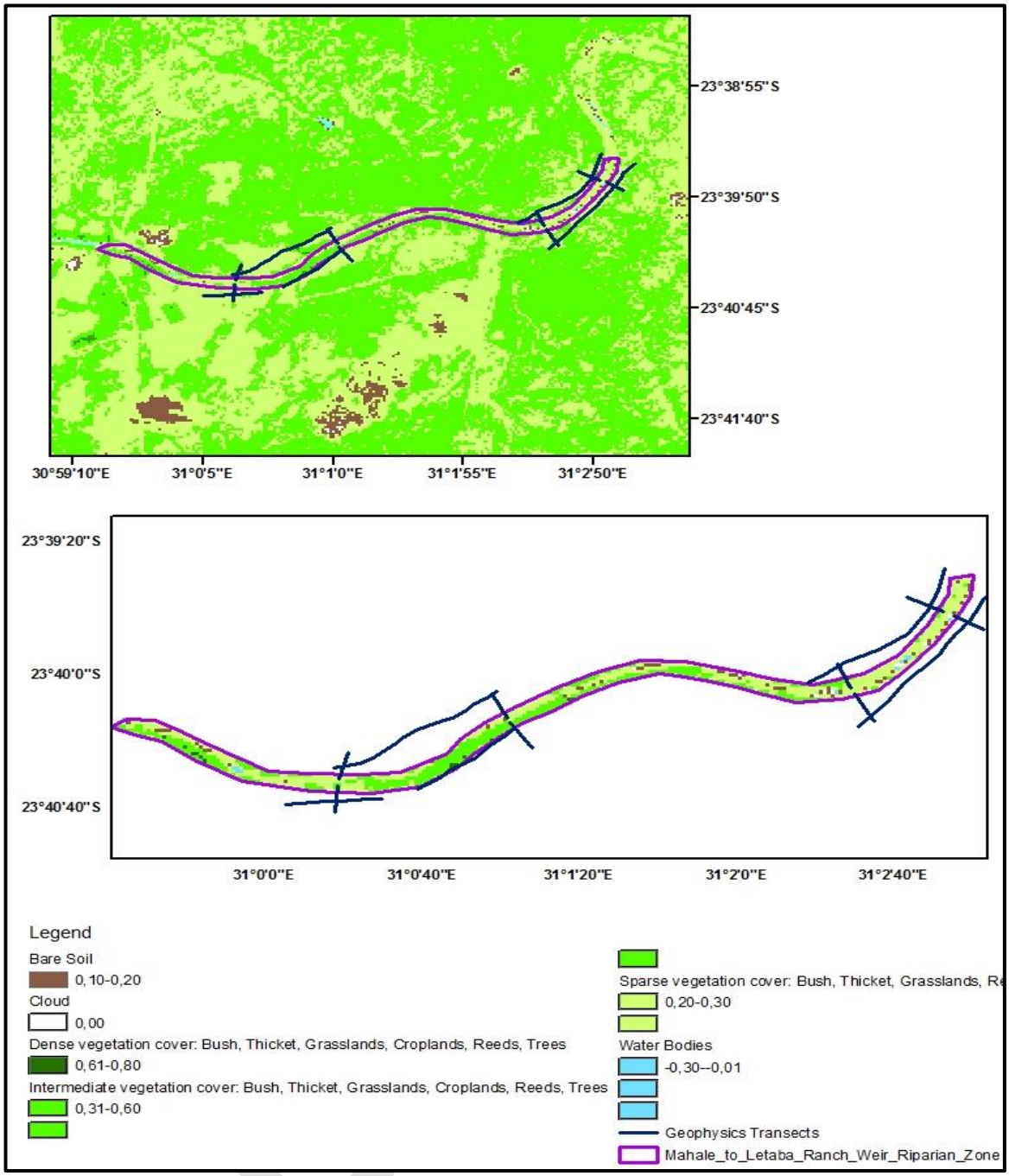

Figure 34 An illustration of the distribution of vegetation biomass and classification of land uses based upon NDVI, for the region between Mahale and Letaba Ranch Weirs on the 21st of June 2015.

5. RESULTS

Hydrogeological characterisation

Two rounds of fluid logging were conducted across the groundwater piezometric network, the first being November 2015 (prior to the onset of extreme drought wet season conditions) followed in August 2016 (thus following the rain season, of which there was only one significant event in March 2016). These will be described on a transect by transect basis (Figure 28)

Transect 1

LF002A (Farms, Regional, Deep)

There is almost no difference in the temperature profile of LF002A (Figure 35), although there is a steady decrease in both profiles with depth. This takes place because of the inflow of fresh water from the top of the borehole to the bottom. The inflow occurs because boreholes will form a preferential pathway for water percolating to and through the groundwater system, thus the warm water from the surface will cool down as it moves to the bottom of the borehole. There is also an increase in the electrical conductivity (EC) between the periods, which is expected due to extremely low rainfall input and evaporation. The result therefore is very little water reaching the saturated zone of the aquifer. The EC also increases to the bottom of the borehole as the heavier salt water and debris from pumping settles at the bottom. The fractures are again indicated at a similar depth of 30m, 35m and 45m with the sharp and sudden increase in conductivity.

LF002B (Farms, Regional, Shallow)

LF002B (Figure 35) shows a slight increase with temperature in the dryer and warmer conditions of August 2016. Again it indicates an inflow of fresh water at the top, similar to the deeper borehole LF002A. A small fracture is again indicated through the sudden increase in EC and the small temperature change at 12.8m where warmer water flows into the borehole.

LF002A/B is located on the fringes of the riparian zone located on the northern bank of the farms. It is situated on a transect that shows a loss to the northern bank form LF004A/B to LF0021 to LF002A/B (transect 1), thus we expected to observe flow in these boreholes.

DRAFT

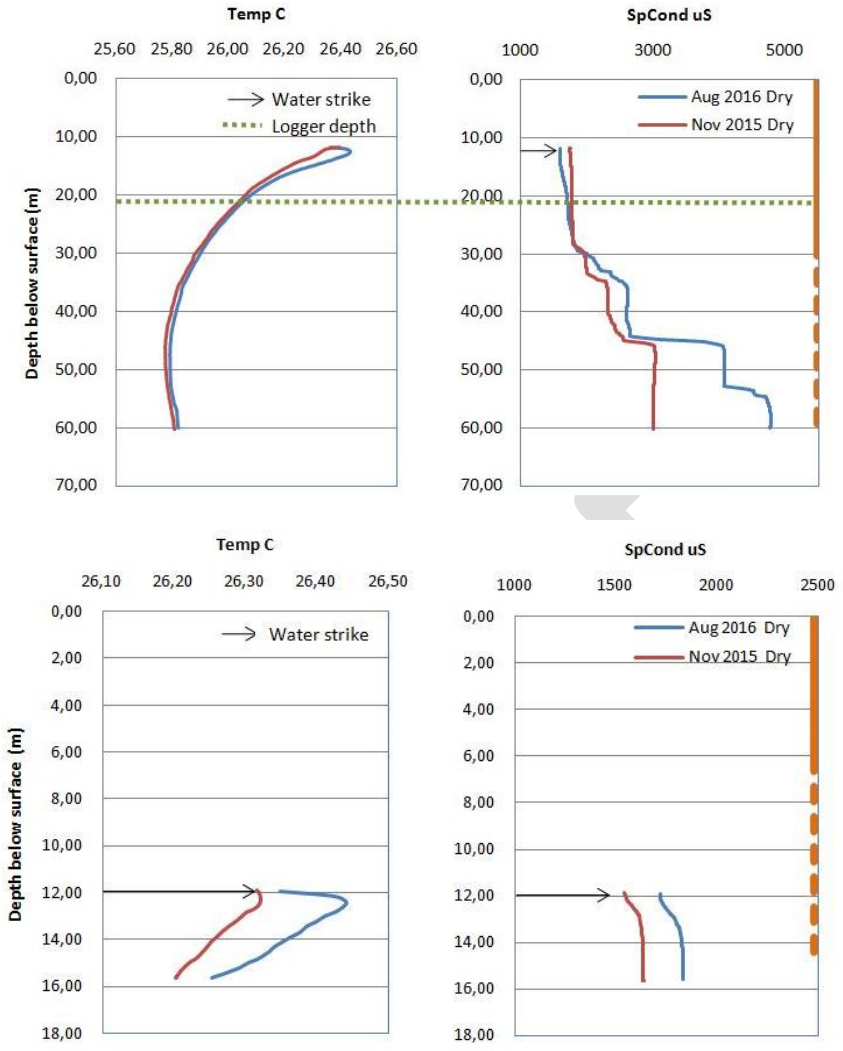

Figure 35 Fluid log of LF002 (A – above, B – below)

LF0021 (Farms, Riparian, Shallow)

The temperature within borehole LF0021 (Figure 36) is warmer in August 2016 and also decreases in with depth to around 18m where it stabilises, indicating increased flow within the aquifer. This indicates that more water is moving through the unconsolidated zone and into the borehole, especially after the March 2016 flood and rainfall events. In addition the EC displays an expected increase in August from the dryer and warmer conditions. Numerous small fractures are indicated by the EC at 13m, 15m, 18m and 21m.

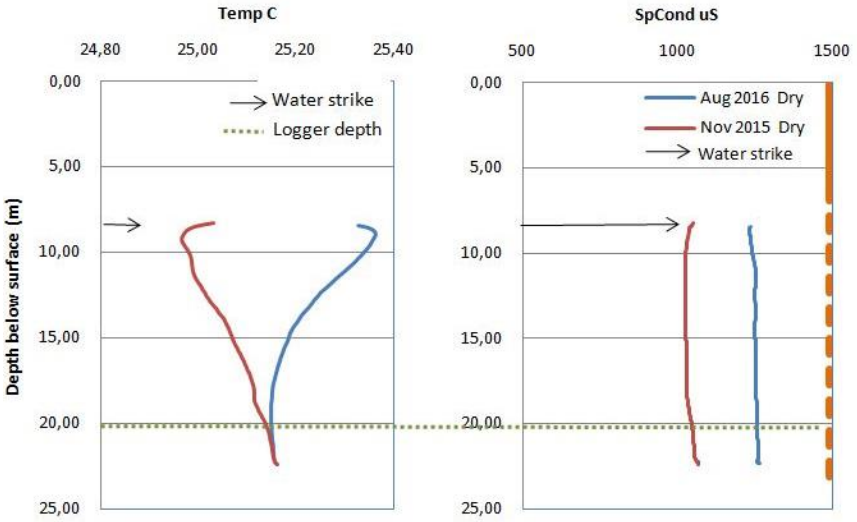

Figure 36: Fluid log of LF0021

LF004A (Farms, Regional, Deep)

The temperature displays a steady increase with depth in both periods (Figure 37). Whilst the temperature profile is similar between the two periods, the conductivity displays a sharp increase after 49m. This indicates that there is not a lot of inflow occurring from water flowing through the unconsolidated zone, but rather from numerous small fractures within the deep consolidated aquifer. The temperature will thus only increase to the bottom where these fractures bring in warmer and high EC water. The end of the solid casing is displayed at 24m with a sharp increase in conductivity. The numerous small fractures are indicated by the increase in temperature and EC at 35m, 53m, 64m and 67m.

LF004B (Farms, Regional, Shallow)

LF004B (Figure 37) shows an increase in temperature with depth in the dryer August 2016 period, this is in contrast to the other shallow boreholes LF003B and LF002B. This indicates that fresh warm water is not flowing in from the unconsolidated zone, but rather from a fracture, similar as the deep borehole LF004A. The EC is surprisingly high within this borehole and lower in the dry season than in wet season, again in contrast to the previous described boreholes. The fracture also surprisingly indicates low EC water flowing in at 15m. The reason for this is that the fracture could possibly be influenced by water from agriculture activities or a high EC profile from contamination during drilling.

DRAFT

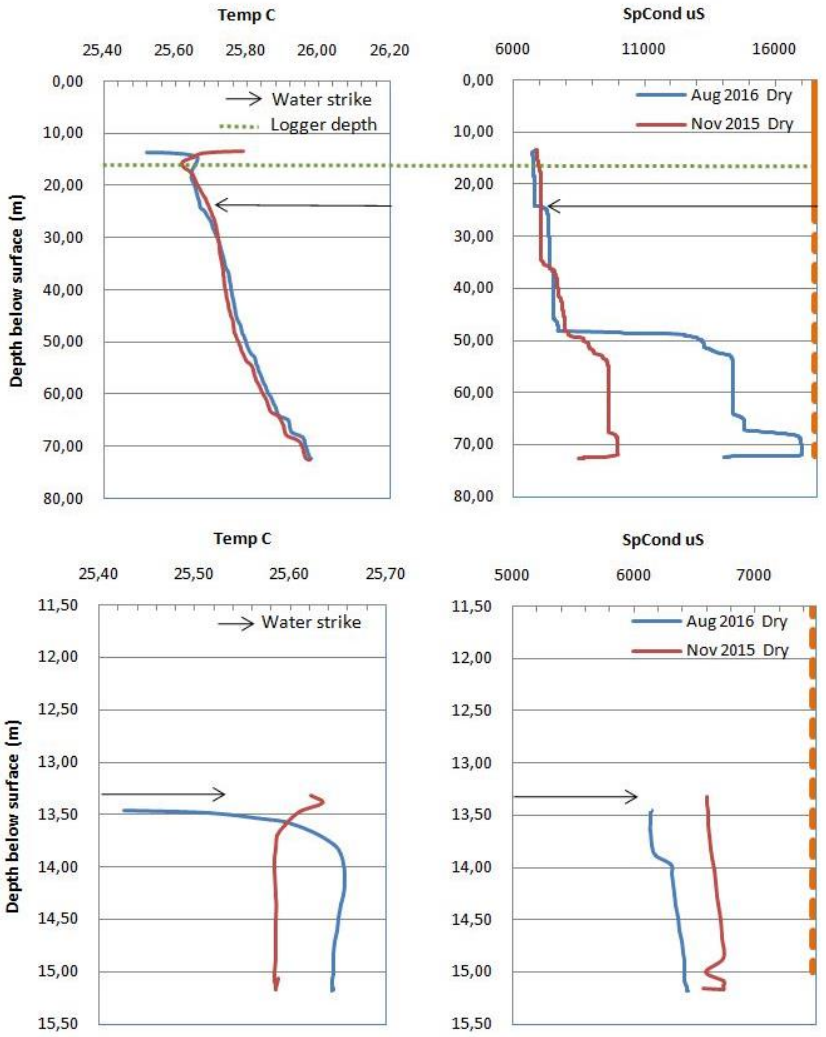

Figure 37: Fluid log of LF004 (A – above, B – below)

Transect 2

LF0031A (Farms, Regional, Deep)

LF0031 displays a similar profile in conductivity and temperature between the two periods (Figure 38). The temperature shows an increase with depth indicating that no flow is coming from the unconsolidated zone but rather from a fracture, similar to LF004A. At 20m there is a sudden increase in temperature and EC, although this is still located within the solid casing indicating a leak in backfill. At 25m there is another increase in temperature and EC that is located exactly where the solid casing stops. This indicates the end of the solid casing as the restricted flow within the solid casing will lower the temperature. The EC will also be lower as the only movement will be heavier salt water moving down the borehole. At 26m a fracture is

indicated by the increase in EC and temperature as warm high EC water is entering through the fracture.

LF0031B (Farms, Regional, Shallow)

The temperature and EC is as expected higher in August 2016 due to the consistently dry and warm conditions during the monitoring period (Figure 38). The temperature indicates some inflow from the unconsolidated zone within August. The fracture is indicated by the temperature curve change, this is also observed in the November 2015 temperature log with a sudden increase in temperature at 17m. The EC supports the temperature with a sudden increase in EC at 17m. Low inflow from the unconsolidated zone was expected at these boreholes. The deeper borehole indicates no inflow from the unconsolidated zone suggesting that the two aquifers are separated from each other.

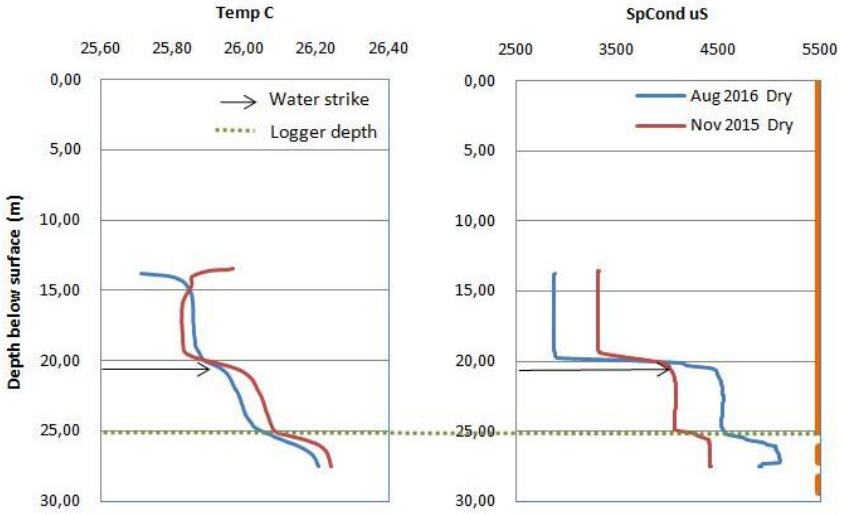

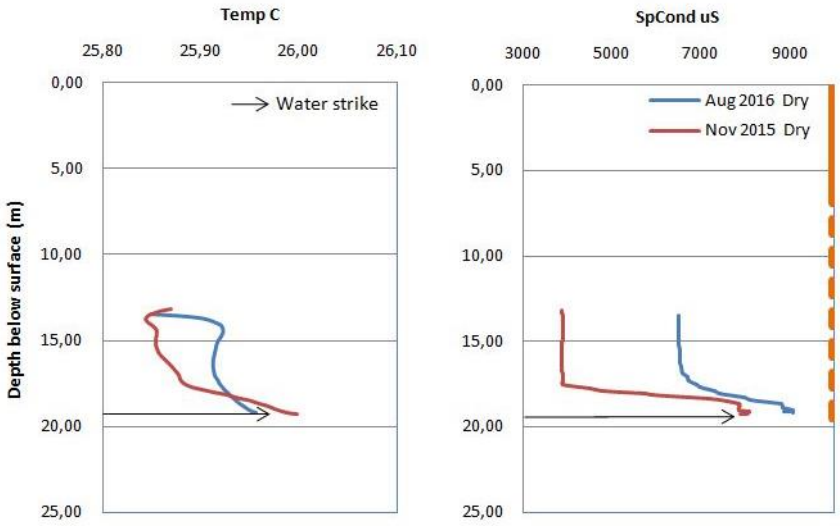

Figure 38 Fluid log of LF0031

LF003A (Farms, Riparian, Deep)

The temperature in LF003A shows no difference between the periods (Figure 39). The inflow of fresher water is again depicted by the decrease in temperature with depth similar to the previous boreholes. The conductivity is again slightly higher in the dryer winter period. Two big fractures are displayed at 23m and 33m, although this is within the solid casing and might indicate a leakage within the solid casing. Numerous very small fractures are indicated further down the borehole by subtle increases in EC.

LF003B (Farms, Riparian, Shallow)

There is a surface inflow suggested in Figure 39, depicted by the decrease in temperature with depth. The conductivity displays a similar profile between the two seasons with a sharp increase after 15m where the solid casing ends. A fracture is indicated by the temperature with a small increase at 19m, as well as the EC with a sudden increase. Most of the fractures are indicated by an increase in temperature and EC. LF003A/B is a riparian borehole located on the northern bank of the farm area.

DRAFT

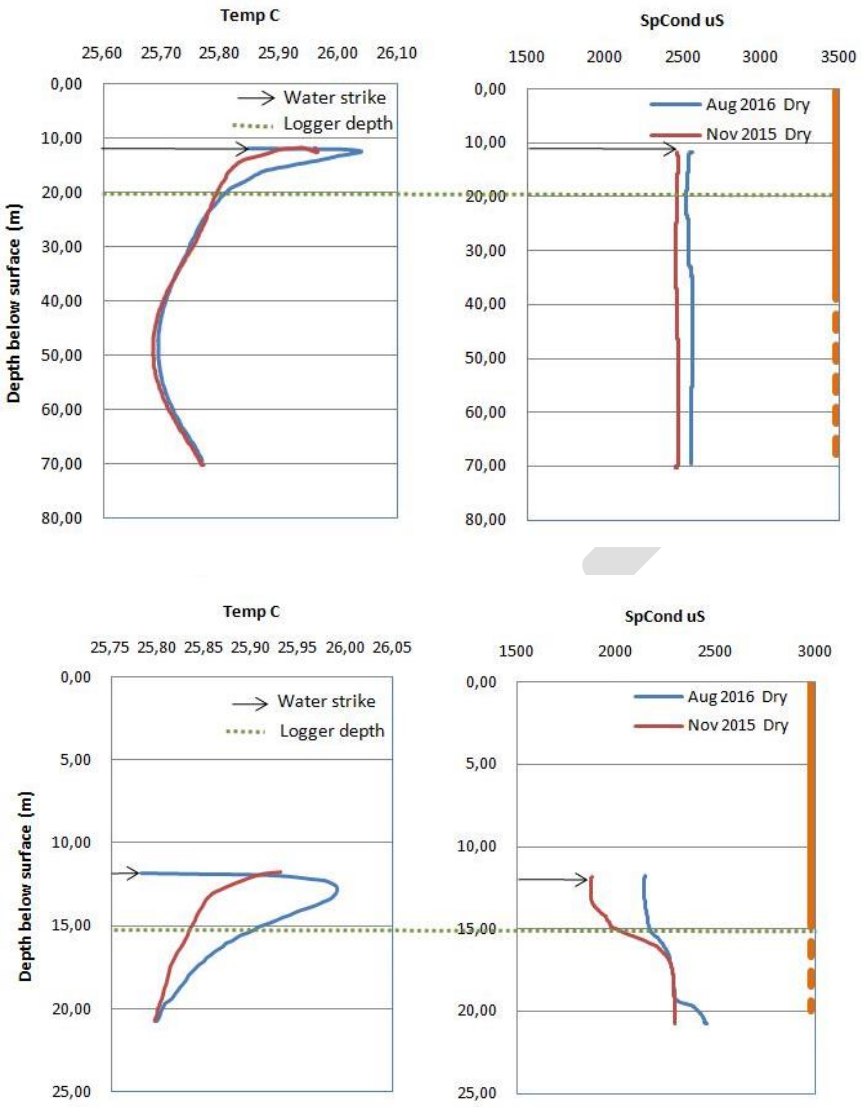

Figure 39 Fluid log of LF003

LF005A (Farms, Riparian, Deep)

LR005A (Figure 40) displays a similar temperature profile between the two monitoring periods with the suggested inflow of fresh water near the top of the borehole, a decrease in temperature toward the bottom of the borehole until a large fracture is obtained. The EC displays the end of the solid casing at 30m with fractures indicated at 44m and 62m by the sudden increase in EC within both periods. The lower EC during August 2016 is due to the location of the borehole as LF005A is located on the southern bank of transect 2 on the farms area within the riparian zone just south of the river. The lower EC is likely due to the contribution from the river (especially after the March 2016 flood) lowering the EC through mixing.

LF005B (Farms, Riparian, Shallow)

The temperature of borehole LF005B (Figure 40) displays the decrease with depth from the inflow of fresh water from the unconsolidated zone, as seen in LF005A. The temperature is similar between the two periods and the conductivity also displays a relatively similar profile. Fractures are indicated at 30m and 40m with an increase in EC and temperature. The fracture at 40m within LF005B is indicated by a sudden increase in conductivity similar to a fracture within LF005A (located only 5m away) at 44m. This indicates that both boreholes intersect the same fracture at around 40m. When the temperatures of the two boreholes are compared it is clear that the temperature drops to around 40m where there is a large fracture. This provides more evidence that water is moving through the unconsolidated zone down the borehole (preferential flow path) and into the fractures.

LF005C (Farms, Riparian, Shallow)

Only one fluid log LF005C (Figure 40) was conducted as very little water was found within the borehole in the initial November 2015 survey. The borehole displays an increase in temperature to the bottom, indicating flow within the fracture zone and no flow from the unconsolidated zone. The EC displays a definite fracture at 13.5m with a slight decrease. This is suggested by the high EC profile around 6000uS, similar to LF004B. Both boreholes are very shallow with less than 1.7m of water, thus evaporation within the borehole will have a bigger effect on its EC. The result is a borehole with very high EC ultimately displaying a decrease in EC at the fracture.

DRAFT

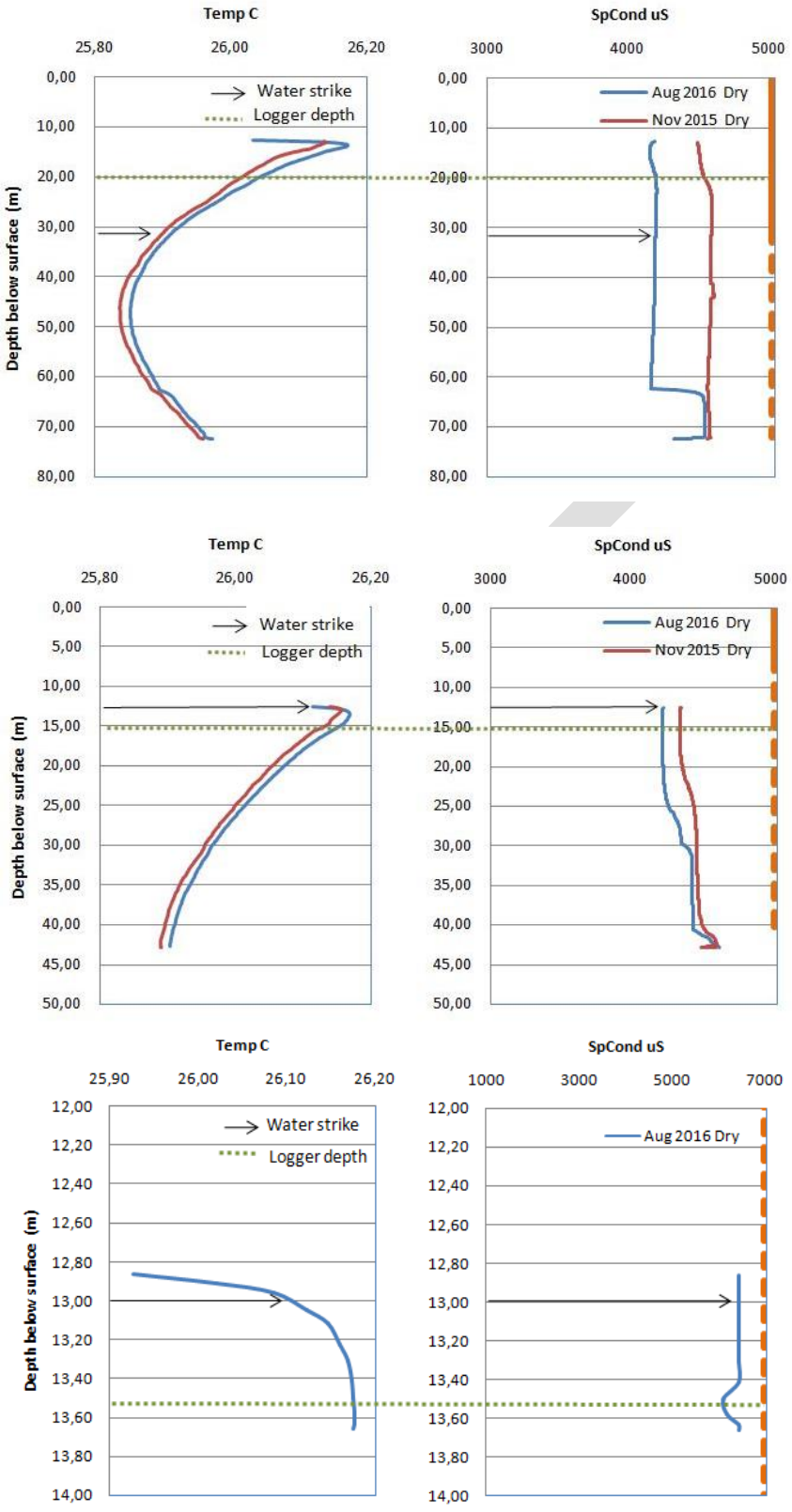

Figure 40 Fluid log of LF005 (A – above, B – mid, C – below)

LF0051A (Farms, Regional, Deep)

The temperature profile is similar between the two periods (Figure 41), with the normal decrease with depth that indicates fresh water flowing in from the top of the borehole to the bottom. This is expected as LF0051A/B is located on the southern bank of transect 2 with the lowest hydraulic heads of all the boreholes on this transect. Thus we would expect the inflow of groundwater from the unconsolidated zone ultimately as the river is losing water to the southern bank. This should also lower the EC as fresher groundwater from the river is entering the borehole. The lowering of the EC can clearly be seen in both periods supporting the theory**.** A sudden increase in EC at 25m indicates that the solid casing has a perforation at this point. The end of the solid casing can be seen at 36m with a small increase in both EC temperature.

LF0051B (Farms, Regional, Shallow)

The temperature displays a decrease with depth (Figure 41) caused by the inflow of groundwater from the unconsolidated zone at the top to the bottom of the borehole or a prominent fracture. The temperature and conductivity as expected is higher in August 2016. A fracture is indicated at 26m (where the temperature starts to stabilize) by a sudden increase in EC and temperature, supported by the EC increase in the August 2016 fluid log.

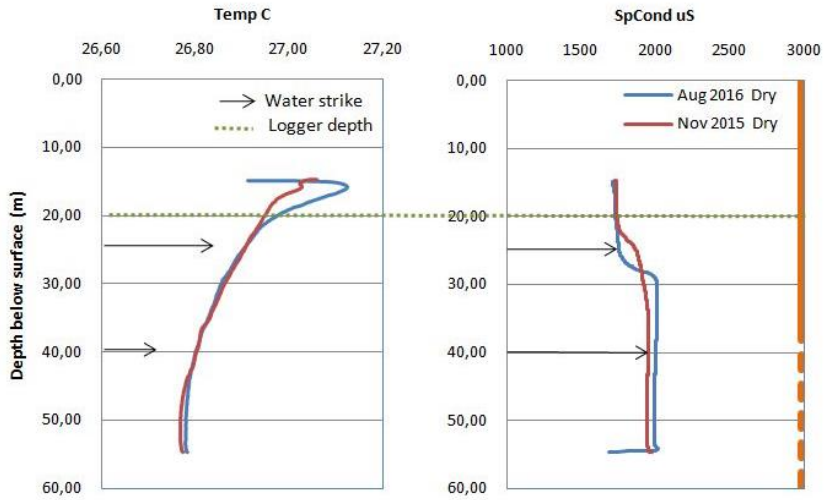

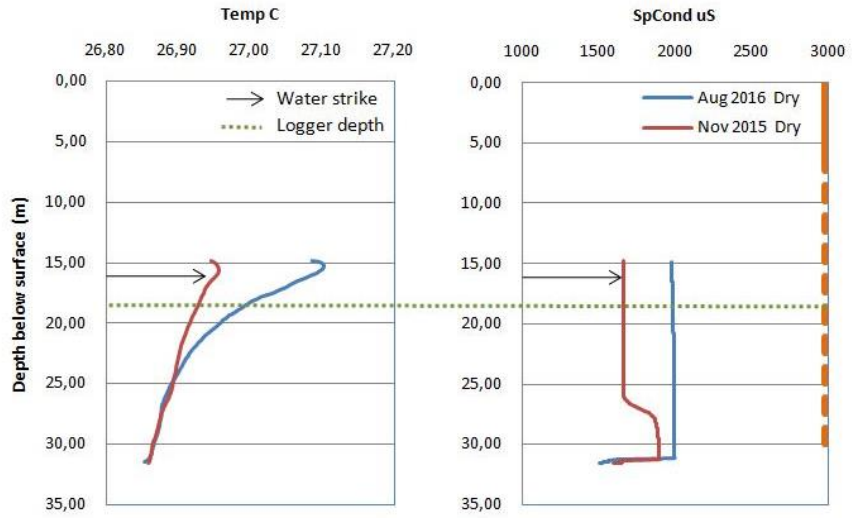

Figure 41 Fluid log of LF0051 (A- above, B – below)

DRAFT

Transect 3

LR002A (Protected area, Regional, Deep)

In LR002A a temperature decrease is shown with depth (Figure 42) indicating the inflow of fresher water from the unconsolidated zone at the top of the borehole to the bottom or prominent fracture. In August 2016 there was a slightly higher temperature as expected. Two fractures where observed with the increase of temperature and EC. The first larger fracture sits at 28m where both EC's indicated the fracture which is confirmed by the temperature decrease which stabilizes beyond this depth. The second fracture is much smaller observed at 32m. The November 2015 EC only displays a straight line from 28m, when the borehole is pumped for hydraulic testing for extensive periods.

LR002A is a deep borehole situated on the northern bank of the protected area. It has the highest hydraulic head of transect 3 and shows that water is moving from the Northern bank to the Southern bank. The borehole did however display the recharge from the unconsolidated zone, indicating that water is moving through this zone towards the river.

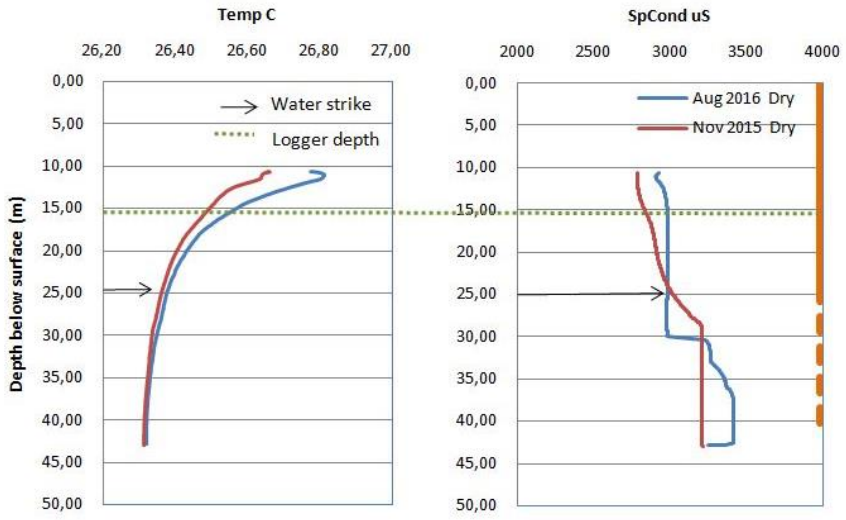

Figure 42 Fluid log of LR002A

LR004A (Protected area, Regional, Deep)

Only one fluid log is available for LR004A (Figure 43), as the borehole was not yet drilled by November 2015. The EC displays no prominent fractures, although the casing is indicated at the correct 30m with a sudden increase in EC. The temperature did however display a very small fracture at 35m.

LR004B (Protected area, Regional, Shallow)

Figure 43 shows a decrease in temperature with depth displays the similar inflow as most of the boreholes with fresh water flowing in at the top to the bottom of the borehole or prominent fracture. The EC displays only one fracture at 24m with a small increase in EC. The temperature indicates the exact same profile up to 24m, where the fracture is located in LF004A. This is also where the water strike occurred, thus it can be assumed that both boreholes intersected the same fracture and that both boreholes are receiving water from the unconsolidated zone.

LR004A/B is located on the southern bank of the protected area. They have the lowest hydraulic heads of transect 3 and had a quick reaction to the March 2016 flood event, indicating that water is being lost from the river in the direction of the boreholes. The EC supports this theory displaying a relatively low EC over all when compared to the opposite river bank at LR002A. The inflow of water through the unconsolidated zone in both boreholes also suggests that the water from the river is being lost to the aquifer around these boreholes moves through the unconsolidated zone.

DRAFT

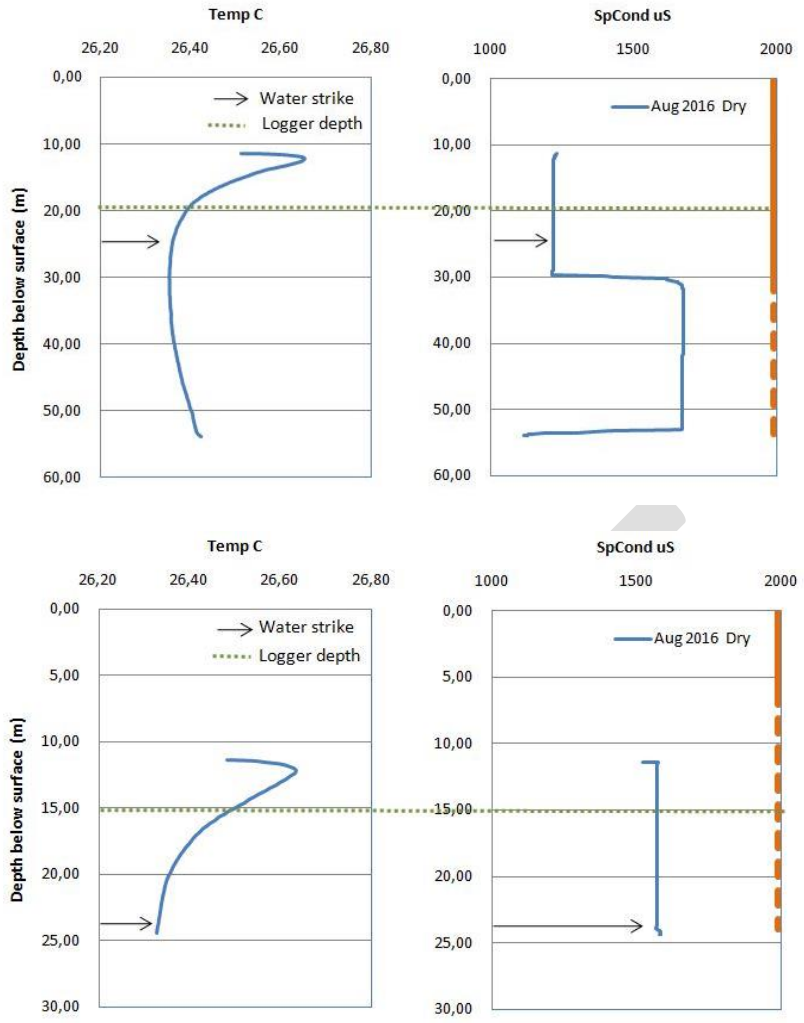

Figure 43 Fluid log of LR004 (A – above, B – below)

<u>Transect 4</u>

LR0011A (Protected area, Riparian, Deep)

The temperature displays a decrease with depth from the inflow of fresh water at the top with almost no difference in temperature between the periods (Figure 44). The first 20m shows a slightly higher temperature indicating warm fresh water entering the borehole from the unconsolidated zone. The EC was much lower in August. The cause is most likely the influence of the March flood, as LR0011A is situated within the riparian zone on the northern bank displaying a quick response to the flood event. Fractures were indicated at 32m and 47m with an increase in temperature and EC, as the warm high EC water enters the borehole.

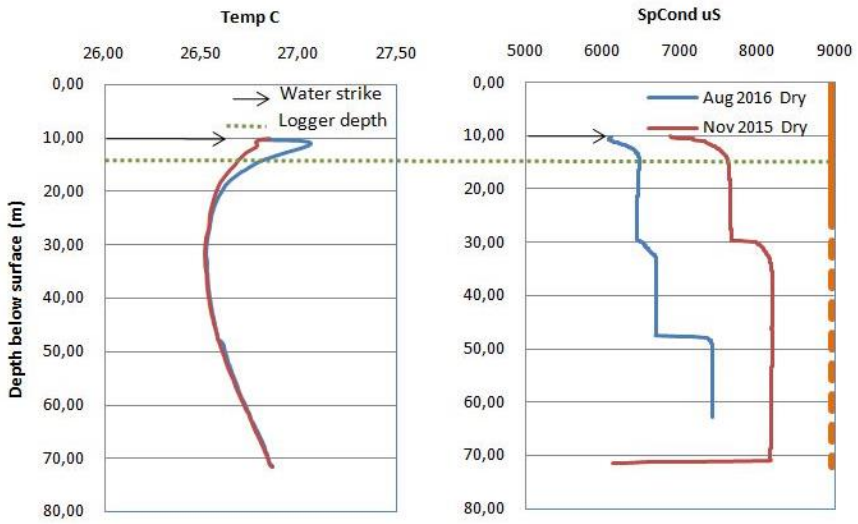

Figure 44 Fluid log of LR0011A

LR001A (Protected area, Riparian, Deep)

No significant difference is found between the temperatures of the two periods (Figure 45). The decrease in temperature with depth found in most of the boreholes is also displayed in LR001A indicating inflow from the unconsolidated zone. The temperature shows a definitive increase at 21m with slight change in the EC, this indicates a perforation leak within the solid casing. Numerous small fractures where indicated at 35m, 42m, 47m and 50m through the increases in temperature and EC. A lower EC is observed in August 2016. LR001A is located within the riparian zone on transect 4 that displayed a very quick response to the March 2016 flood event. The result was mixing of fresher low EC river water, ultimately lowering the EC profile of the aquifer around LR001A.

DRAFT

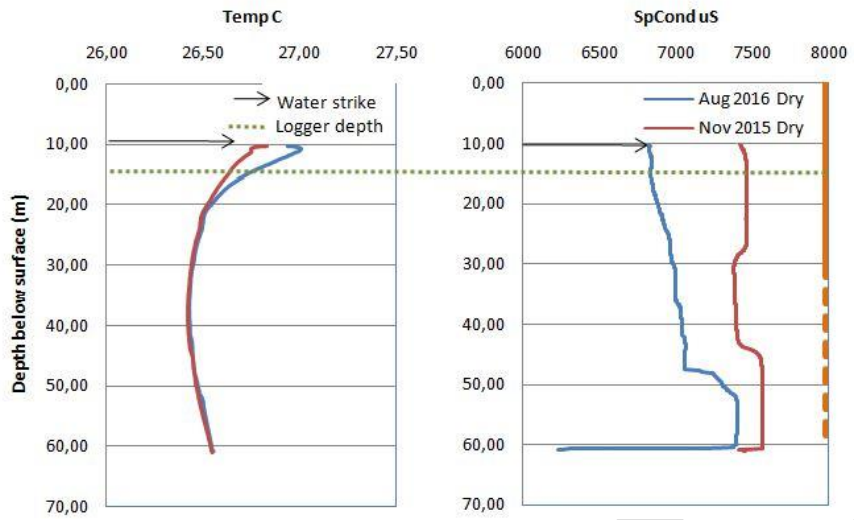

Figure 45 Fluid log of LR001A

LR005A (Protected area, Regional, Deep)

The temperature displays an anticipated decrease with depth due to inflow of fresh water at the top (Figure 47). The temperature and EC remains similar over the two periods with both indicating a perforation leak in the solid casing at 20m. Only one prominent fracture was indicated at 57m.

LR005B (Protected area, Riparian, Shallow)

The temperature in August 2016 displays an increase in temperature as anticipated for this dry and warm period (Figure 47). The temperature decreases with depth indicating water flowing in from the unconsolidated zone. The temperature starts to stabilize around 16m and stabilizing at around 20m. Two fractures are confirmed with a slight increase of EC at 16m and 20m.

The decreases in temperature from both boreholes show that groundwater is moving through the unconsolidated zone, as well as the deep fractured aquifer towards the river. The slightly lower EC within the top 25m shows that the water that moves into the aquifer is lower in EC and fresher than the high EC groundwater within the fractures. This lowering of EC could also be the effect of the March 2016 flood contributions to the aquifer, as both boreholes had a delayed reaction to the flood.

DRAFT

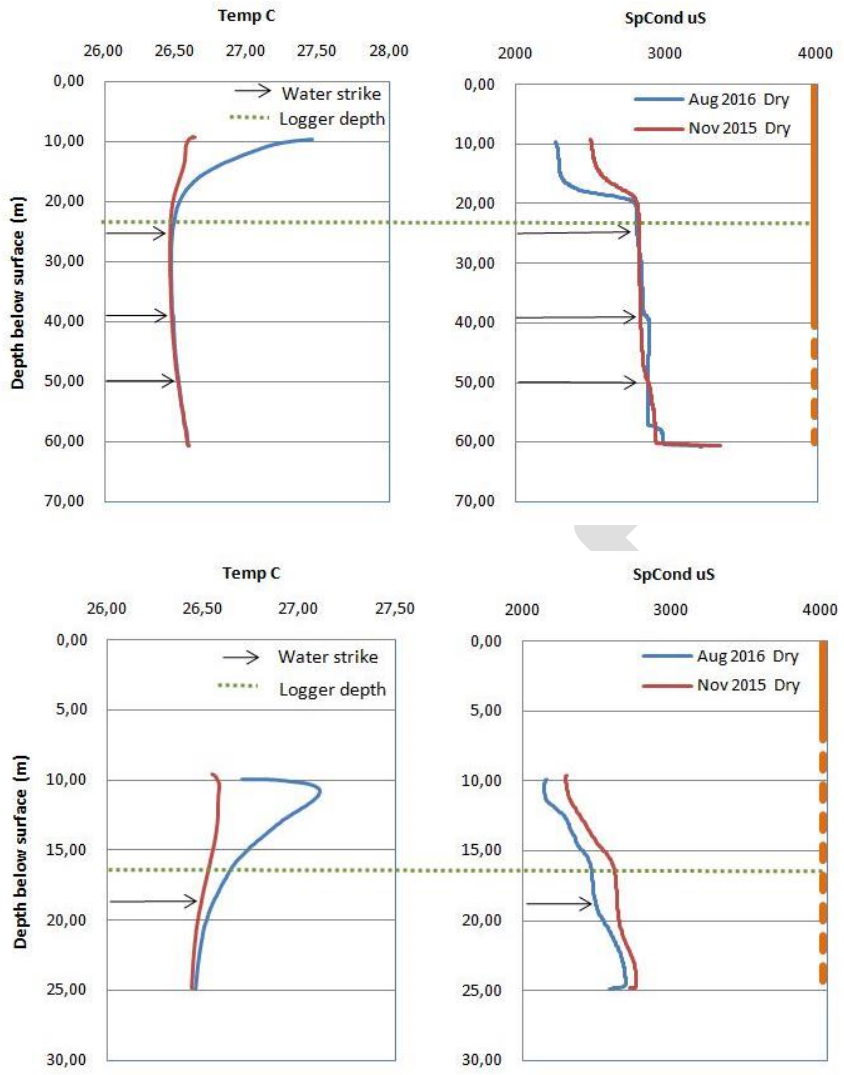

Figure 47 Fluid log of LR005 (A – above, B – below)

LR003 (Protected area, Riparian, Shallow)

Only one fluid log is available for LR003 (Figure 48), because it never had a water strike and was initially dry. The inflow of groundwater from the unconsolidated zone can be seen in the temperature log with a decrease to the bottom of the borehole. The EC is extremely high increasing to 16000 uS and displaying no fractures. This indicates no flow through the borehole, only flow into the borehole from the top.

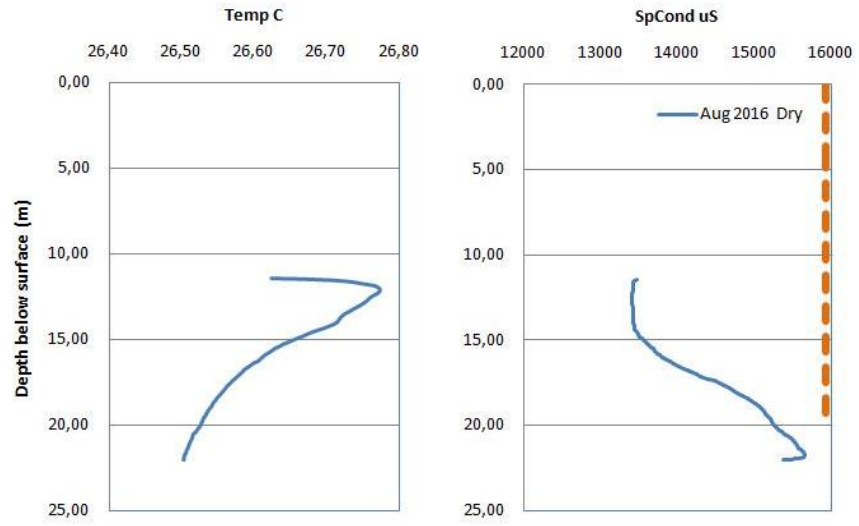

Figure 48 Fluid log of LR003

Dolerite Dyke transect

LRW001 (Protected area, River bed, Shallow)

Only one fluid log is available for LRW001 (Figure 49), because the borehole was only drilled in November 2015. The temperature increases with depth indicating that no water is moving through the unconsolidated zone, but only through the fracture. The fracture is indicated with an increase in both conductivity and temperature at 8m, as the warmer and high EC water flows into the borehole from the fracture.

LRW002 (Protected area, River bed, Shallow)

Only one fluid log is available for LRW002 (Figure 49), because the borehole was only drilled in November 2015. The temperature increases with depth indicating that no water is moving through the unconsolidated zone, but only through the fracture. The fracture is indicated by an increase in temperature at 4.6m.

LRW001 is located within the Letaba River streambed on the Northern side (downstream) of a large dolerite dyke (with a small dam wall on top of it) running through the river, ultimately connecting with the Letaba weir. This causes a damming of the river water as well as groundwater. LRW002 was purposefully drilled on the southern side (upstream) of this dolerite dyke to determine the processes and water movement across it.

LRW001 indicates a very high EC of 7000 uS, this is anticipated as no contact occurs with water from the river. The temperature slowly increases from 24°C to 26°C in a relatively straight line

DRAFT

indicating no inflow of groundwater from the unconsolidated zone, but only from the fracture. This is supported by the high increase in EC at the fracture.

LRW002 displays a much lower temperature and EC. The reason for this is that the dolerite dyke blocks the water forcing the river water to move alongside the dyke in the direction of the Letaba Rancg gauging weir (North-East). This forces the colder river water to flow into LRW002. The result will be a lower temperature and EC with the borehole. This can clearly be seen with the cold river water flowing in at 21°C slowly increasing to the warmer groundwater flowing in the fracture. The EC is also evidence of this with LRW002 displaying a low EC of 1500 uS. The only anomaly is the EC should be higher at the fracture of 4.6m, although this can be explained by the low EC river water flowing and diluting the high EC from the fracture.

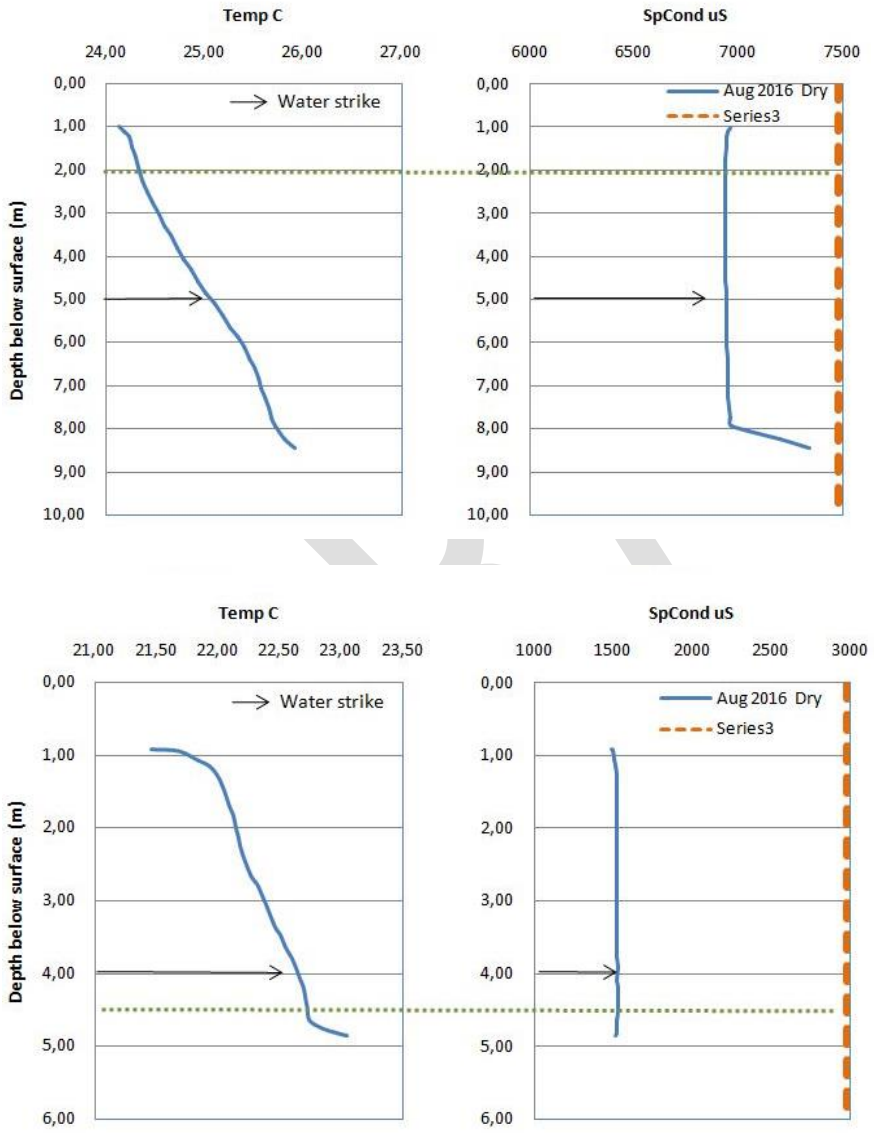

Figure 49 Fluid log of LRW001 (above) and LRW002 (below)

Summary

The high difference in EC between the two periods show that the aquifer is strongly dependent on rainfall events especially regional boreholes located outside the riparian zone of the river (e.g. LF0031, LF0051). The large effect the March 2016 flood event had on riparian zone, as well as sections where the river was losing water to the ground water system was evident and displayed the interconnectedness of the river and the groundwater system.

DRAFT

Groundwater Hydraulic Gradient Distribution

As an example the following section plots the water levels as observed on 15 February 2016 in cross-section relating to the position of the river. Included are the final values for K and T in order to build an interpretation of *potential* losses or gains to the Letaba river from the surrounding aquifer(s). These data are then use to derive a cumulative time-series of potential gains/losses between the river and the surrounding aquifer along the entire river reach.

Figure 50 shows the most upstream transect, with the hydraulic gradient showing a potential groundwater flow from south (LF004) to north (LF002). The T values show that there is a high flow within the shallow fractured aquifer from the north, although this is lower in the deep hard rock aquifer. After intersecting with the river the T values suggest a slight loss to the river but, a greater loss to the riparian zone as indicated by LF0021. The shallow borehole LF002B indicates a large river loss to the northern bank, although the deeper hard rock aquifer seems to be detached from it.

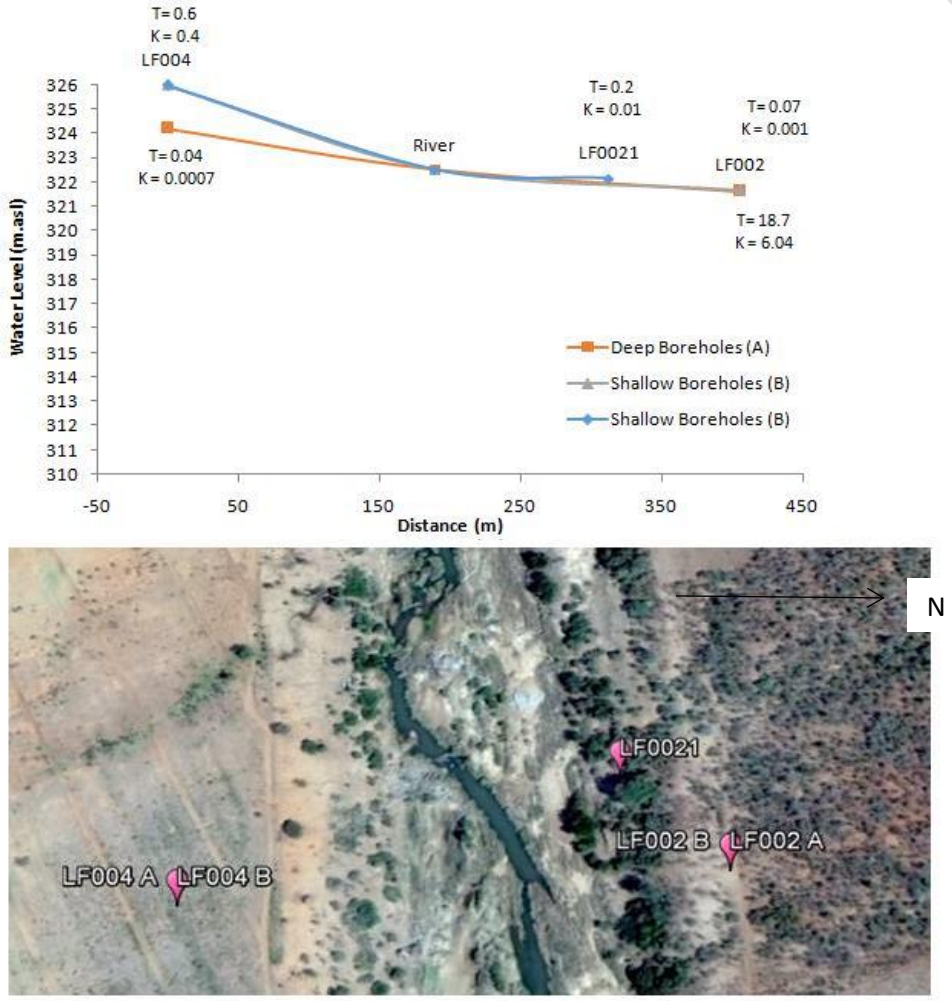

Figure 50 Cross-section plot of transect LF004 to LF002, February 2016

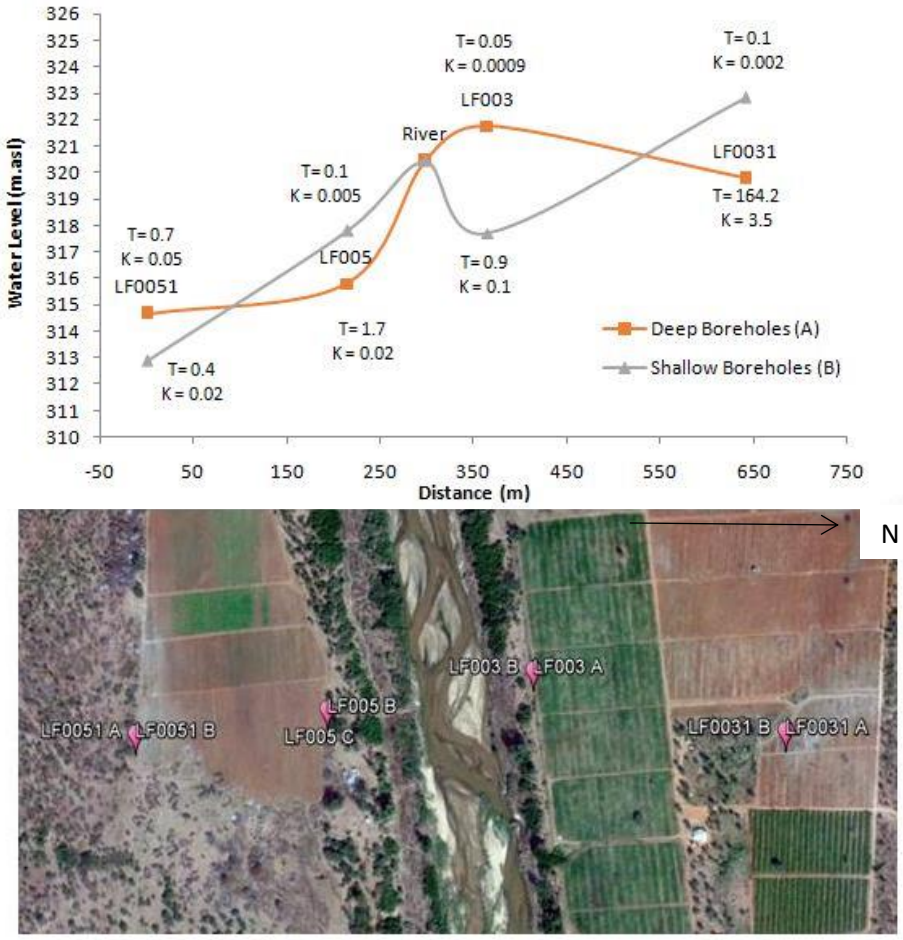

Figure 51 Cross-section plot of transect LF0051 to LF0031, February 2016

Figure 51 indicate the hydraulic gradient from north (LF0031) to south (LF0051). There is a definitive loss to the aquifer from the river on the southern bank in the weathered and hard rock indicated by a high hydraulic gradient. LF003 seems to be an anomaly and might be disconnected from the regional aquifer as it indicates very low flow from the T values. A possible explanation could be the water still flows from north to south but, because there is an increase in the hard rock elevation as seen in the geophysics, it "pinches" the water at LF003 increasing the hydraulic gradient a smaller scale, inducing flow and "pushing" the groundwater over the elevated hardrock.

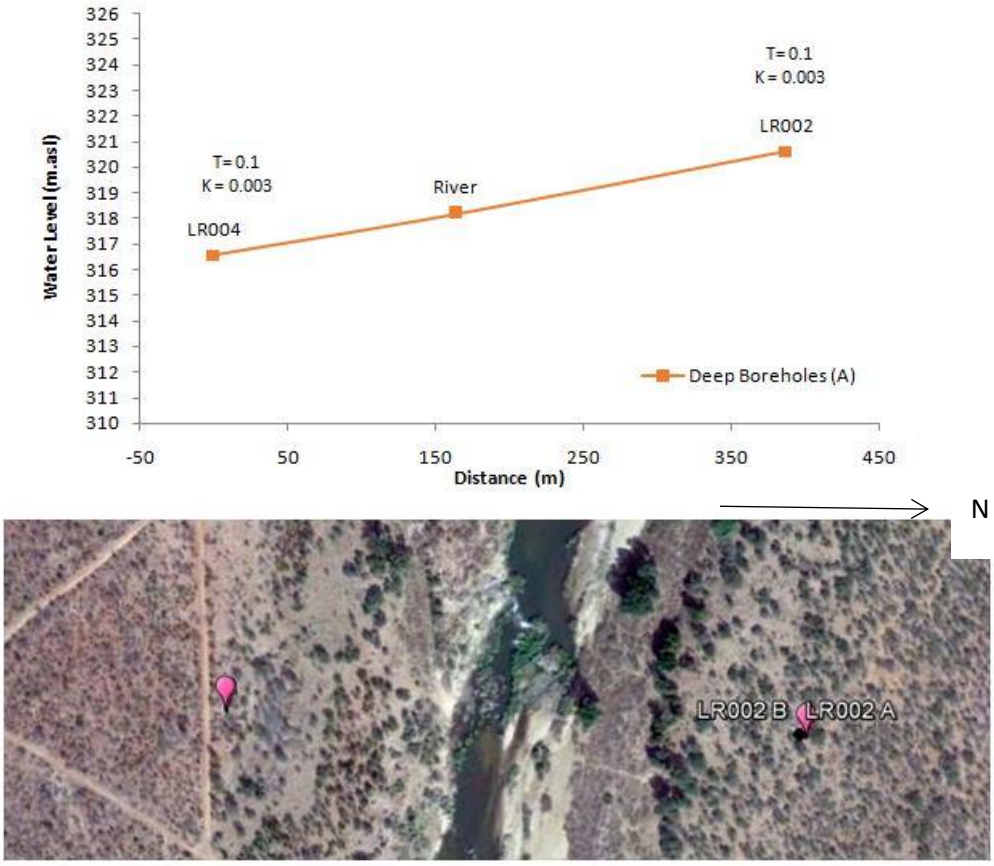

Figure 52 Cross-section plot of transect LR004 to LR002, February 2016

In Figure 52 it appears that the groundwater flows from the northern bank to the southern bank. The deep hard rock aquifer does not appear to be largely affected by the intersection of the river. From the T values the deep hardrock aquifer seems to be detached from the river with almost no change in values.

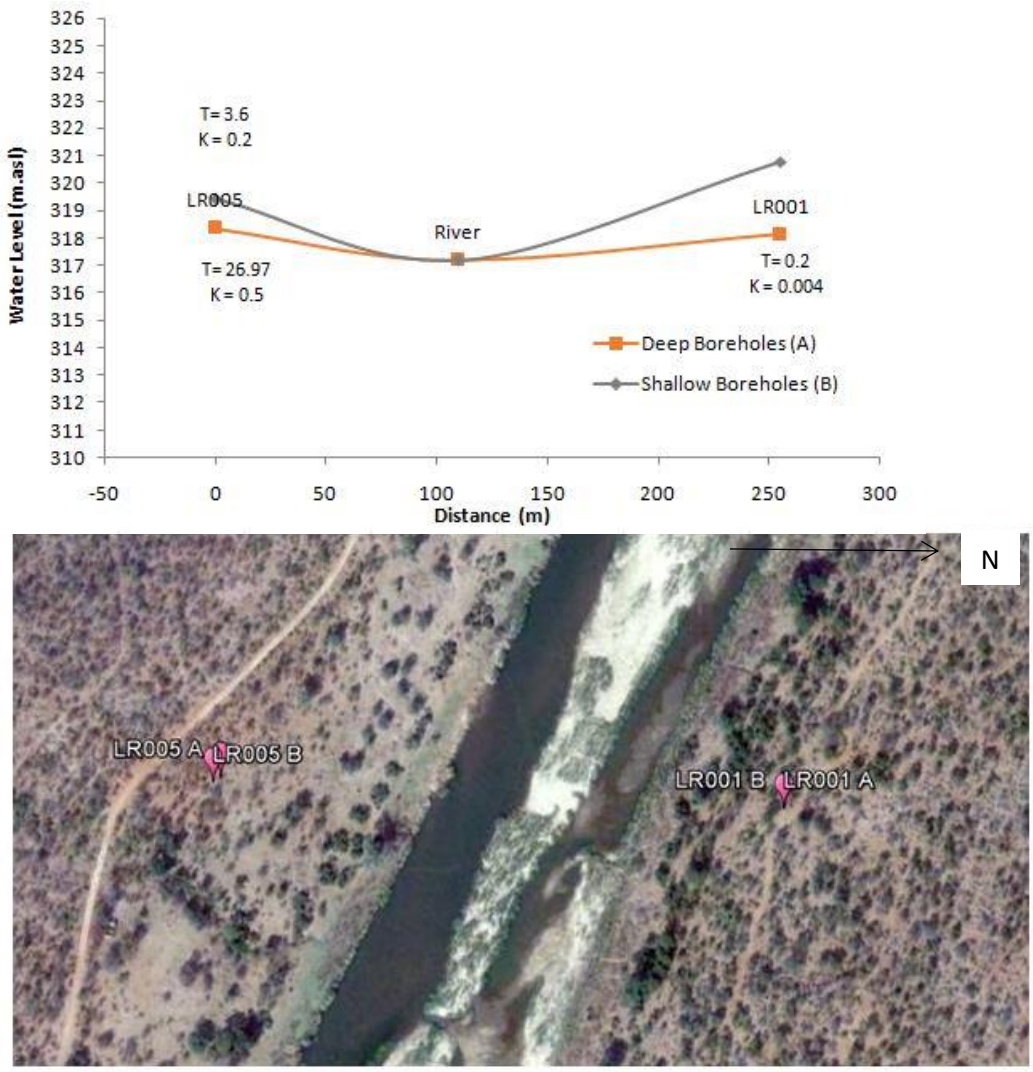

Figure 53 Cross-section plot of transect LR005 to LR001, February 2016

In Figure 53 both the deep hard rock aquifer and the shallow weathered aquifer display a large potential contribution from the groundwater to the river from both the south and north. It is likely that the shallow weathered aquifer contributes much more than the hard rock aquifer although this will be impacted by riparian vegetation transpiration. Through flow of the aquifer is not displayed in this transect as in all the other transects although, there is a dolerite dyke running through the river between these two borehole positions in a North – East and South West direction. It is therefore possible that this dyke might be separating two contributing aquifers.

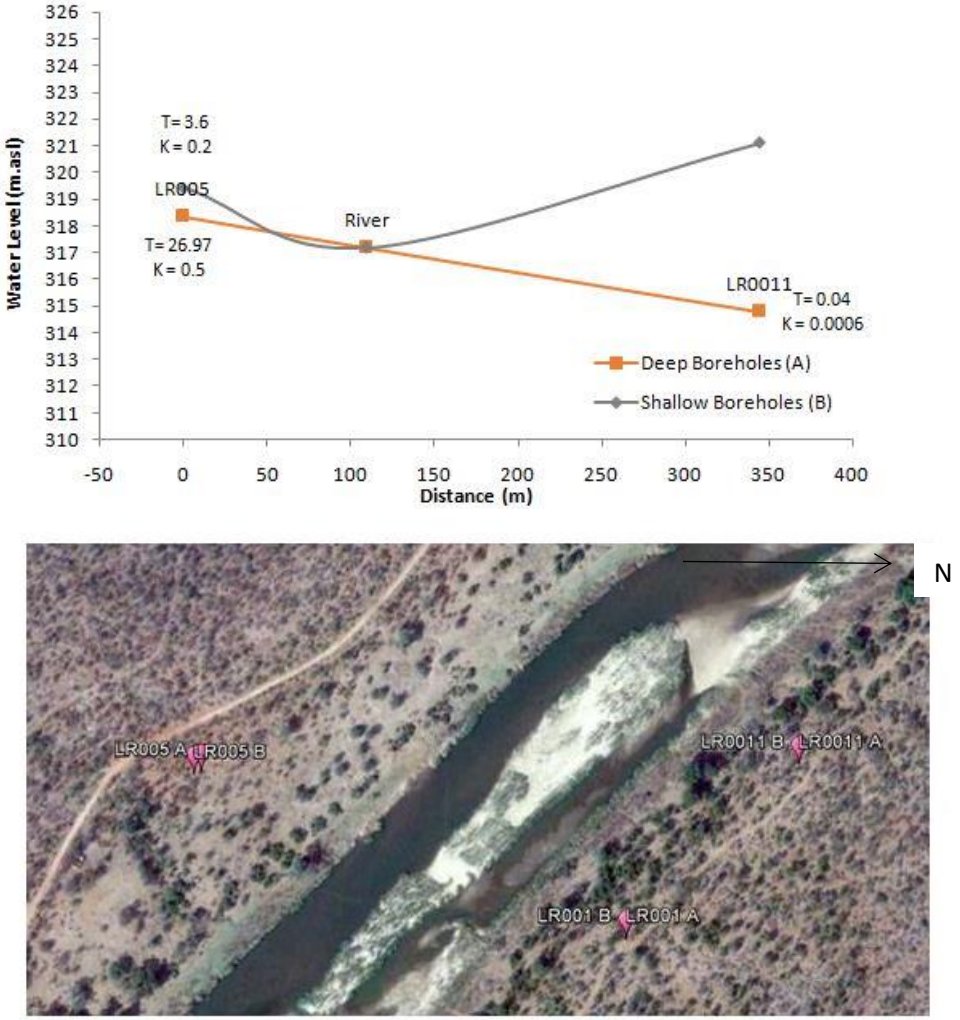

Figure 54 Cross-section plot of transect LR005 to LR0011, February 2016

The hydraulic gradients in Figure 54 suggest a through flow of the deep hard rock aquifer with a large contribution from the southern bank to the river depicted by the T values. This through flow is similar to the other transects and might indicate that the dolerite dyke does in fact separate the aquifer from LR001. The shallow weathered aquifer from the northern bank does not show a large loss to the river drainage (but this still requires hydraulic data characterisation), this can also be seen in the manual water levels where only small fluctuations occurred in the water level during the season.

Initial Transmission Loss Estimation

Following the groundwater hydraulic characterisation (Table 9) an initial transmission loss estimate can be made for the section of river, as related to the groundwater component.

Table 9 Hydraulic Characteristics of Boreholes at Study Site

BOREHOLE	Slug K (m/day)	Depth	Storativity	Q L/s	Final T (m^2/day)
LF0021	0.00	15.00	0.04	0.17	0.030
LF002A	0.02	48.20	0.00	0.15	0.080
LF002B	to high for slug		0.50	0.70	18.000
LF0031A	3.54		0.00	STEP	164.200
LF0031B	0.00	6.60		SLUG	0.003
LF003A	0.13	60.00	0.01	0.22	0.050
LF003B	0.12		0.04	0.40	1.000
LF004A	0.02	58.00	0.00	0.15	0.870
LF004B	0.41	1.63		SLUG	0.668
LF0051A	0.35	39.00	0.00	1.00	13.650
LF0051B	0.02	15.00	0.00	0.15	0.300
LF005A	0.02	59.00	0.00	0.15	1.180
LF005B	0.00	29.00	0.00	0.10	0.058
LF005C	0.14	1.20		SLUG	0.168
LR0011A	0.01	61.00	0.00	0.11	0.305
LR001A	0.02	49.00	0.02	0.41	0.980
LR002A	0.01	31.00	0.00	0.10	0.155
LR003A	0.00	3.60	0.00	0.10	0.014
LR004A	0.02	40.00	0.00	0.16	0.680
LR004B	0.17	12.00	0.00	0.33	2.040
LR005A	0.53		0.05	1.60	26.970
LR005B	0.27	14.20	0.14	0.71	3.834

In accordance with the 4 geohydrological transects described an estimate was made of the approximate river reach lengths represented by the surrounding aquifers, as depicted in Figure 55 which divides the river between Mahale and Letaba Ranch into 4 representative river reaches upon which the interaction between the river and the aquifer can be estimated in terms of either gains or losses from the water course.

DRAFT

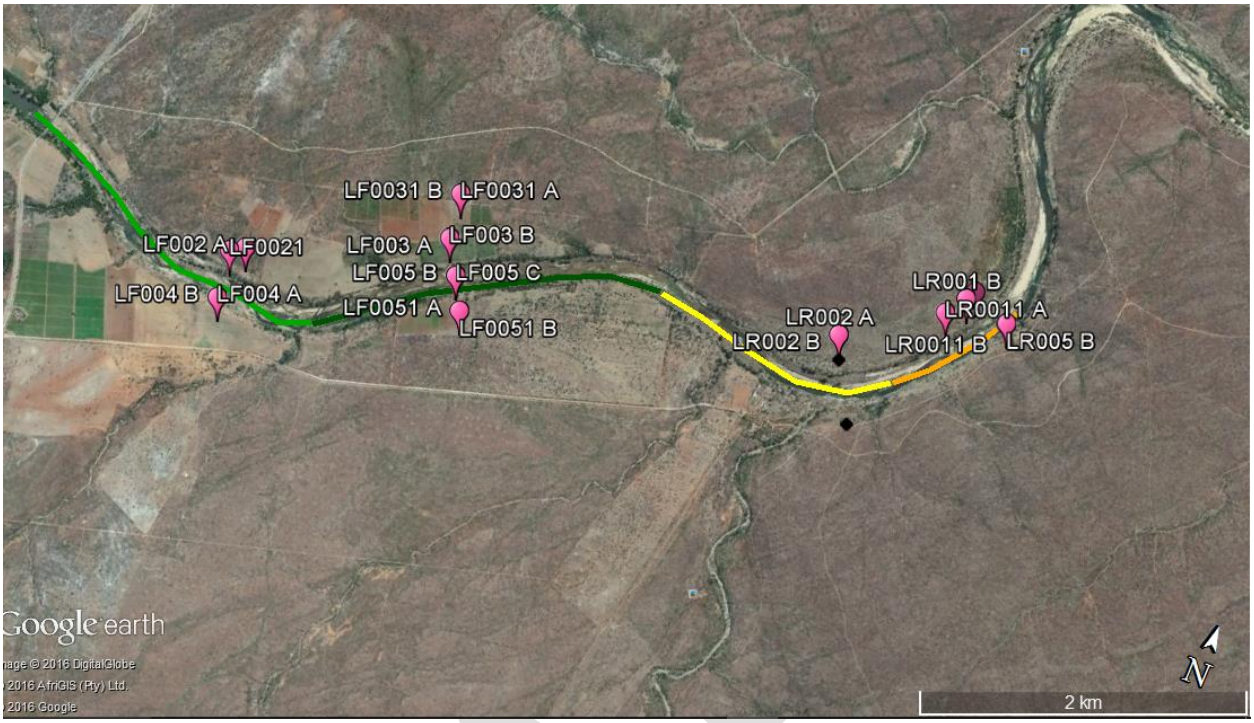

Figure 55 Assumed river reaches between Mahale and Letaba Ranch weirs associated with geohydrological transects (green represents farming areas and yellow the protected areas).

Transmission losses along a river can be estimated using the following equation:

Equation 6 $Q = TiL$

Where Q is discharge (m^3), T is transmissivity, i is the hydraulic gradient between the river and the surrounding aquifer (dimensionless), L is the length of river reach (m)

This equation was applied to each river reach distinguishing between hydraulic parameters for deep and shallow boreholes and applied to the hydraulic gradients determined for the study site as depicted Table 9.

It is interesting to note that based on Table 10 there appears to be a net loss from the river to the surrounding aquifer in the transects representing the farming areas, and this is potentially greater into the deeper hard rock zone. Moreover there is a marginal decrease at the hydraulic gradient reduces over time. Meanwhile further downstream in the protected areas there is a potential flow gain from the surrounding aquifer especially in the deep hard rock zone. Here there is a noticeable decrease in potential gain from the aquifer to the river comparing February to September.

DRAFT

It is therefore important to take this into context of the prevailing hydrology for the study period in which the upstream Mahale weir was discharging only through low flow outlets with an estimated flow of between 0.4-0.5 m^3/sec or 34560 to 43200 m^3/day. Hydro-census information for river abstractions (surface water only) between these two weirs allows for an estimate of total daily abstractions of 52 m^3/day.

Table 10 Transmission Loss parameters determined for the Letaba river study site comparing wet season (15 February 2016) with dry season (16 September 2016) (yellow highlighted values mean borehole properties could not be determined for the shallow boreholes due to insufficient head, so these values were inferred from the deep boreholes)

					15/02/2016		16/09/2016	
		River Section	Actual Section Length (L)	*T* m/day	*i*	Q m^3/day	*i*	Q m^3/day
Deep BH data (A)	Farms	LF002	2200	0.08	-0.004	-0.72	-0.004	-0.78
		LF004	2200	0.87	0.009	17.03	0.008	16.20
		LF003	2180	0.05	0.020	2.19	0.020	2.19
		LF005	2180	1.18	-0.055	-142.00	-0.055	-140.58
					Total	**-123.49**		**-122.97**
	Reserves	LR002	1580	0.155	0.011	2.67	0.011	2.65
		LR004	1580	0.68	-0.010	-10.64	-0.011	-12.33
		LR001	880	0.98	0.006	5.52	0.006	5.44
		LR005	880	3.834	0.011	35.76	0.008	27.98
					Total	**33.32**	**Total**	**23.74**
Shallow BH data (B)	Farms	LF002	2200	18	-0.003	-114.84	-0.003	-119.72
		LF004	2200	0.6683	0.018	26.91	0.018	26.06
		LF003	2180	1	-0.041	-88.94	-0.041	-89.37
		LF005	2180	0.058	-0.032	-3.98	-0.031	-3.95
					Total	**-180.86**		**-186.98**
	Reserves	LR002	1580	0.155	-0.001	-0.24	0.015	3.78
		LR004	1580	2.04	-0.015	-47.38	-0.016	-52.55
		LR001	880	0.98	0.025	21.22	0.024	20.35
		LR005	880	3.834	0.020	68.83	0.018	62.02
					Total	**42.42**	**Total**	**33.59**

This information is integrated into a time-series (Figure 56) which suggests a sustained contribution from the deep regional aquifer of approximately +14.2 m^3/day, although one observes that the hydraulic gradient to the river decreases toward the end of the reporting period in September (further data to be incorporated for the final version of this report). However there is a potential drawdown of the river toward the unconsolidated shallow aquifer throughout the study period, which potentially averages -25.5 m^3/day.

DRAFT

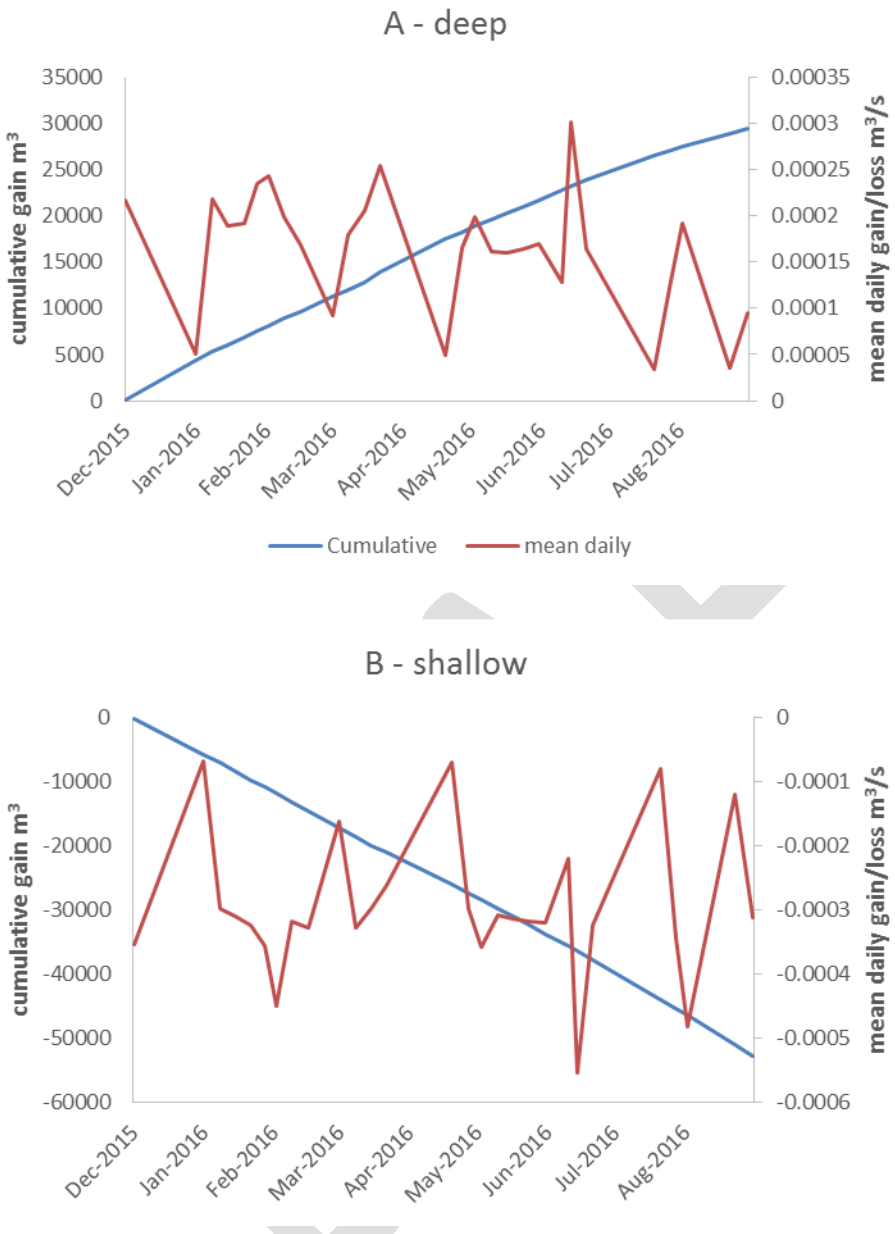

Figure 56 Time-series of potential gains/losses along the study site (related to deep hard rock aquifer and to shallow unconsolidated aquifer)

Updated conceptual model: groundwater-surface water interaction

The data presented on borehole fluid logging and hydraulic gradients towards the river were used to derive a conceptual model of groundwater-surface water interactions along the study site reaches of the Letaba River. Further valuable information was derived from the single large streamflow event that occurred at site during the drought during March 2016 flood (Figure 13). These will be discussed according to transect names (Figure 28).

DRAFT

Assessing peak flow transmission losses

Transect 1

Transect 1 includes borehole nests LF002, LF0021 and LF004. This studies initial conceptual model, supported by the hydraulic gradient data interpreted that groundwater was moving from LF004A in the south toward the river with water being lost from the river to LF002 and LF0021 on the northern bank. This assertion was supported by the boreholes reaction to the March 2016 peak flows. Both LF002 and LF0021 displayed (Figure 57) a subtle delayed response, meanwhile LF004 did not display any reaction (not plotted). This data suggests that water was lost to the northern bank at transect 1, although at a relative slow rate. The fluid logging supports this with a lower EC found in these boreholes on the northern bank from the loss of river water to the groundwater.

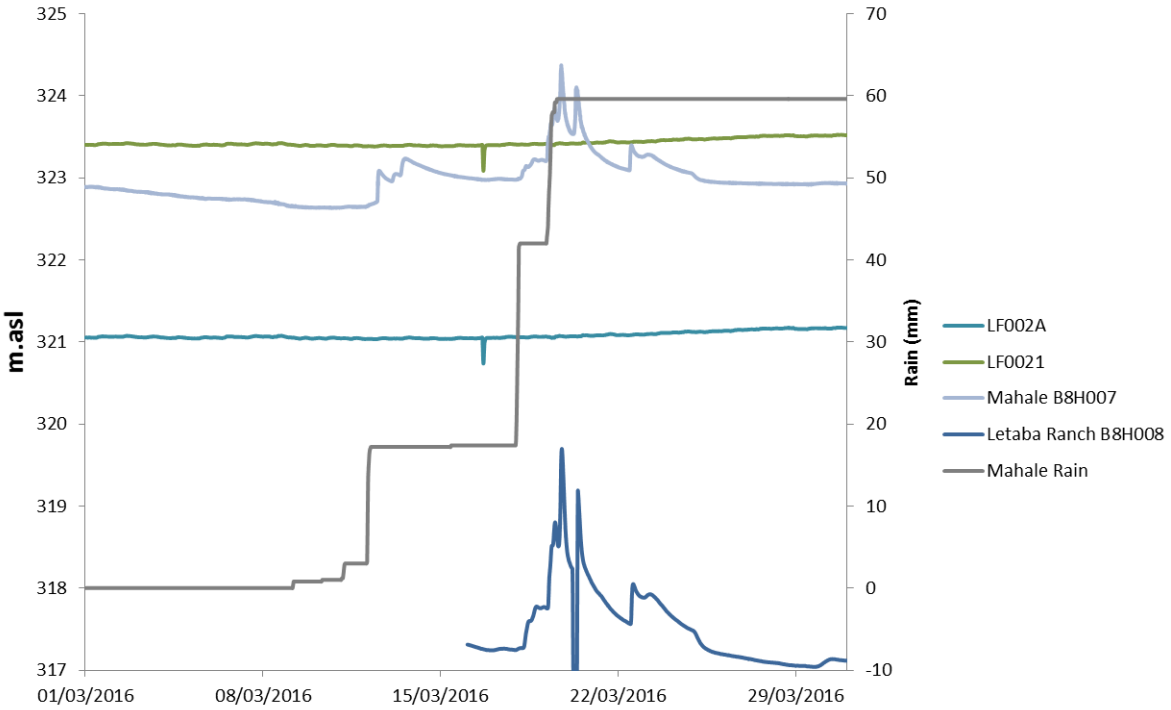

Figure 57 Key responses to March 2016 rain and peak flow along Transect 1 (stream stages plotted against datum at upstream and downstream sites for reference)

Transect 2

Transect 2 includes borehole's LF0031 & LF003 on the northern bank, and LF005 & LF0051 on the southern bank. Both deep and shallow holes at LF005 displayed (Figure 58) a quick and definite response to the flood. The water level in LF0051A further to the south did start responding only on the 19/03/2016 indicating a delayed rainfall response. The previous conceptual model interpreted that groundwater was moving from the northern bank, intersecting the river before losing water to the southern bank, with the deeper aquifer possibly being detached from the river. This was supported in that neither borehole at LF003 displayed a reaction to the March 2016 peak flow with little reaction to the rain events (not plotted).

Flow within the unconsolidated to consolidated zone through the boreholes on this transect were indicated by all the boreholes with a decrease in temperature with depth. The temperature also suggested movement of groundwater within all the boreholes. An EC of around 4000 uS is found within most of the boreholes (supporting the theory), except for LF0051 (A/B).

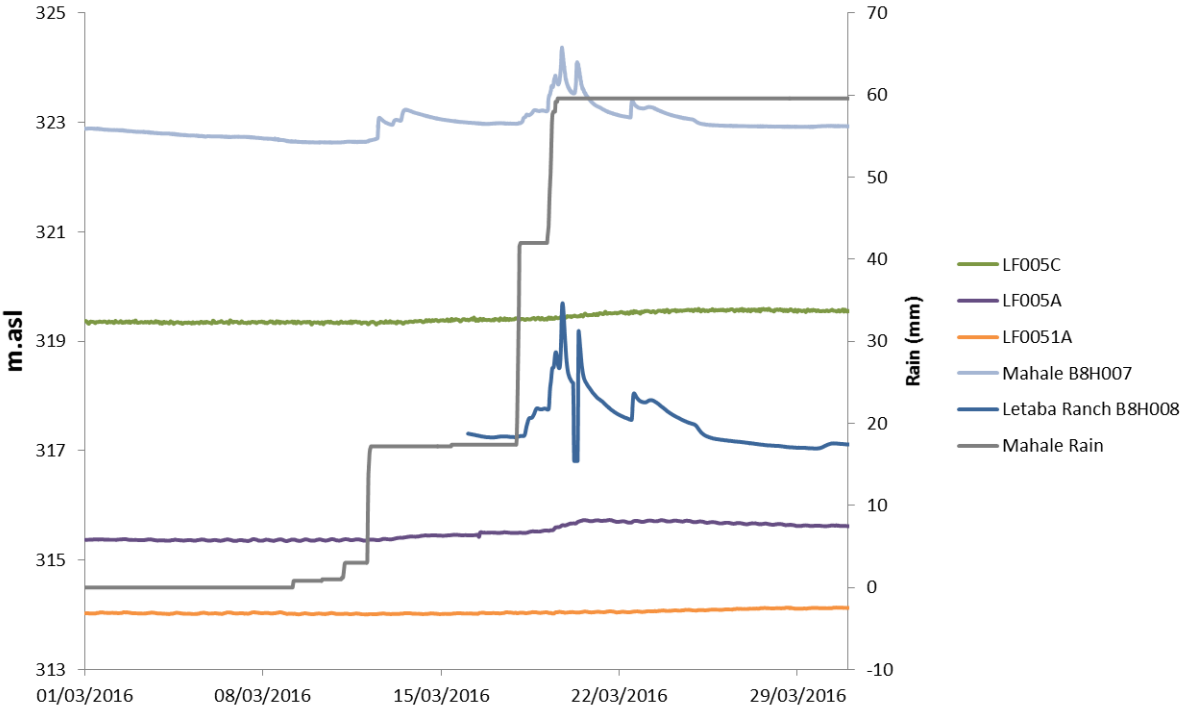

Figure 58 Key responses to March 2016 rain and peak flow along Transect 2 (stream stages plotted against datum at upstream and downstream sites for reference)

Transect 3

Transect 3 includes borehole nests at LR002 on the northern bank and LR004 on the southern bank, with the initial conceptual model suggesting that groundwater was moving from the northern bank to the southern bank as result of the hydraulic gradient across the

transect. The March 2016 peak flow reactions only partially suggest this theory, because both LR002A and LR004A/B reacted to the flood on the same day (13/03/2016), see Figure 59. Although LR004A/B is located almost twice the distance from the river when it is in flood, indicating that water is definitely being lost to the southern bank while water is only lost to the northern bank when the river is flood or high flow situations. During base flow situations water continues to flow from the northern bank to the southern bank. The fluid log supports this theory with the temperature displaying a good flow within all the boreholes and a higher EC of around 3000 uS in LR002A and lower EC of around 1500 uS within both shallow and deep boreholes at LR004, suggesting that water is being lost from the river to the southern bank.

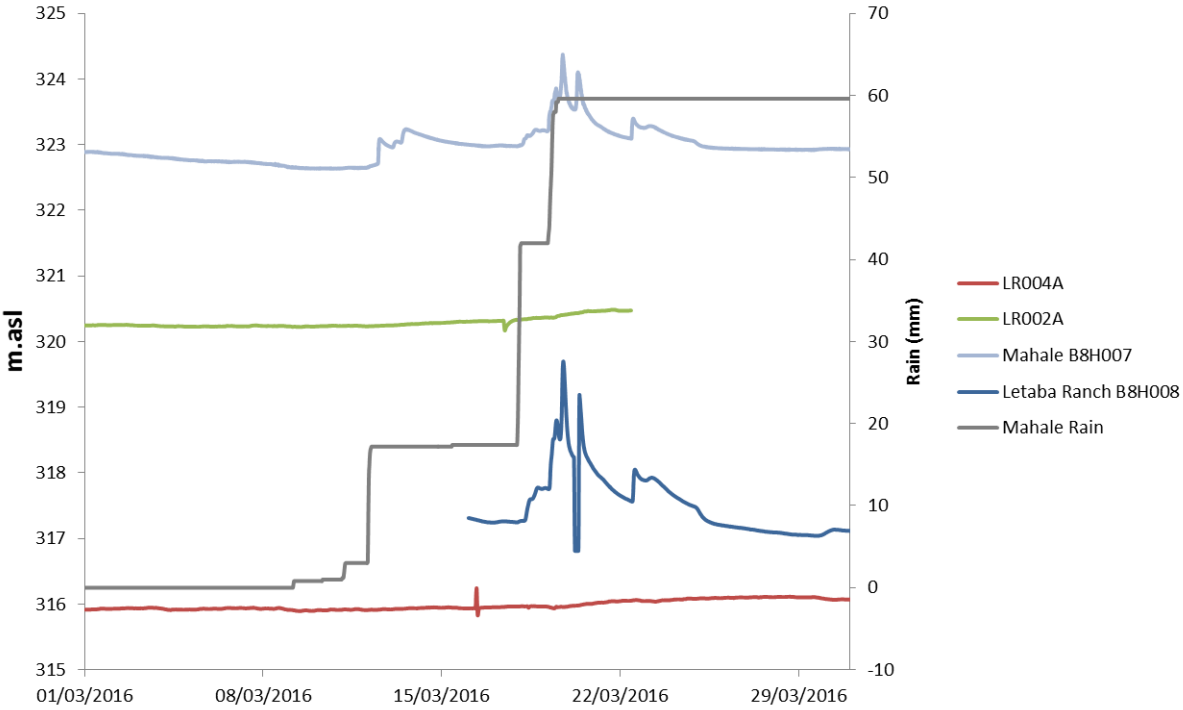

Figure 59 Key responses to March 2016 rain and peak flow along Transect 3 (stream stages plotted against datum at upstream and downstream sites for reference)

Transect 4

Transect 4 includes borehole's at LR001 on the northern bank and LR005 on the southern bank Figure 60. The hydraulic gradients across this transect suggest that groundwater moves from both north and south toward the river. The peak flow events of March 2016 suggest that this reverses to bank storage/recharge from the river as both LR005A and LR001A respond to the streamflow hydrograph, particularly obvious at LR001A. This indicates that during base flow the groundwater is contributing to the river from both sides and during flood conditions the river contributes to the groundwater. The fluid log supports this theory with good flow indicated within all the boreholes, as well as water flowing through the unconsolidated zone into the boreholes noted from the decrease in temperature with depth.

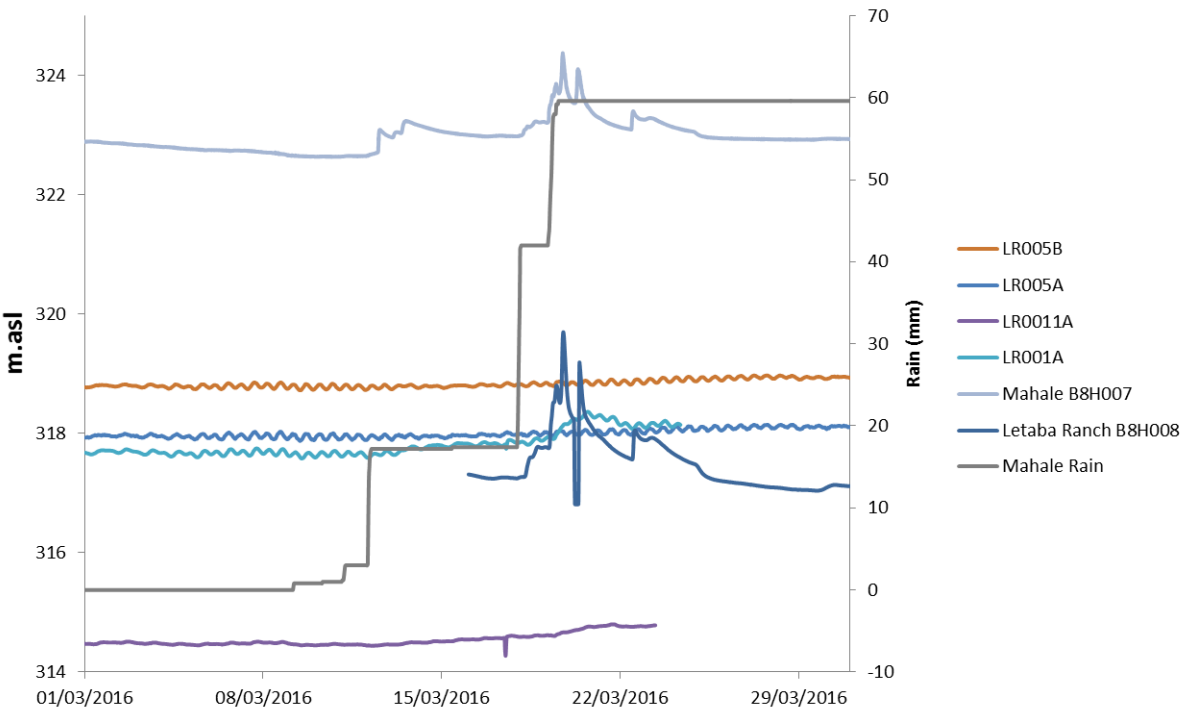

Figure 60 Key responses to March 2016 rain and peak flow along Transect 4 (stream stages plotted against datum at upstream and downstream sites for reference)

DRAFT

Groundwater flow direction from hydraulic heads

The hydraulic heads of all the boreholes where plotted as contours in Surfer™ to integrate groundwater movement in relation the Letaba River. This focused on understanding groundwater movement before and after the flood/rains of March 2016 (Figure 62 and Figure 63) as well as a dry and wet season comparison (Figure 61 to Figure 64).

Transect 1

As discussed in the section above and supported by the hydraulic heads, the groundwater is moving towards the northern bank of traverse 1 (Figure 61). A small difference could be seen between the hydraulic heads before and after the March 2016 events. Greater hydraulic heads where observed on the northern bank, although not on the southern bank supporting the theory of transmission loss to the northern bank from the river. No large differences were observed between the hydraulic heads of the wet and dry season, although this can be assigned to the very little rainfall that occurred between these periods.

Transect 2

The discussion above is supported by the hydraulic head distribution where the groundwater is moving from the northern bank to the southern bank intersecting the river (Figure 61). The difference in hydraulic heads before and after the March peak flows displayed only a slight increase in hydraulic head on the southern bank again supporting the theory. This slight reaction might indicate that the fractured rock aquifer is detached from the system. Again no big differences were observed between the wet and dry season due to little rainfall that occurred.

Transect 3

The discussion above is supported by the hydraulic head distribution where the groundwater is moving from the northern bank to the southern bank (Figure 61). An increase in hydraulic heads is observed on the southern bank, as well as the northern bank. This indicates that during peak flows water is lost to both banks and during low flows only to the southern bank. A visible decrease in hydraulic heads was observed between the wet and dry season this was anticipated due to the drought conditions.

Transect 4

The groundwater is moving from both banks towards the river. An increase in hydraulic heads are observed after the March flood, supporting the theory that the river contributes to the groundwater during peak flow, while this process is reversed during low flow periods. A slight decrease in hydraulic head is observed in the dry season (Figure 64), as anticipated due to the little rain that fell within this period.

These process as described are all captured visually in the conceptual model of the site in Figure 66.

DRAFT

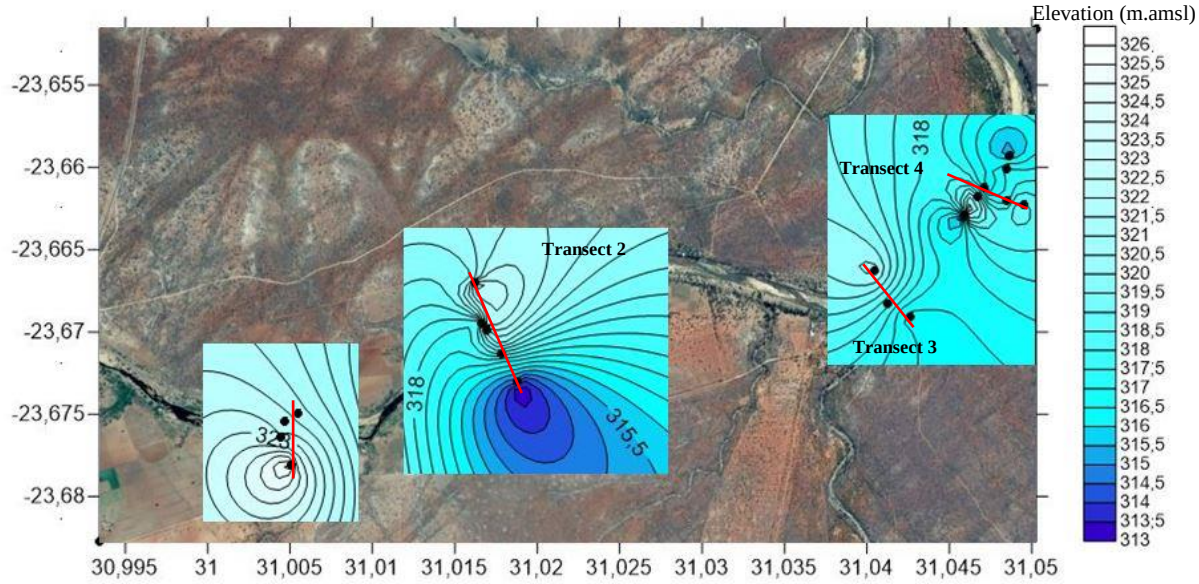

Figure 61 Borehole and River heads before the flood event (30/11/2015).

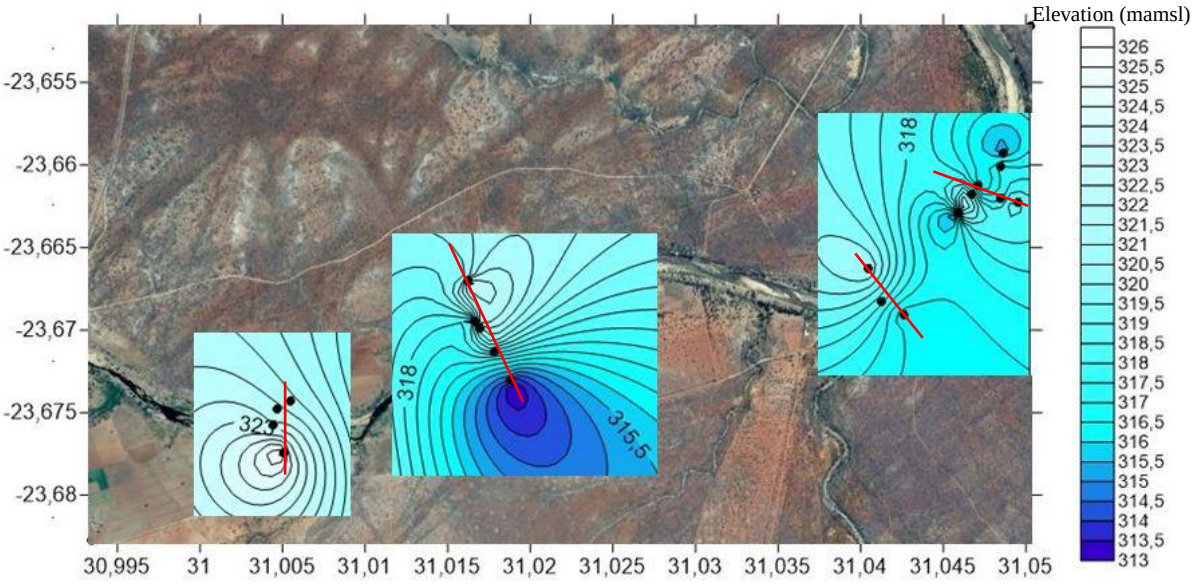

Figure 62 Borehole and River heads before the flood event (15/02/2016).

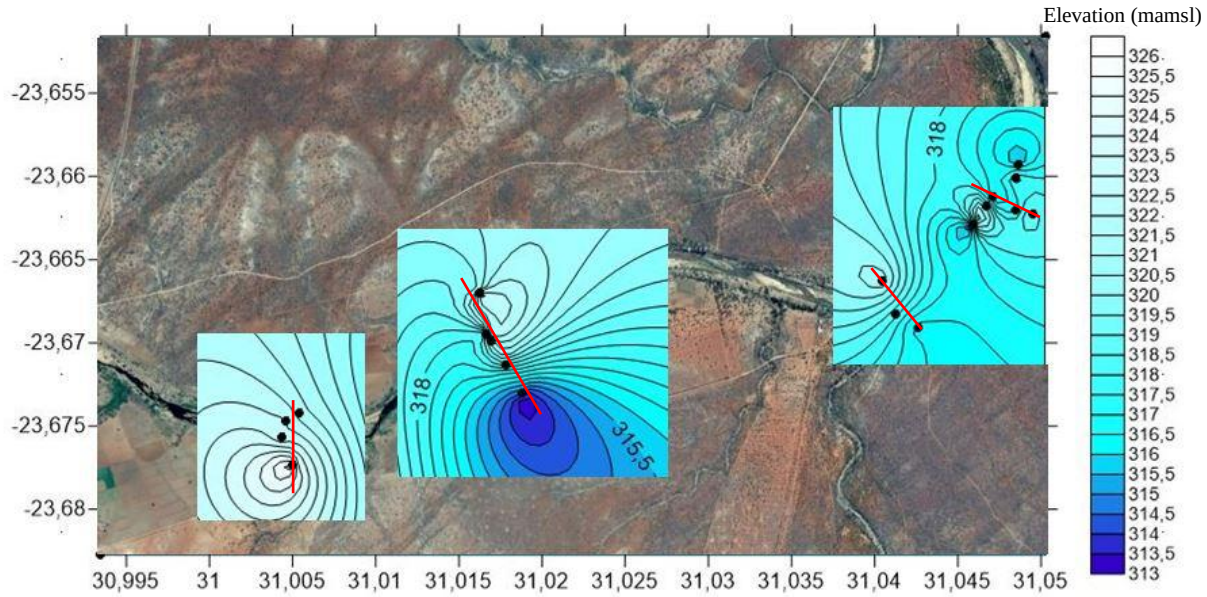

Figure 63 Borehole and River heads after the flood event (28/03/2016).

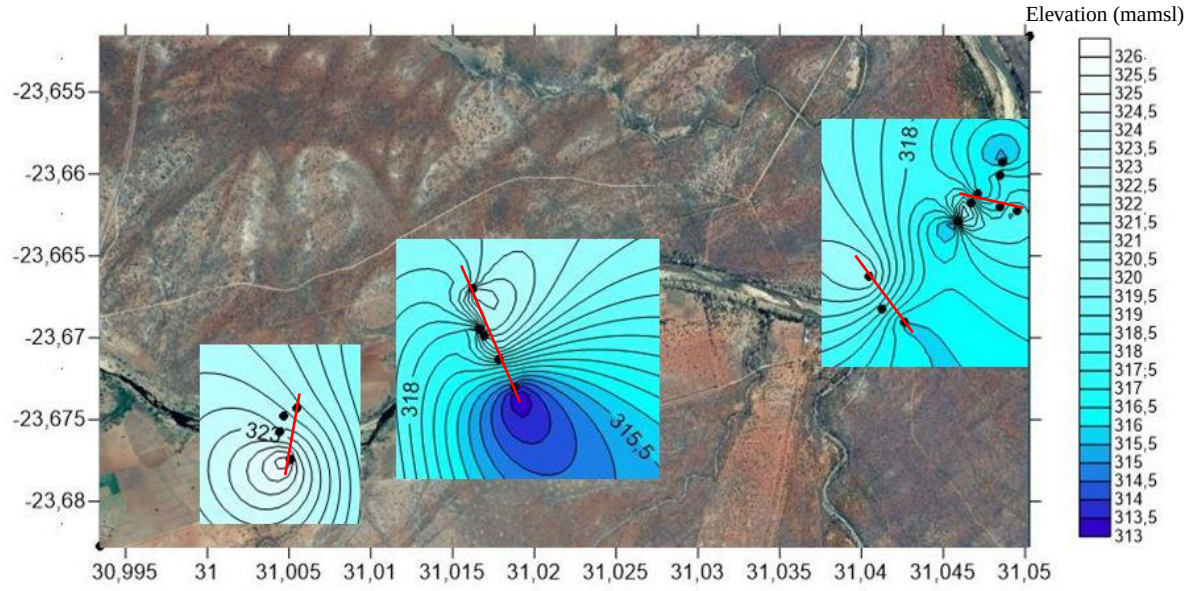

Figure 64 Borehole and River heads after the flood event (08/08/2016).

Groundwater stream flow process across dolerite dyke

LRW002 is located on the southern side (upstream) of a dolerite dyke with LRW001 located on the northern side (downstream), see Figure 65, this is described briefly here in terms of the responses of these boreholes within the active river macro-channel. The first indication of the flood event on 13/03/2016 was indicated at the Mahale weir upstream. The second indication was by LRW002, with a delayed response in LRW001. The reason being the dolerite dyke interrupts the groundwater moving through the unconsolidated/consolidated zone. This is supported by the fluid logging with LRW002 displaying lower temperatures of around 22°C from the interaction with river water, compared to LRW001 with a temperature between 24 and 26°C. The EC also supports this with a low EC of around 1500uS from the mixing with river water, compared to LRW001 with a high EC of around 7000uS.

After the second peak of the flood the two boreholes acted similarly, as the river had now created connectivity over the dolerite dyke. After the flood passed LRW002 displayed a faster decrease in water level due to a continual drawdown towards the river. The result was a more steady decrease in water level for LRW001.

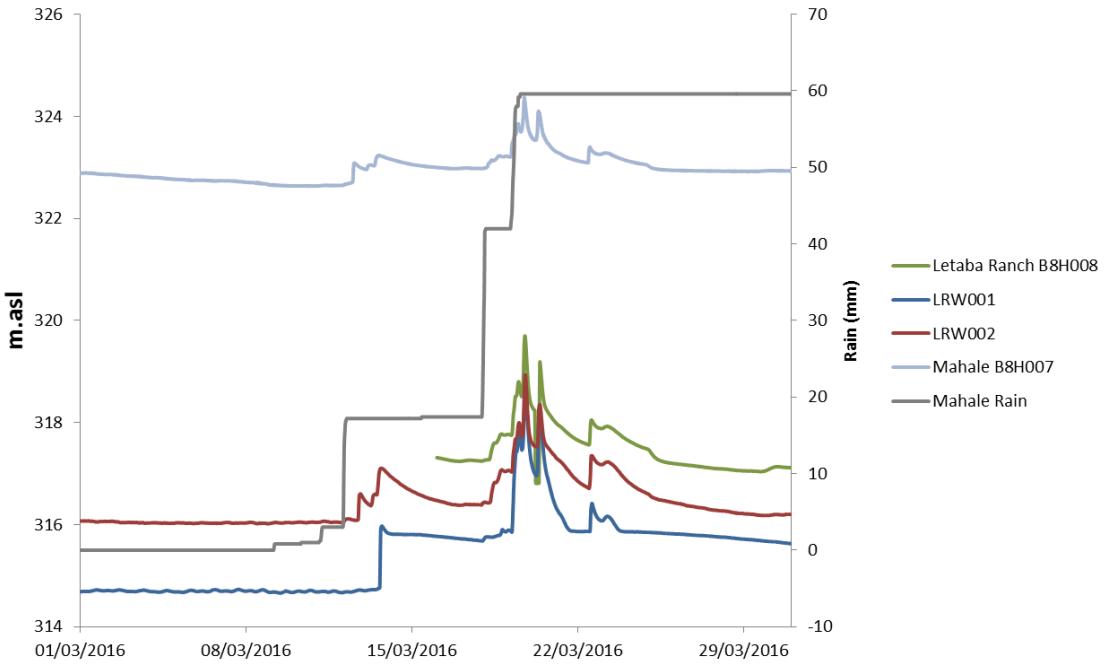

Figure 65 Groundwater-Streamflow processes across dolerite dyke (NB. The dyke also has concrete wall built upon it as part of the rating structure for the Letaba Ranch gauge B8H008).

DRAFT

Conceptual model

The previous sections have detailed the hydrometric results from the piezometric borehole network. Based on this and the fluid logging results from the boreholes, hydrometric time-series, and three longitudinal hydrochemical profiles of the entire river reach (Figure 9) it is possible to present a conceptual model for the study site from a geohydrological perspective (Figure 66).

Figure 9 compares the survey of November 2014 which can be considered representative of the dry season, but following a wet cycle climatically. With the October 2015 survey also in the dry season it does follow a significantly below average rainfall year. This figure reveals two interesting aspects. The first being the apparently lower EC in the November 2014 survey, with a clear increase in EC in the river reach represented by the LF003-LF005 transect in the farming area, which then returns to a lower EC further downstream. This contrasts with the higher EC throughout in October 2015 with no EC elevation at the LF003-LF005 transect. By the time of the 3rd survey in April 2016 EC had lowered significantly and remained so throughout the longitudinal profile. Two factors may explain this: low flows in the Letaba river were significantly lower in the 2015 survey (<0.5 m^3 at Letaba Ranch) compared to the former in 2014 (~1.0 m^3 at Letaba Ranch) and therefore subject to greater concentration of salts from natural processes as well as anthropogenic activities (the low ECs in the April 2016 survey likely a result of the March 2016 flood event); whilst the 2014-

15 being a low rainfall year may have prevented a significant hydraulic gradient from the weathered zone and disturbed landscapes of the farming region on the northern bank of the river (LF003-LF0031). This hydraulic gradient will have reduced during the very dry period of 2015-16. This is of course speculative as we have no groundwater observations to verify for the early period, but certainly an aspect to consider in long term monitoring of the site.

Meanwhile other aspects to consider from the fluid logging are the low EC readings for LF002 suggesting continuous connection to river surface water at least in the November 2015 survey which implies losses to the northern bank in the most upstream part of the study and the hydraulic gradient data supports this. Moreover, LF004 on the southern side of the river shows increasing EC to a depth of 30m with corresponding increase in temperature with depth, this is seen in both fluid logging surveys, suggesting sustained groundwater contributions from elsewhere in the landscape.

At the lowest end of the study site the fluid logs suggest that there is a sustained groundwater contribution from the northerly directions into the river channel, as suggested by decreasing temperature and stable EC with depth at LR001. With similar observations in the boreholes at LR005 also supports sustained groundwater contributions to surface flow in the river from a southerly direction. The new data from the flood event of March 2016 also suggest that the river recharge from the groundwater can be reversed during peak flow especially at the lower end of the study site within the protected areas.

DRAFT

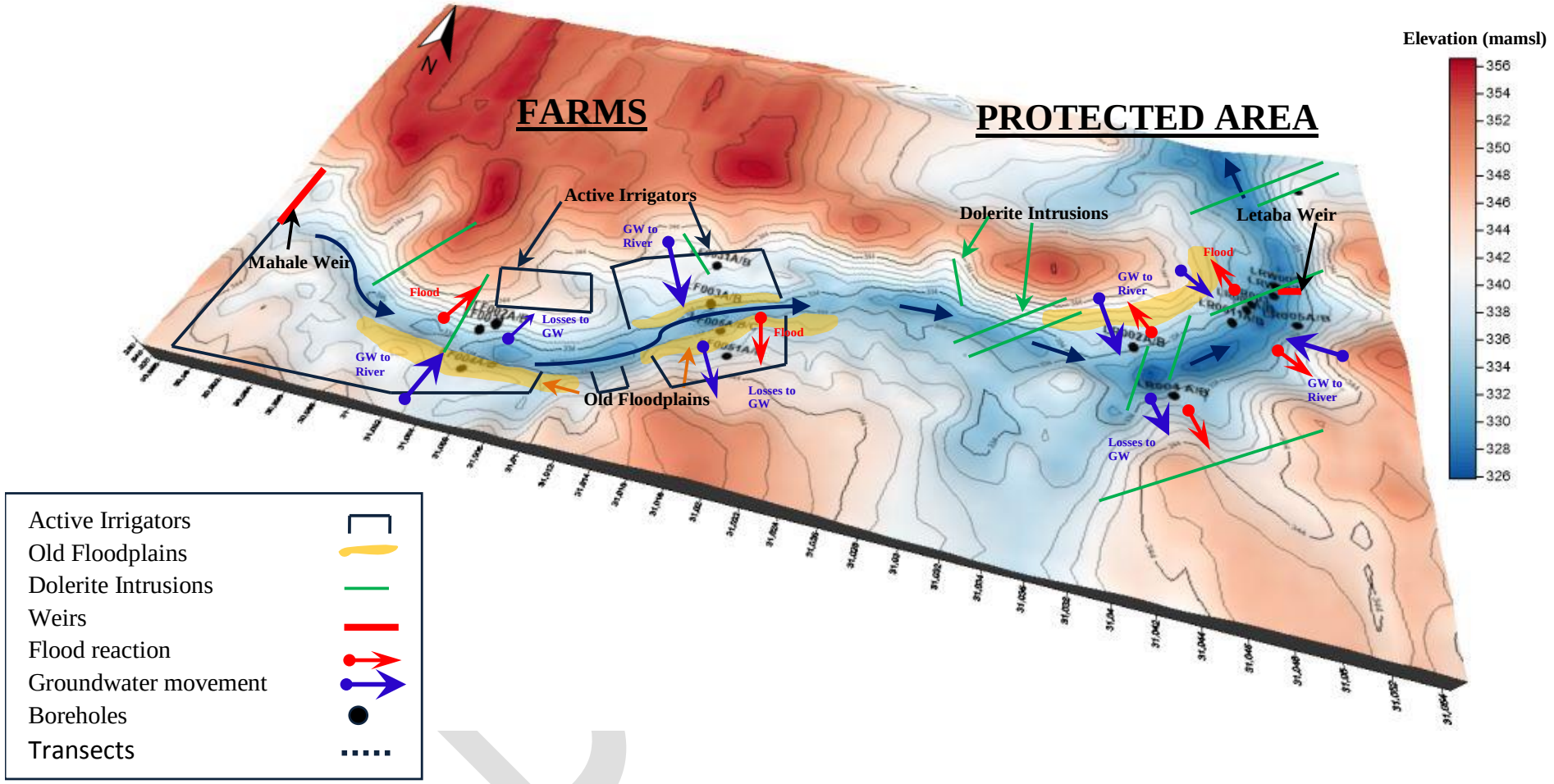

Figure 66 Conceptual Model of Geohydrological Process Connectivity along the Groot Letaba river study site

Stable Isotopes in the Riparian Zone

Isotopic Composition of Rainfall

δ^2H in rainfall ranged from -22.9 to 15.3‰, with a mean value of 0.2‰ (± 11.6 ‰). Whereas $\delta^{18}O$ in rainfall ranged from -4.3 to 0.9 ‰, with a mean value of -1.7 ‰ (± 1.6 ‰). The LMWL for our study site, as shown in Figure 67, was established as $\delta^2H = 7.06\delta^{18}O + 12.13$, with a R^2 value of 0.89. The slope of the LMWL is lower than the slope of the global meteoric water line (GMWL), described respectively in Craig (1961) and Liu et al. (2014), as $\delta^2H = 8\delta^{18}O + 10$ and $\delta^2H = 7.94\delta^{18}O + 3.92$. The lower slope of the LMWL can be attributed to rapid evaporation of falling raindrops (Ma and Song, 2016), which would be expected in this semi-arid region. It is also quite clear that the rainfall during the study period was dominated by convective rainfall with lighter isotopes, the exception being the rain of March 2016 which had a much more depleted signature.

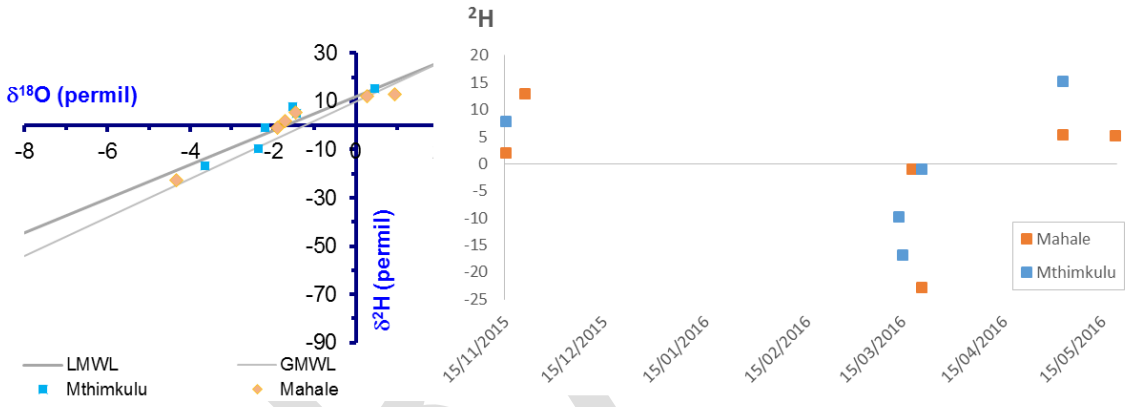

Figure 67 Stable isotopes of rainfall during the study period against GMWL (left) and time-series (right)

Isotopic composition of riparian zone water

The δ^2H and $\delta^{18}O$ of streamflow, soil water and xylem water plot below the LMWL, showing evaporative enrichment in these samples relative to rainfall, as shown in Figure 68. δ^2H and $\delta^{18}O$ values for groundwater and soil water (100 cm) plot closer to the GMWL providing evidence that precipitation is one of the principal sources contributing to groundwater recharge at this site.

δ^2H in stream water ranged from -9.2 to -7.6 ‰, with a mean value of -8.3 ‰ (± 0.6 ‰). Whereas $\delta^{18}O$ in stream water ranged from -1.9 to -1.2 ‰, with a mean value of -1.5 (± 0.3 ‰). $\delta^{18}O$ and δ^2H in stream water are relatively enriched in comparison to the other samples, indicating a strong evaporation effect.

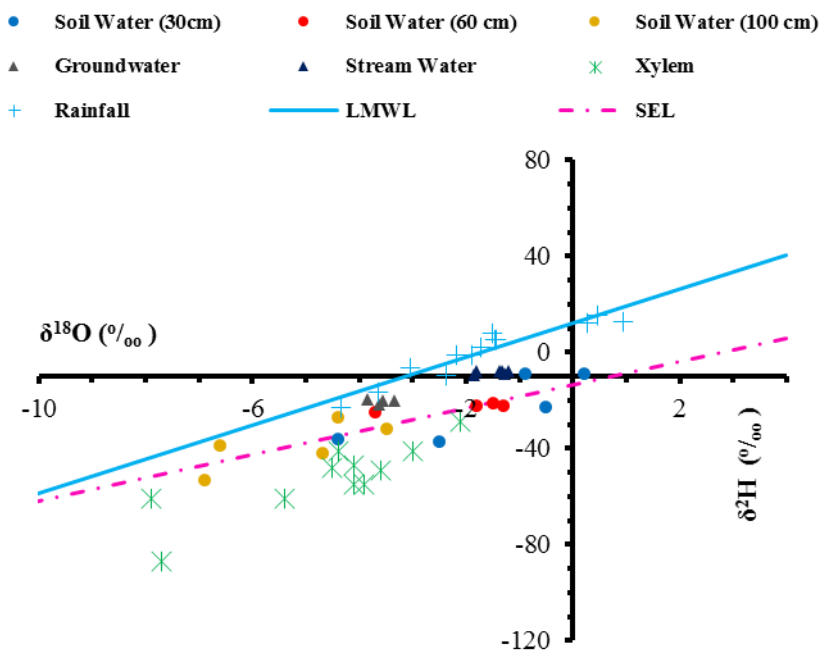

Figure 68 A plot of δ^2H versus $\delta^{18}O$ values for all the study samples.

δ^2H in soil water (30, 60 and 100cm) ranged from -53 to -9.0 ‰, with a mean value of -28.4 ‰ (± 12.3 ‰). Whereas $\delta^{18}O$ in soil water (30, 60 and 100cm) ranged from -6.9 to 0.2 ‰, with a mean value of -3.0 (± 2.2 ‰). δ^2H and $\delta^{18}O$ in soil water were enriched in the top soil layers and depleted with depth. Mean δ^2H and $\delta^{18}O$ values for soil water in the upper soil layers (between 0 and 60 cm) were -22.7 ‰ (± 9.8 ‰) and -1.8 ‰ (± 1.5 ‰), respectively. Whereas mean δ^2H and $\delta^{18}O$ values for soil water at a depth of 100 cm was more negative, with δ^2H of -38.6 (± 10.0 ‰) and -5.2 (± 1.5 ‰) $\delta^{18}O$ of, respectively.

δ^2H in xylem water ranged from -87 to -29.0 ‰, with a mean value of -52.2 ‰ (± 14.9 ‰). Whereas $\delta^{18}O$ in xylem water ranged from -7.9 to -2.1 ‰, with a mean value of -4.6 (± 1.8 °‰). The δ^2H and $\delta^{18}O$ values of xylem water generally plot close to the fitting line of the soil water δ^2H and $\delta^{18}O$ (SEL) relationship as shown in Figure 68, indicating that soil water is one of the main contributors to the vegetation during transpiration.

Proportional contribution of potential water sources to plant water use during transpiration

In this study, Simmr[5] was used to quantify the proportional contribution of the various water sources to plant water uptake during transpiration. The isotopic composition of soil water in the upper soil layers (between 0 and 30 cm) was generally clearly distinguishable from deeper down in the profile, therefore this was treated as a separate source. The input data to Simmr was the measured δ^2H and $\delta^{18}O$ for xylem water, rainfall, soil water (30 and 60 cm), soil water (100 cm) groundwater and stream water.

[5] The Stable isotope mixing model package in R designed to solve mixing equations for stable isotope data using a Bayesian statistical framework (Parnell, 2016).

According to Philips (2012) the isotopic composition of δ^2H and $\delta^{18}O$ in the xylem water must fall between those of the potential water source end-members, in order to be explained as a mixture of them. While the model is able to compute a mathematical solution of the proportion of sources that sum to 1.

The proportion of one of the sources will be negative, while the proportion of one of the remaining sources will be greater than one, neither of which is hydrologically possible (Philips, 2012). In such circumstances it is highly probable that there is an additional source which has not been considered or there remains a degree of uncertainty associated with the isotopic composition of δ^2H and $\delta^{18}O$ in the xylem water or the sources.

In general, the δ^2H and $\delta^{18}O$ in the xylem water of our samples is more depleted relative to the δ^2H and $\delta^{18}O$ of all possible sources. This is shown in the simple-end member plot (Figure 69) of δ^2H and $\delta^{18}O$ in the xylem water and the potential water sources. Consequently, Simmr could not be applied to determine the general proportional contribution of water sources to plant water uptake during transpiration, as the abovementioned assumption required to implement the mixing model successfully, was not satisfied.

However, δ^2H and $\delta^{18}O$ in the xylem water for three individual trees at sampling points 1 (*D. mespiliformis*), 2 (*C. Microphyllum*) and 6 (*F. sycomorus*), respectively, were between those of the potential water source end-members. Therefore, it was possible to implement Simmr, to quantify the potential contribution of water from a particular source at these particular sampling points, during plant water uptake.

The average contribution of rainfall, soil water (30 and 60 cm), soil water (100 cm), groundwater and stream water to plant water uptake for each of the aforementioned tree species is given in **Table 11**. The results shown in Figure 68 and Figure 69, as well as **Table 11** indicate that soil water (especially at greater depths) is a major contributing source of water during transpiration, in the study area.

DRAFT

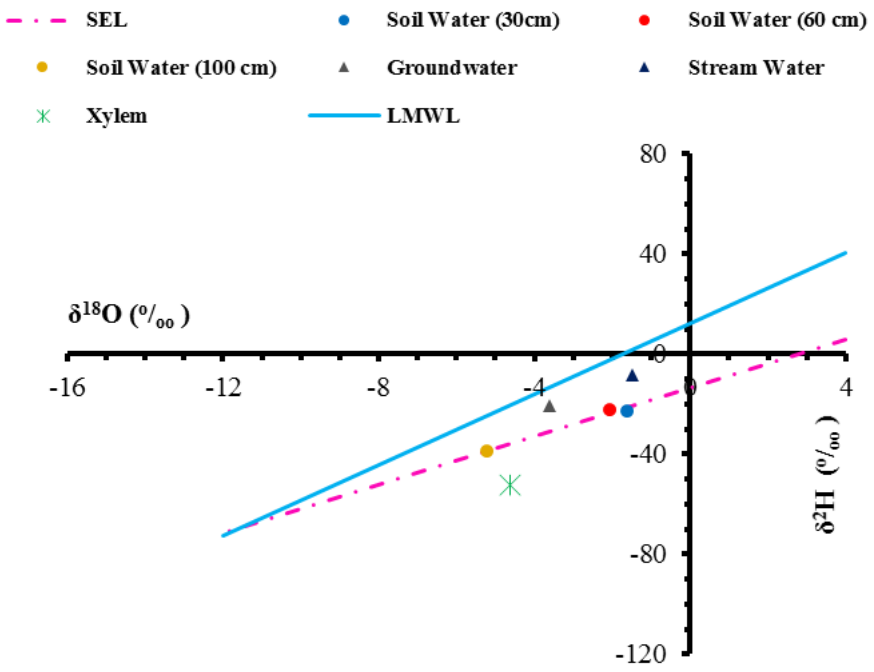

Figure 69 A plot of δ^2H versus $\delta^{18}O$ values for the simple end-members.

Table 11 Average contribution of each water source sampled for plant water taken up by three common riparian species, at sampling points 1, 2 and 6.

Tree Species	*D. mespiliformis*	*C. Microphyllum*	*F. sycomorus*
Rainfall	0.40 %	6.00 %	2.50 %
Groundwater	20.90 %	5.60 %	2.10 %
Stream water	0.40 %	10.50 %	3.30 %
Soil (30 and 60 cm)	78.10 %	7.50 %	3.70 %
Soil (100 cm)	N/A	68.70 %	87.70 %

δ^2H and $\delta^{18}O$ values of xylem water were shown to generally plot closest to the SEL, indicating that soil water is one of the main contributors to the vegetation during transpiration. However, the isotopic composition of δ^2H and $\delta^{18}O$ in the xylem water was generally more depleted relative to the other samples and did not fall between those of the potential water source end-members, in order to be explained as a mixture of them. A conceivable explanation for this occurrence is that there is an additional water source which has not been sampled, and this is likely to be soil water at a depth of more than 100cm.

DRAFT

Total Evaporation

Eddy Co-Variance

The results presented below discuss the inter-annual comparisons of EC_{ET} measurements. Only those EC_{ET} measurements for the corresponding dates i.e. 17th Jun to 13th August and 21st Aug to 17th October are presented and discussed. Furthermore, the FAO 56 Penman-Monteith reference evaporation is included in the graphical illustrations and statistical analyses to compare if the ranges of the EC_{ET} measurements are within a similar magnitude as ET_0.

Inter annual comparison of EC_{ET} for 2015 and 2016 during the period 17th June to 13th August, at Site 1

Figure 70, as well as the results of the statistical comparisons presented in Table 12 indicates that the EC_{ET} for 2016 is significantly higher than the EC_{ET} for 2015 for site 1. The ET measured in 2016 has approximately increased by a factor of 3 when compared to the ET measured in 2015 during this period. The Root Mean Square Error (RMSE) indicates that on average the EC_{ET} for 2016 is 1.67 mm d^{-1} higher than the EC_{ET} for 2015. While the result of the ANOVA test at the 95 % confidence level reaffirms that there is a significant difference between the 2015 and 2016 EC_{ET}.

Table 12 Statistical comparison of ET_0 and EC_{ET} for 2015 and 2016 during the period 17th June to 13th August, at Site 1

	ET_0 2015	EC_{ET} 2015	ET_0 2016	EC_{ET} 2016
Total	137,69	52,32	141,33	133,39
Average	2,42	0,92	2,48	2,34
Max	3,79	1,42	3,55	3,93
Min	0,41	0,46	0,27	0,77
Median	2,48	0,94	2,62	2,22
Variance	0,26	0,04	0,49	0,77
Std Dev	0,51	0,19	0,70	0,88
RMSE				1,67
ANOVA p value				0,00

DRAFT

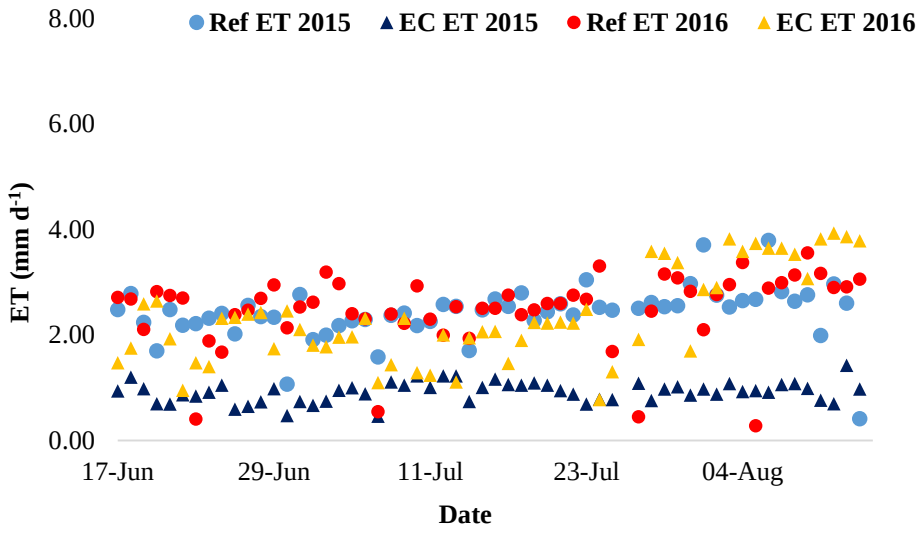

Figure 70 A comparison of ET_0 and EC_{ET} for 2015 and 2016 during the period 17th June to 13th August, at Site 1

Inter annual comparison of EC_{ET} for 2015 and 2016 during the period 22nd August to 17th October, at Site 2

Figure 71, as well as the results of the statistical comparisons presented in Table 13, indicates that the EC_{ET} for 2016 is significantly higher than the EC_{ET} for 2015 for site 2. The ET measured in 2016 has approximately increased by a factor of 1.4 when compared to the ET measured in 2015 during this period. The Root Mean Square Error (RMSE) indicates that on average the EC_{ET} for 2016 is 1.83 mm d^{-1} higher than the EC_{ET} for 2015. While the result of the ANOVA test at the 95 % confidence level reaffirms that there is a significant difference between the 2015 and 2016 EC_{ET}.

Table 13 Statistical comparison of ET_0 and EC_{ET} for 2015 and 2016 during the period 22nd August to 17th October, at Site 2

	ET_0 2015	EC_{ET} 2015	ET_0 2016	EC_{ET} 2016
Total	200,03	151,52	216,22	205,12
Average	3,57	2,71	3,86	3,66
Max	5,65	4,97	5,80	5,45
Min	0,75	0,60	1,34	1,49
Median	3,59	2,87	3,74	3,96
Variance	1,44	1,49	0,70	1,12
Std Dev	1,20	1,22	0,83	1,06
RMSE				1,83
ANOVA p value				0,00

DRAFT

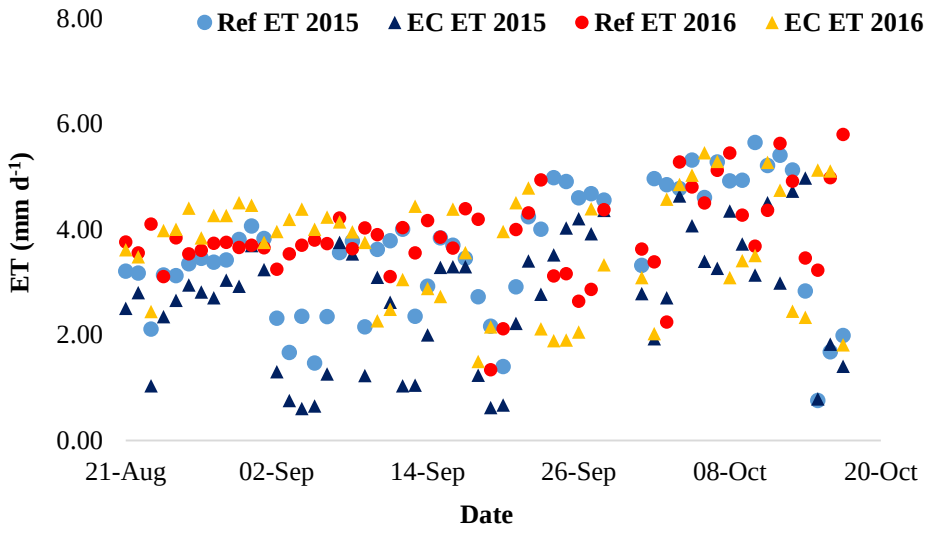

Figure 71 A comparison of ET_0 and EC_{ET} for 2015 and 2016 during the period 22nd August to 17th October, at Site 2

Inter annual comparison of ECET for 2015 and 2016

The results presented in Table 14 as well as the graphical illustration shown in Figure 72, indicates that the EC_{ET} for 2016 is significantly higher than the EC_{ET} for 2015. The ET measured in 2016 has approximately increased by a factor of 1.7 when compared to the ET measured in 2015 during this period. The Root Mean Square Error (RMSE) indicates that on average the EC_{ET} for 2016 is 1.76 mm d^{-1} higher than the EC_{ET} for 2015. While the result of the ANOVA test at the 95 % confidence level reaffirms that there is a significant difference between the 2015 and 2016 EC_{ET}.

Table 14 Statistical comparison of ET_0 and EC_{ET} for 2015 and 2016

	ET_0 2015	EC_{ET} 2015	ET_0 2016	EC_{ET} 2016
Total	337,72	203,83	357,55	338,51
Average	2,99	1,80	3,16	3,00
Max	5,65	4,97	5,80	5,45
Min	0,41	0,46	0,27	0,77
Median	2,65	1,08	3,10	2,88
Variance	1,17	1,56	1,07	1,37
Std Dev	1,08	1,25	1,03	1,17
RMSE				1,76
ANOVA p value				0,00

DRAFT

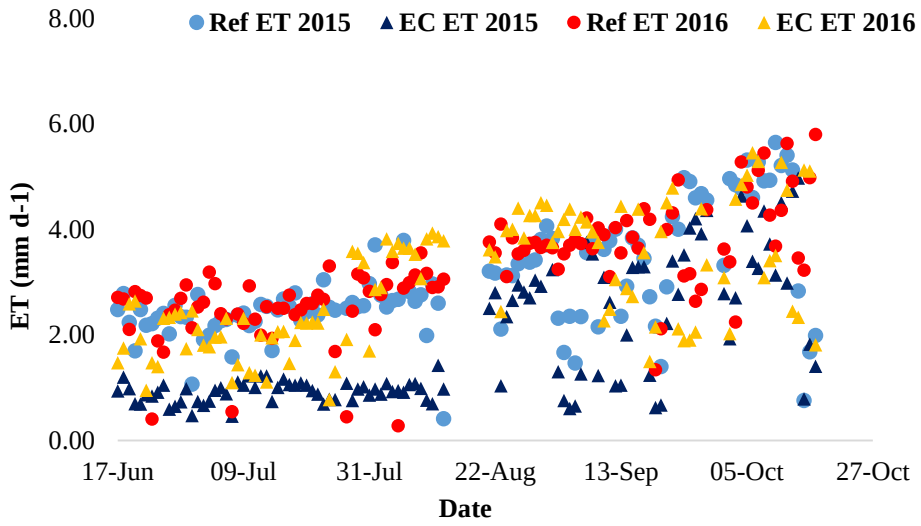

Figure 72 A comparison of ET_0 and EC_{ET} for 2015 and 2016

Summary

In order to understand the inter annual variations seen in the measured ET, the climatic factors which drive ET were analyzed to identify any specific trends which may have contributed to the differences in the 2015 and 2016 EC_{ET}. As ET is mainly a physical process driven by radiation and the vapour pressure deficit (VPD) (Penman, 1948; Xu et al., 2014), measurements of these variables for 2015 and 2016 during the period 17th June to 17th October, were compared. These are shown in Figure 73 to Figure 75 , respectively. In addition, average temperature measurements during the aforementioned period are shown in Figure 76.

The results presented indicate that the daily ET measured at Site 2 is higher than at Site 1 for both 2015 and 2016. This is largely due to the influence of climatic factors during this period of investigation. According to Xu et al. (2014) ET is generally positively correlated to climatic factors (Radiation, VPD and temperature) and responds rapidly to variations in radiation and VPD (Monteith, 1965). As shown in Figure 73 to Figure 75, the values for these climatic factors are generally higher for Site 2.

In addition to climatic factors, biotic factors such as leaf area index (LAI) and stomatal conductance of the canopy, *inter alia*, play a substantial role in driving ET (Monteith, 1965; Bernier et al., 2006; Pejam et al., 2006; Bucci et al., 2008). Assuming that the stomatal conductance of the canopy at both sites is similar (tree species and age of the vegetation is similar for both sites), the greater canopy coverage for Site 2, as well as the higher values associated with the climatic variables at this site, subsequently resulted in higher daily ET.

DRAFT

While the intra-annual variability for 2016 EC_{ET} follows a similar trend to the 2015 EC_{ET}. There is a significant increase in EC_{ET} for 2016. Comparisons between the 2015 and 2016 Solar Radiation, Net Radiation, VPD and Temperature shown in Figures 5 to 8, illustrate that in general there are no significant differences in the daily Solar Radiation, Net Radiation and temperature for 2015 and 2016. However, the daily VPD is significantly higher in 2016. These observations are reaffirmed by the results of the ANOVA test at the 95 % confidence interval, shown in **Table 15**. While there is a significant increase in the VPD for 2016, the 2016 VPD is generally only higher than the 2015 VPD at Site 2.

Table 15

	Solar Radiation	Net Radiation	VPD	Temperature
ANOVA p value	0.61	0.32	0.00	0.94

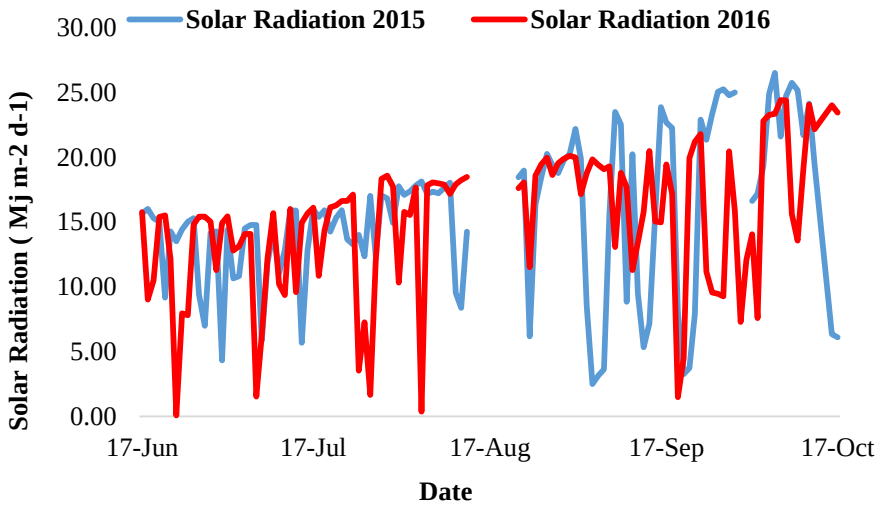

Figure 73 A comparison of Solar Radiation for 2015 and 2016 during the period 17th June to 17th October

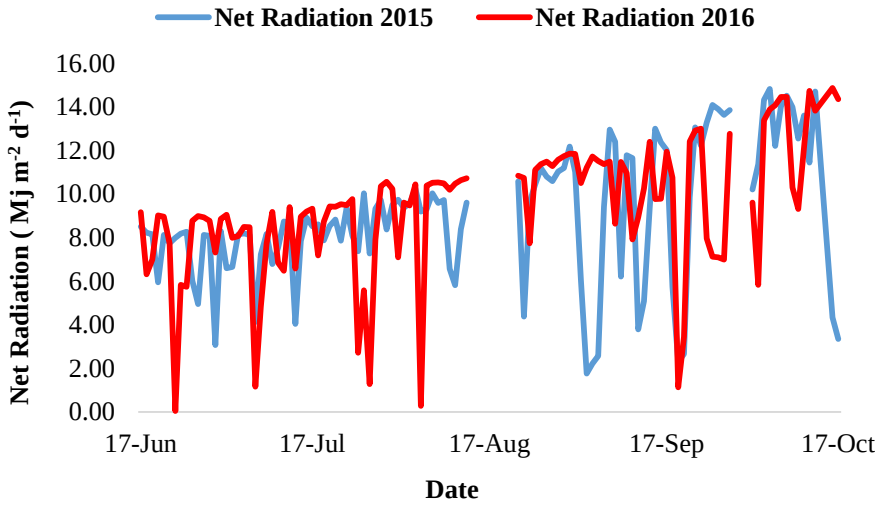

Figure 74 A comparison of Net Radiation for 2015 and 2016 during the period 17th June to 17th October

With respect to the increasing rates of ET for 2016, the absolute difference in EC_{ET} at Site 2 is 53.6 mm. While the absolute difference in EC_{ET} at Site 1 is 80.07 mm. Climatic and biotic factors are generally the factors which control ET, however, during periods of water stress, soil water content becomes the main controlling factor of ET (Alfieri et al., 2007). The EC system was situated at Site 1 during the dry season (Winter) and then moved to Site 2 just prior to the beginning of the wet season (Spring).

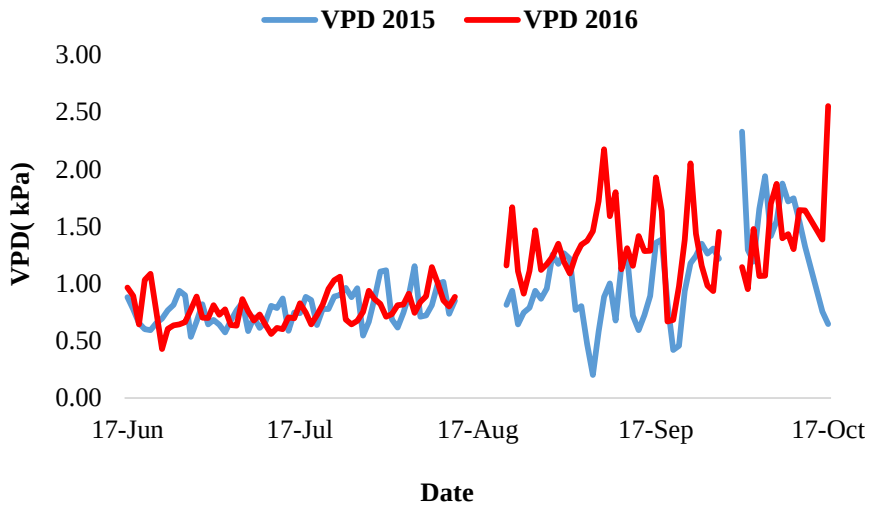

Figure 75 A comparison of VPD for 2015 and 2016 during the period 17th June to 17th October

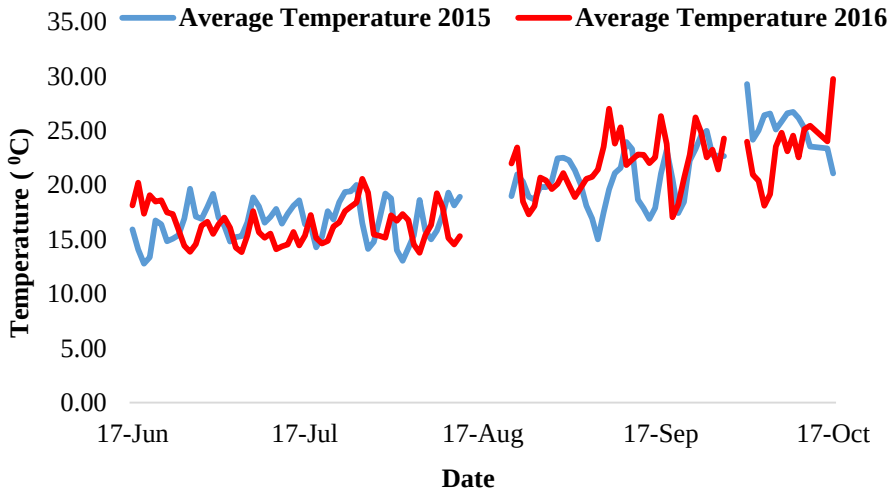

Figure 76 A comparison of temperature for 2015 and 2016 during the period 17th June to 17th October

During the wet season ET is limited by available energy, while during the dry season ET is limited by water availability. The greater study area is currently experiencing one of the most severe droughts in decades. While the study site is situated within a riparian environment, water availability is quite variable along the portion of river that was study and has been further impacted by the drought.

During the measurement period in 2015 there were a few minor precipitation events which would have contributed to soil water recharge. However, from November 2015 to October 2016 there were a few heavy precipitation events which would have contributed a much higher volume of water to soil water recharge. Considering ET is controlled by soil water availability during periods of water stress, the increase in soil moisture *via* these precipitation events, could have potentially resulted in the higher EC_{ET} for 2016, especially at Site 1.

Summary

In this study an Eddy Covariance system was installed within the riparian zone along a portion of the Groot Letaba River, in order to quantify the ET during the 2015 and 2016 dry season. These measurements are to be used to validate ET estimates acquired from implementing the SEBS model. In this manuscript we have reported on the intra/inter annual variability of ET for our study area.

In general, the study area experiences two distinct seasons, a dry period in winter and a wet season in summer. Consequently, the system experiences both water limiting and energy limiting periods during the year which influences ET rates. Daily ET measured at Site 2 was shown to be higher than at Site 1 for both 2015 and 2016. This was largely attributed to the influence of climatic and biotic factors during the period of investigation.

DRAFT

REFERENCES

Alidoost, F, Sharifi, MA and Stein. A. 2015. Region and pixel-based image fusion for disaggregation of actual evapotranspiration. International Journal of Image and Data Fusion. DOI: 10.1080/19479832.2015.1055834.

Allen, R, Bastiaanssen, W and Waters, R. 2002. SEBAL Expert Training Tutorial, August 19-23, 2002. Personal communication. The Idaho Department of Water Resources, Idaho State University.

Allen, R, Tasumi, M, Morse, A, Trezza, R, Wright, J, Bastiaanssen, W, Kramber, W, Lorite, I and Robison, C. 2007. Satellite-Based Energy Balance for Mapping Evapotranspiration with Internalized Calibration METRIC—Applications. Journal of Irrigation and Drainage Engineering 1334: 395–406.

Allen, RG, Pereira LS, Raes D and Smith, M. 1998. Crop evaporation: Guidelines for computing crop water requirements, FAO Irrigation and Drainage Paper no. 56. Food and Agriculture Organization of the United Nations, Rome, Italy. ISBN 92-5-104219-5.

Allen, RG, Pereira, LS, Smith, M, Raes, D and Wright JL. 2005b. FAO-56 dual crop coefficient method for estimating evaporation form soil and application extensions. Journal of Irrigation and Drainage Engineering ASCE 1311:2–13.

Allen, RG, Pruitt, WO, Wright, JL, Howell, TA, Ventura, F, Snyder, R, Itenfisu ,D, Steduto, P, Berengena, J, Yrisarry, JB, Smith, M, Pereira, LS, Raes, D, Perrier, A, Alves, I, Walter, I and Elliott, R. 2006. A recommendation on standardized surface resistance for hourly calculation of reference ETo by the FAO56 Penman-Monteith method. Agric. Water Management 81: 1–22.

Arthington, A.H., et al., 2006. The challenge of providing environmental flow rules to sustain river ecosystems. Ecological Applications, 16 (4), 1311 – 1318.

Bhattarai, N, Quackenbush, LJ, Dougherty, M and Marzen, LJ 2015. A simple Landsat–MODIS fusion approach for monitoring seasonal evapotranspiration at 30 m spatial resolution. International Journal of Remote Sensing 361: 115-143.

Bierkens, MFP, Finke, PA and Willigen, DE. 2000. Upscaling and Downscaling Methods for Environmental Research. Dordrecht: Wageningen University and Research Centre. Kluwer Academic.

Boroto, J and Gorgens, AHM. 2003. Limpopo River: an overview of alternative methods for estimating transmission losses. Hydrology of Mediterranean and Semiarid regions. Proc. Montpellier Conference. IAHS Publ. 278.

Cataldo, J, Behr, C, Montalto, F and Pierce, RJ. 2010. Prediction of Transmission Losses in Ephemeral Streams, Western U.S.A. The Open Hydrology Journal 4: 19-34.

Cooper, H.H. and Jacob, C.E. (1946). A generalized graphical method for evaluating formation constants and summarizing well field history. American Geophysical Union Transactions 27: 526-534.

Costa, AC, Foerster, S, de Araujo, JC and Bronstert, A. 2013. Analysis of channel transmission losses in a dryland river reach in north-eastern Brazil using streamflow series, groundwater level series and multi-temporal satellite data. Hydrological Processes 27: 1046–1060.

Costelloe, JF, Grayson, RB, Argent, RM, and McMahon, TA. 2003. Modelling the flow regime of an arid zone floodplain river, Diamantina River, Australia. Environmental Modelling and Software 18: 693–703.

Department of Water Affairs and Forestry. 2006. Letaba River System Annual Operating Analysis. DWAF Report No: WMA 02/000/00/0406.

DWA, 2011 DEVELOPMENT OF OPERATTNG RULES FOR THE INTEGRATEON OF THE BLYDE AND OLIFANTS RIVER SYSTEMS DWA REPORT NO.: P WMA O4/B60/00/8510

DWA 2013. Classification of Water Resources and Determination of the Resource Quality Objectives in the Letaba Catchment. Ecological Water Requirements. Prepared by: Rivers for Africa eFlows Consulting (Pty) Ltd. DWA Report, RDM/WMA02/00/CON/CLA/0313.

DWA, 2014. DEVELOPMENT OF A RECONCILIATION STRATEGY FOR THE LUVUVHU AND LETABA WATER SUPPLY SYSTEM: RECONCILIATION STRATEGY. Report No. P WMA 02/B810/00/1412/10

Everson CS., 2001. The water balance of a first order catchment in the montane grasslands of South Africa. Journal of Hydrology 241: 110-123.

Ghorbani, A, Mossivand, MA and Ouri, AE. 2012. Utility of the Normalised Difference Vegetation Index (NDVI) for land/canopy cover mapping in Khalkhal County (Iran). *Annals of Biological Research* 3(12):5494-5503.

Gokmen, M, Vekerdy, Z, Verhoef, A, Verhoef, A, Batelaan, O and Tol, C. 2012. Integration of soil moisture in SEBS for improving evapotranspiration estimation under water stress conditions. Remote Sens Environ 121: 261–274. DOI: 10.1016/j.rse.2012.02.003

Ha, W, Gowda, PH and Howell, TA. 2013. A review of downscaling methods for remote sensing-based irrigation management: Part I. Irrigation Science 31: 831–850.

Hacker, F. 2005. Model for Water Availability in Semi-Arid Environments WASA: Estimation of transmission losses by infiltration at rivers in the semi-arid Federal State of Ceara Brazil. MSc Thesis, University of Potsdam, Germany.

Heritage, GL, Moon, BP and Large, ARG. 2001. The February 2000 floods on the Letaba River, South Africa: an examination of magnitude and frequency. Koedoe 44 2: 1-6.

DRAFT

Hong, S. Hendrickx. JMH and Borchers. B. 2011. Down-scaling of SEBAL derived evapotranspiration maps from MODIS 250 m to Landsat 30 m scales. International Journal of Remote Sensing 3221: 6457–6477.

Hughes, D.A. 1999. Towards the incorporation of magnitude-frequency concepts into the Building Block Methodology used for quantifying ecological flow requirements of South African rivers. Water SA 25 (3): 279-284.

Hughes, DA and Sami, K. 1992. Transmission losses to alluvium and associated moisture dynamics in a semi-arid ephemeral channel system in southern Africa. Hydrological Processes 6: 45-53.

Hughes, DA, Mallory, SJL and Louw D. 2008. Methods and software for the real-time implementation of the ecological reserve-explanations and user manual. WRC Report 1582/1/08.

Hughes, D.A. 2001. Providing hydrological information and data analysis tools for the determination of ecological instream flow requirements for South African rivers. Journal of Hydrology 241: 140-151.

Jarmain, C, Everson, CS, Savage, MJ, Mengistu, MG, Clulow, AD, Walker, S and Gush, MB, 2009a. Refining tools for evaporation monitoring in support of water resources management. WRC Report No 1567/1/08. ISBN 978-1-77005-798-2.

Katambara, Z and Ndiritu, JG. 2010. A hybrid conceptual-fuzzy inference streamflow modelling for the Letaba River system in South Africa. Physics and Chemistry of the Earth 3513-14: 582-595.

King, J.M. and M.D. Louw. 1998. Instream flow assessments for regulated rivers in South Africa using the Building Block Methodology. Aquatic Ecosystem Health and Management 1: 109-124.Kongo et al. 2007,

Kruseman, G.P. and De Ridder, N.A. (1994). Analysis and Evaluation of Pumping Test Data. 2nd ed.

Lane, LJ. 1990. Transmission losses, flood peaks and groundwater recharge. Hydraulics/hydrology of arid lands H2AL: proceedings of the International Society of Civil Engineers, Hydraulics Division 1990.

Lange, J. 2005. Dynamics of transmission losses in a large arid stream channel. Journal of Hydrology 306: 112–126.

Li, Y, Zhou, J, Wang, H, Li, D, Jin, R, Zhou, Y and Zhou, Q. 2015. Integrating soil moisture retrieved from L-band microwave radiation into an energy balance model to improve evapotranspiration estimation on the irrigated oases of arid regions in northwest China. Agricultural and Forest Meteorology 214-215: 306–318.

Liang, S. 2004. Quantitative Remote Sensing of Land Surfaces. New York: JohnWiley and Sons.

DRAFT

Liou, Y and Kar, SK. 2014. Evapotranspiration Estimation with Remote Sensing and Various Surface Energy Balance Algorithm: A Review. Energies 7: 2821-2849.

Loke, M.H. 1999. Electrical imaging surveys for environmental and engineering studies: A practical guide to 2-D and 3-D surveys. www.terrajp.co.jp/lokenote.pdfMalan and Day, 2003

McLoughlin, C., A. Deacon, H. Sithole & T. Gyedu-Ababio. 2011. History, rationale, and lessons learned: Thresholds of potential concern in Kruger National Park river adaptive management. Koedoe 53(2): 1-27

Molle et al., 2010: Molle, F, Wester, P and Hirsch, P. 2010. River basin closure: Processes, implications and responses. Agricultural Water Management 97: 569-577.

Moon, B.P. and G.L. Heritage. 2001. The contemporary geomorphology of the Letaba River in the Kruger National Park. Koedoe 44 (1): 45-55O'Keeffe, 2008

Pardo et al., 2014: Pardo, N, Sanchez, LM, Timmermans, J, Su, Z, Perez, IA and Garcia, MA. 2014. SEBS validation in a Spanish rotating crop. Agricultural and Forest Meteorology 195-196: 132-142.

Poff, N.L., et al., 2009. The ecological limits of hydrological alteration (ELOHA): a new framework for developing regional environmental flow standards. Freshwater Biology, 55 (1), 147 – 170.

Pollard, S and du Toit, D. 2011b. Towards the sustainability of freshwater systems in South Africa: An exploration of factors that enable and constrain meeting the ecological Reserve within the context of Integrated Water Resources Management in the catchments of the lowveld. WRC Report No K8/1711.

Pollard, S and du Toit D. 2011a. Towards Adaptive Integrated Water Resources Management in Southern Africa: The Role of Self-organisation and Multi-scale Feedbacks for Learning and Responsiveness in the Letaba and Crocodile Catchments. Water resources management 25 15: 4019-4035.

Pollard et al. 2012 through a historical contextual assessment of compliance

Ramsey, RD, Wright Jr, DL and McGinty C. 2004. Enhanced Thematic Mapper to Monitor Vegetation Cover in Shrub-Steppe Environments. Geocarto International 19(2): 39-47.

Riddell, ES, Pollard, SR, Mallory, S and Sawunyama, T. In press. A methodology for historical assessment of compliance with environmental water allocations: Lessons from the Crocodile East River, South Africa. Hydrological Sciences Journal.

Robinson et al., 2008: Robinson, DA, Campbell, CS, Hopmans, JW, Hornbuckle, BK, Jones, SB, Knight, R, Ogden, F, Selker, J, Wendroth, O. 2008. Soil moisture measurement for ecological and hydrological watershed-scale observatories: a review. Vadose Zone Journal 7: 358-389.

DRAFT

Santos, C, Lorite, IJ, Tasumi, M, Allen, RG and Fereres, E. 2008. Integrating satellite-based evapotranspiration with simulation models for irrigation management at the scheme level. Irrigation Science 263: 277-288.

Sawunyama, T and Hughes, DA. 2010. Using satellite-based rainfall data to support the implementation of environmental water requirements in South Africa. Water SA 364.

Seneviratne, SI, Luthi, D, Litschi, M and Schar, C. 2006. Land–atmosphere coupling and climate change in Europe. Nature 443: 205–209.

Shanafield, M and Cook, PG. 2014. Transmission losses, infiltration and groundwater recharge through ephemeral and intermittent streambeds: A review of applied methods. Journal of Hydrology 511: 518–529.

Singh, RK, Senay, GB, Velpuri, NM, Bohms, S and Verdin, JP, 2014b. On the Downscaling of Actual Evapotranspiration Maps Based on Combination of MODIS and Landsat-Based Actual Evapotranspiration Estimates. Remote Sensing 6: 10483-10509.

Spiliotopolous, M, Adaktylou, N, Loukas, A, Michalopoulou, H, Mylopoulos, N and Toulios, L. 2013. A spatial downscaling procedure of MODIS derived actual evapotranspiration using Landsat images at central Greece. Proceedings of SPIE - The International Society for Optical Engineering - August 2013. DOI: 10.1117/12.2027536.

State of the Rivers Report. 2001. Letaba and Luvuvhu Rivers Systems. WRC Report no.: TT 165/01. Water Research Commission, Pretoria, RSA

Su et al., 1999: Su, Z., Pelgrum, H. and Menenti, M. 1999. Aggregation effects of surface heterogeneity in land surface processes. Hydrology Earth System Science 34: 549-563.

Su, 2002: Su, Z. 2002. The Surface Balance Energy System SEBS for estimating turbulent heat fluxes. Hydrology and Earth System Sciences, 61: 85-99.

Uhlenbrook, S., J. Wenninger, S. Lorentz. 2005. What happens after the catchment caught the storm? Hydrological processes at the small, semi-arid Weatherley catchment, South Africa. Advances in Geosciences 2: 237-241.

Vlok, W. and J.S. Engelbrecht. 2000. Some aspects of the ecology of the Groot Letaba River in the Northern Province, South Africa. African Journal of Aquatic Science 25 (1): 76-83

Walters 1990: Walters, MO 1990. Transmission losses in arid regions. Journal of Hydraulic Engineering ASCE 116:129-38.

Wenninger, J., S. Uhlenbrook, S. Lorentz, C. Leibundgut. 2008. Identification of runoff generation processes using combined hydrometric, tracer and geophysical methods in a headwater catchment in South Africa. Hydrological Sciences Journal 53 (1): 65-80.

Water Research Commission WRC. 2001. State of the Rivers Report: Letaba and Luvuvhu Rivers Systems. WRC Report No TT 165/01, Water Research Commission, Pretoria, RSA.

DRAFT

Wu, X, Zhou, J, Wang, H, Li, Y and Zhong, B. 2014. Evaluation of irrigation water use efficiency using remote sensing in the middle reach of the Heihe river, in the semi-arid Northwestern China. Hydrol Process 2014. DOI: 10.1002/hyp.10365.

Yang, D, Chen, H and Lei, H. 2010. Estimation of evapotranspiration using a remote sensing model over agricultural land in the North China Plain. International Journal of Remote Sensing 3114: 3783–3798.

Zhuo, G, Ba, L, Ciren, P and Bu, L. 2014. Study on daily surface evapotranspiration with SEBS in Tibet Autonomous Region. Journal of Geographical Sciences 241: 113-128.

DRAFT

Appendix I Letaba River Transmissions Losses Maps

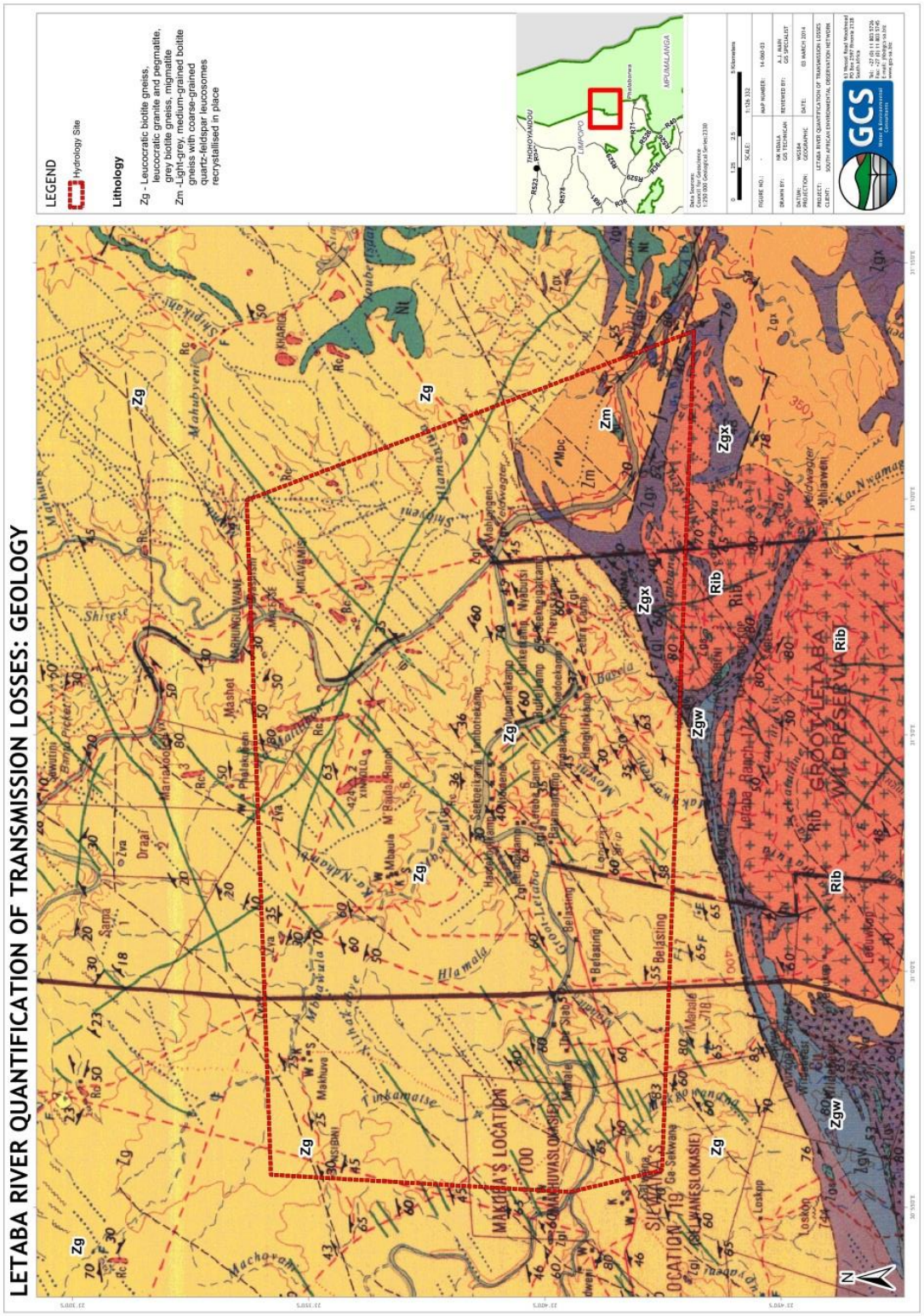

Geology of the site illustrating the dominant geology and dykes

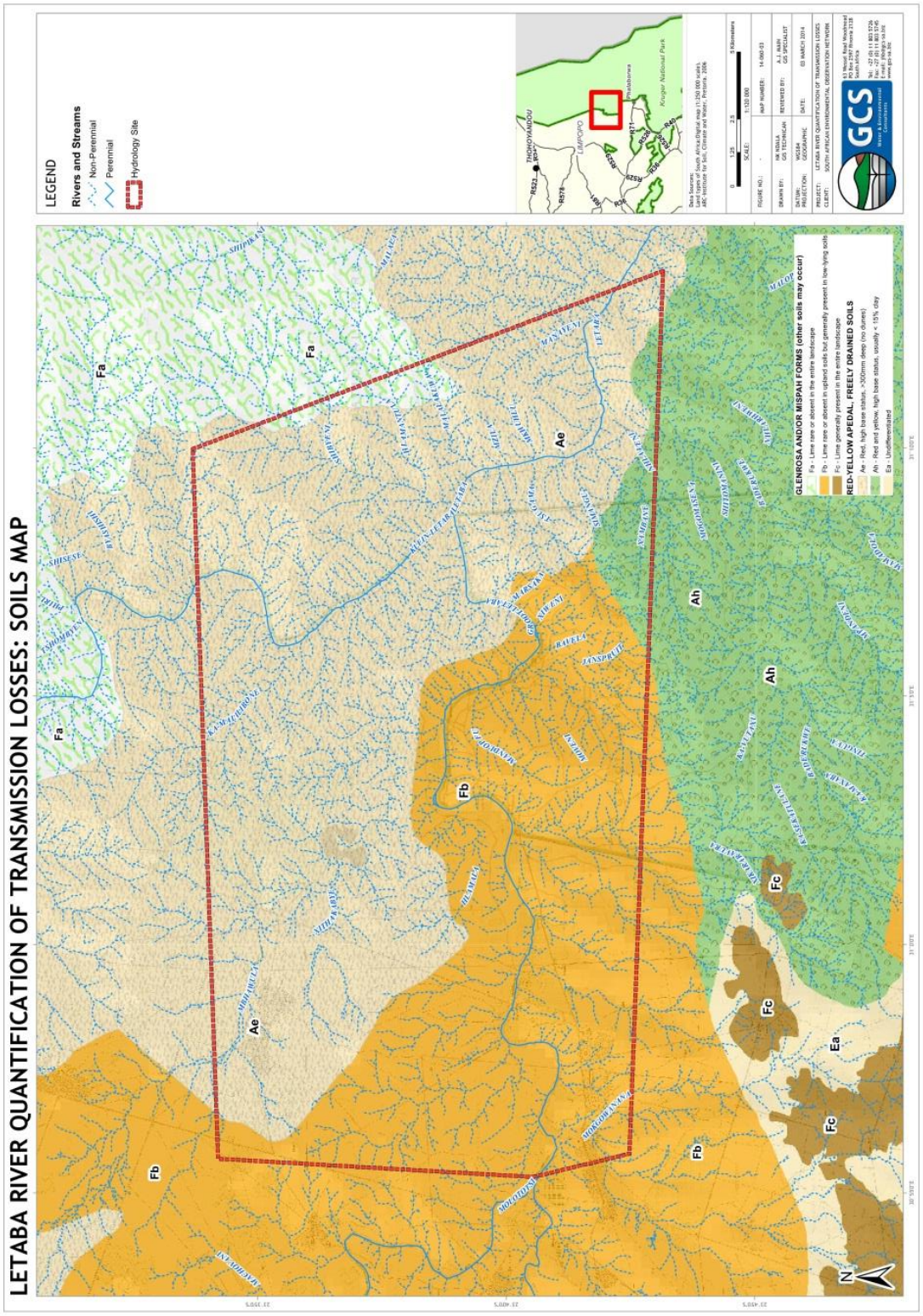

The dominant soil types and perennial/ non perennial streams

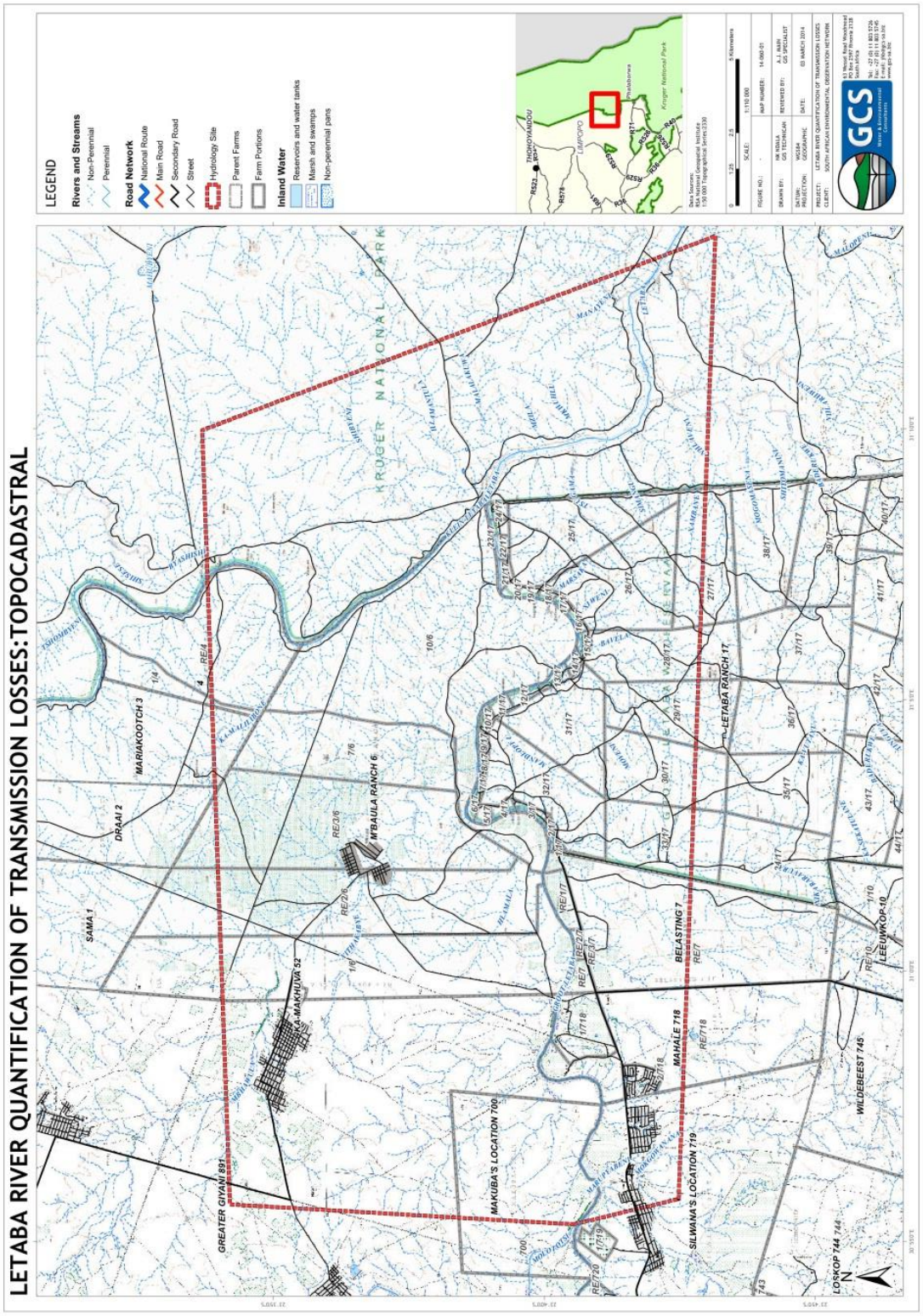

Topocadastral map of the study site delineating farms, ranches and rural communities.

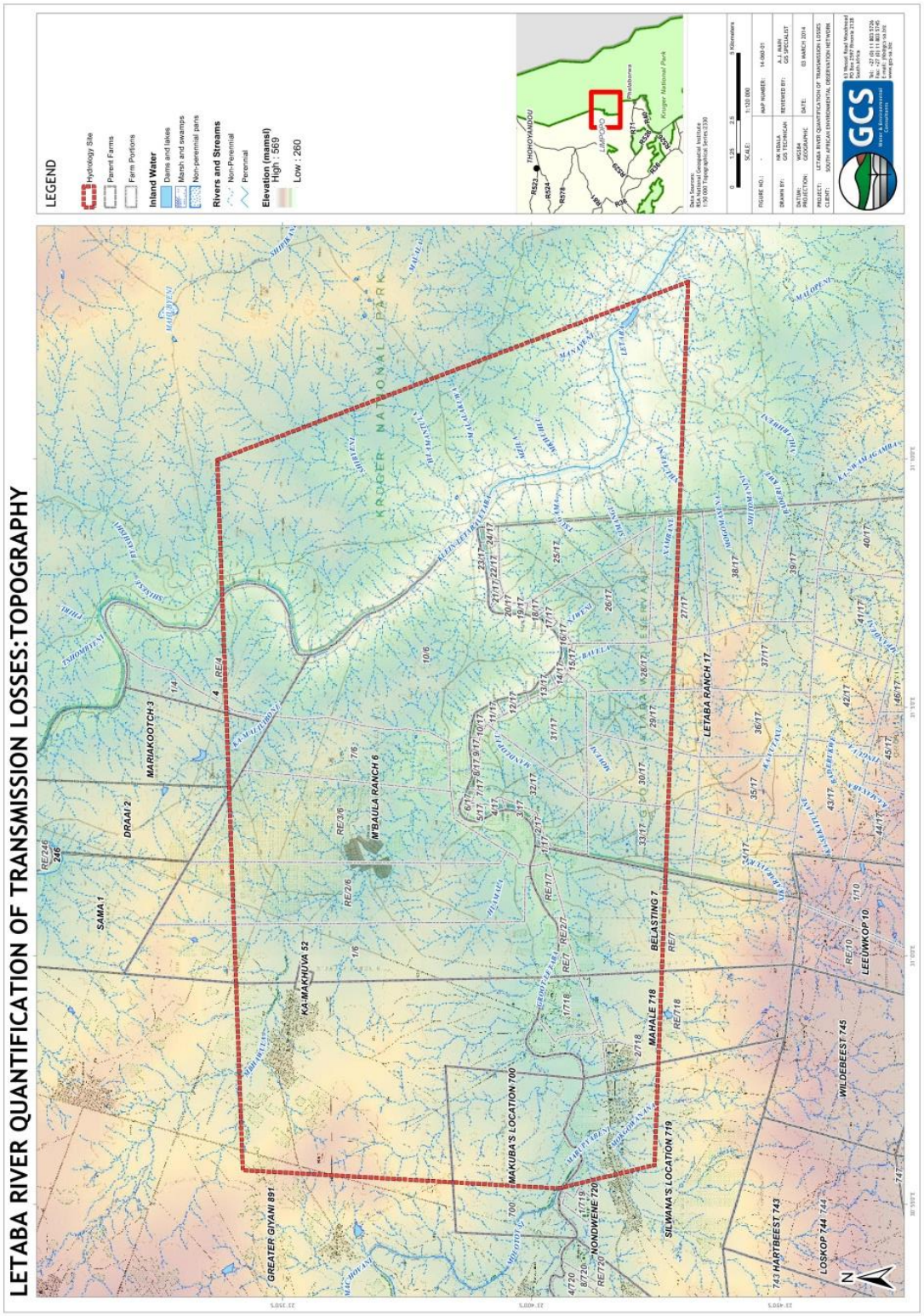

Topographical map of the study site

Appendix II Magnetic Surveys

Magnetic Surveys

Magnetic surveys are applied in many fields, such as geological mapping and geohydrological surveys. During a field campaign conducted in June 2015, magnetic surveys were used to characterise and confirm the presence of structural intrusions (or magnetic dykes) along the Letaba River. Geophysics transects conducted in 2014 using Electrical Resistivity Tomography (ERT) were resurveyed using a Geotron Proton Magnetometer (G5 Model). The magnetic survey data was coupled and overlaid with the geophysics survey data in order to verify the presence of possible dyke intrusions which were recorded during the ERT surveys.

DRAFT

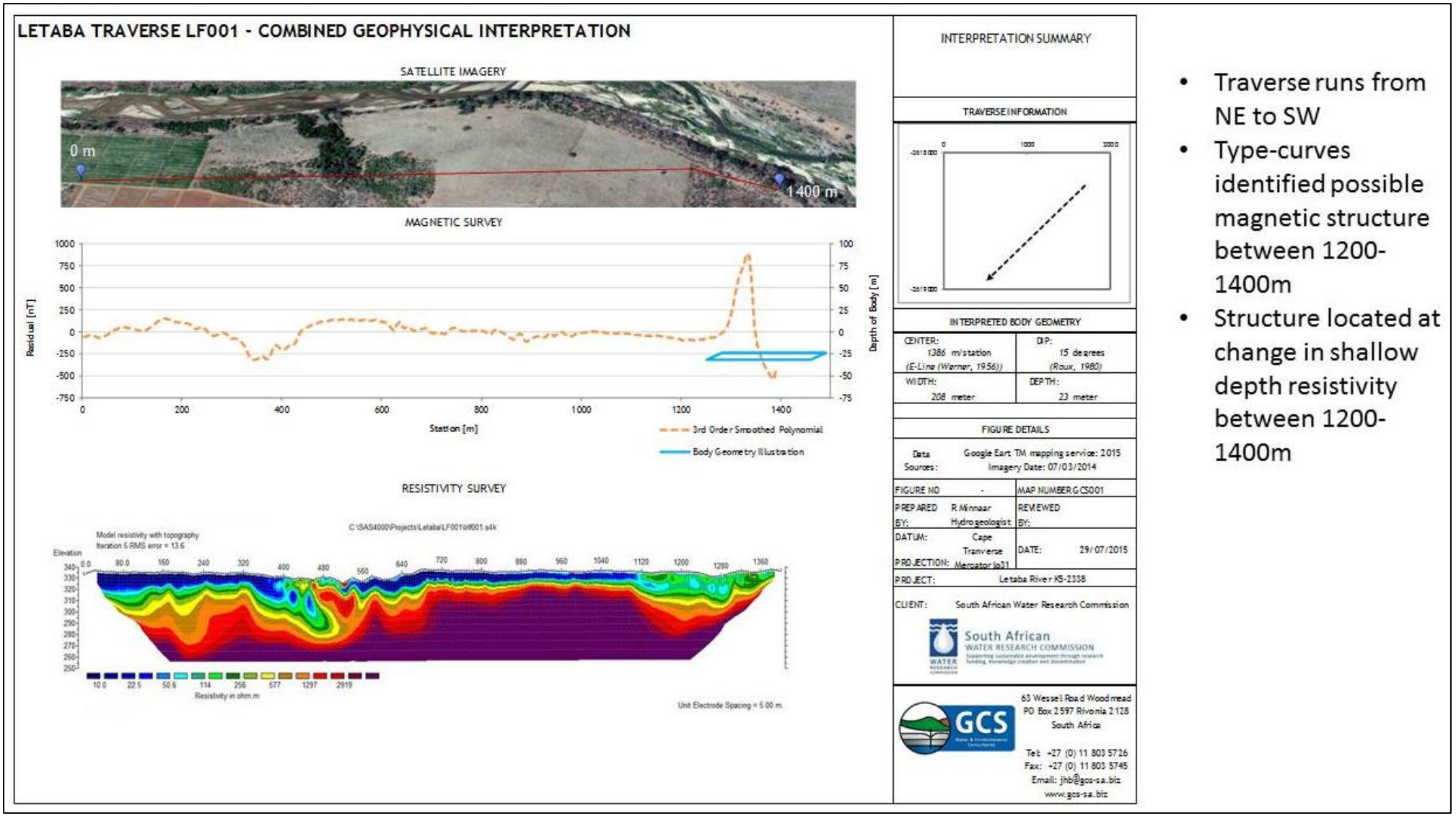

- Traverse runs from NE to SW
- Type-curves identified possible magnetic structure between 1200-1400m
- Structure located at change in shallow depth resistivity between 1200-1400m

Figure 77 Combined Geophysical Interpretation LF001

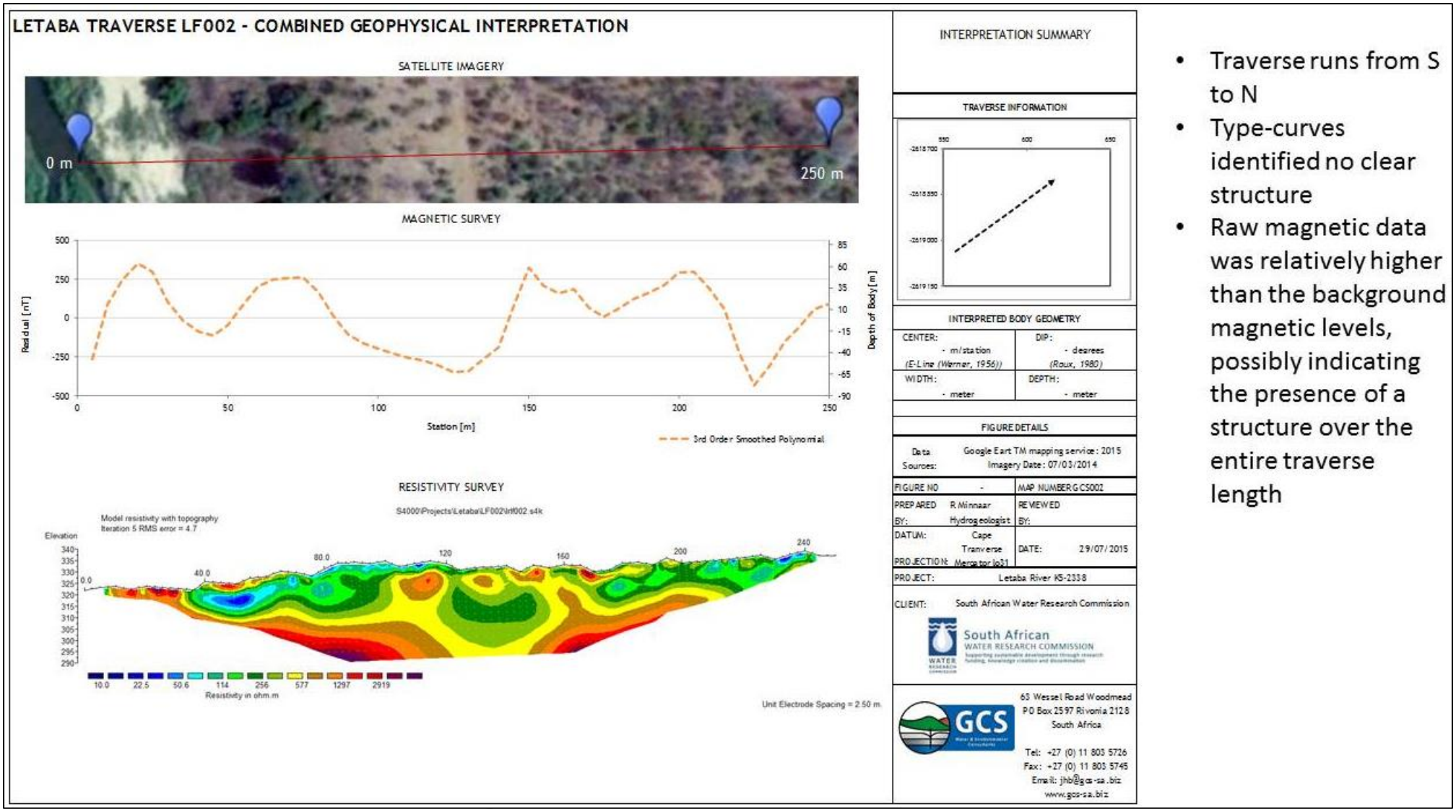

- Traverse runs from S to N
- Type-curves identified no clear structure
- Raw magnetic data was relatively higher than the background magnetic levels, possibly indicating the presence of a structure over the entire traverse length

Figure 78 Combined Geophysical Interpretation LF002

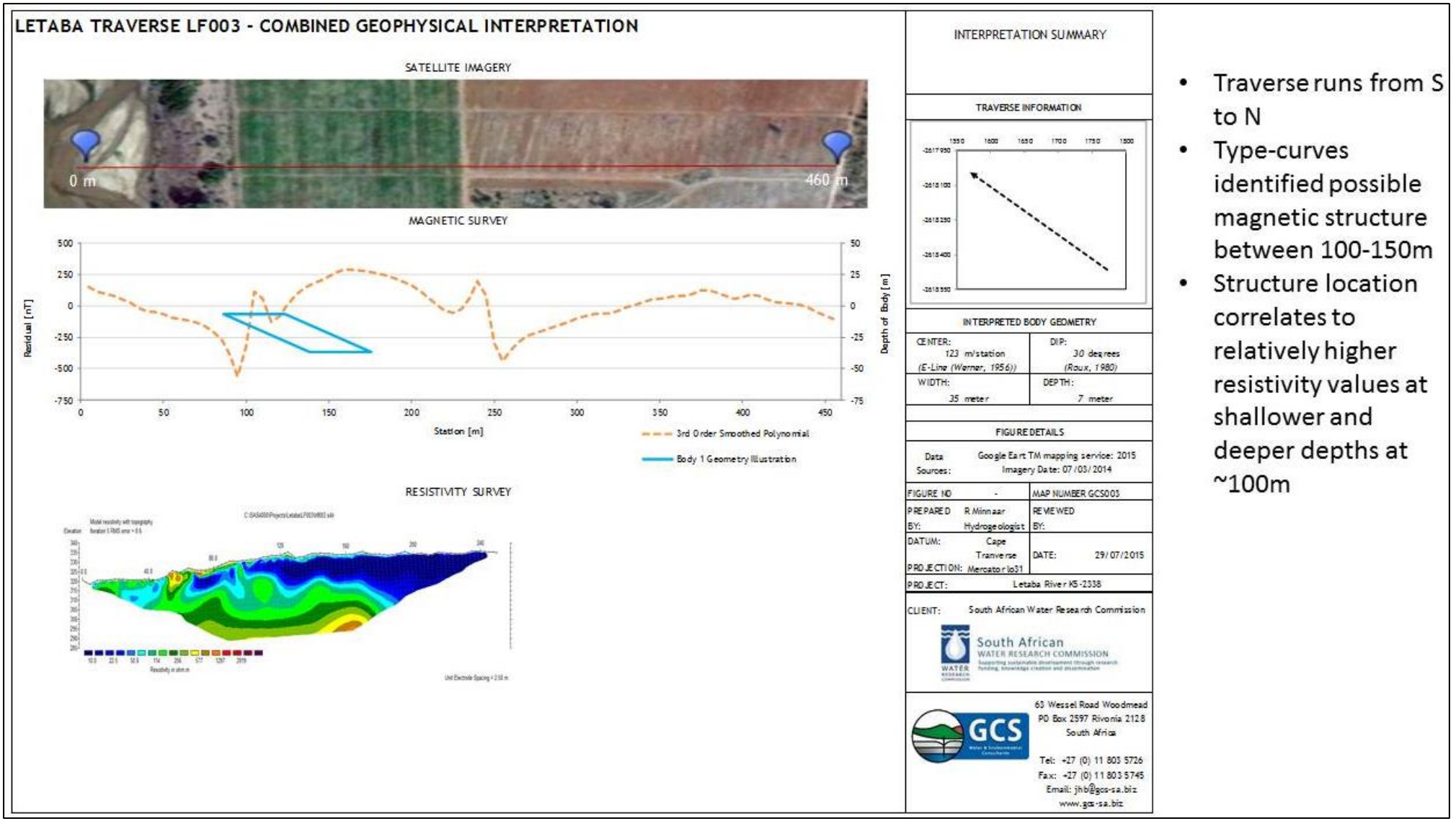

- Traverse runs from S to N
- Type-curves identified possible magnetic structure between 100-150m
- Structure location correlates to relatively higher resistivity values at shallower and deeper depths at ~100m

Figure 79 Combined Geophysical Interpretation LF003

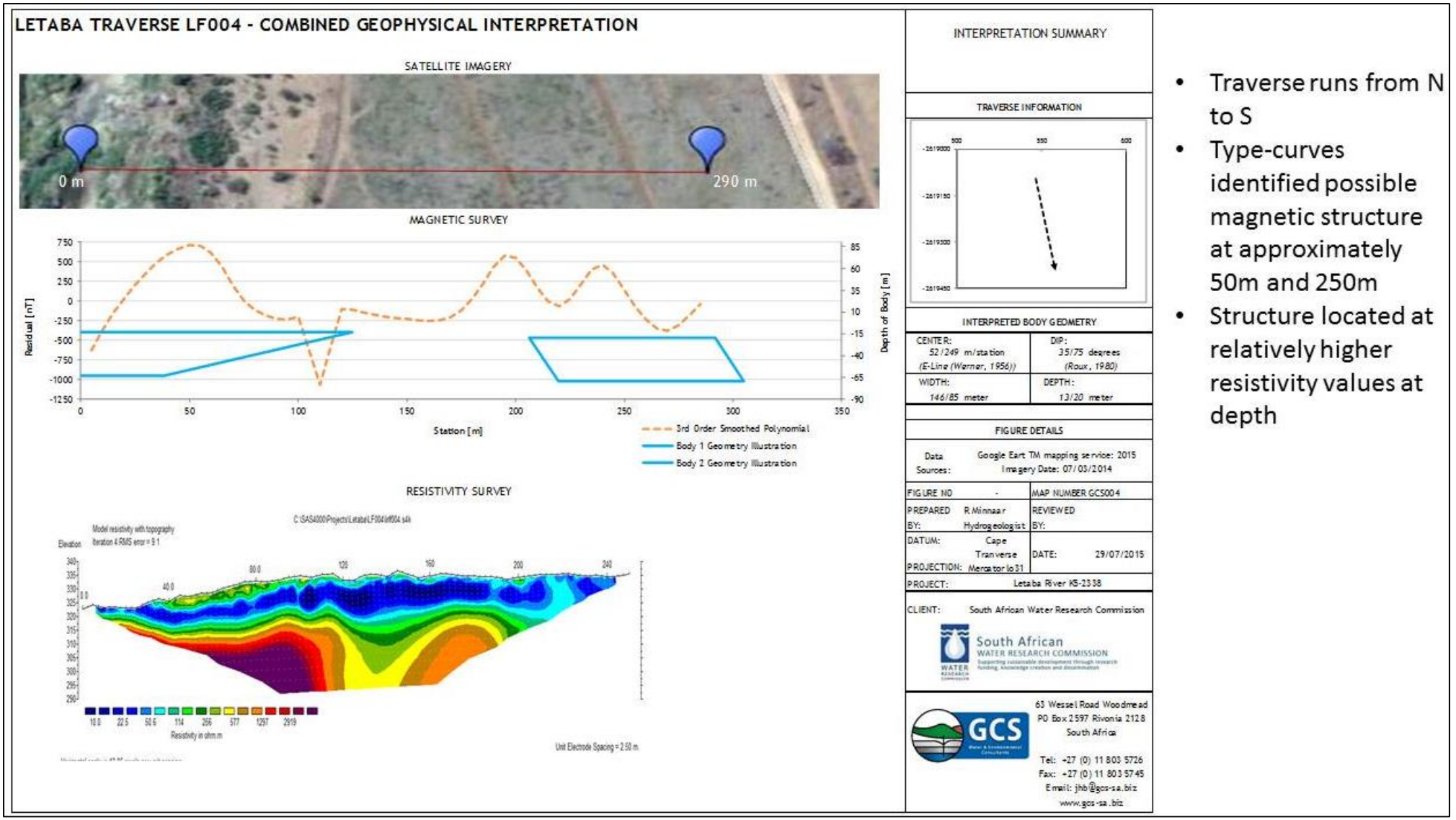

- Traverse runs from N to S
- Type-curves identified possible magnetic structure at approximately 50m and 250m
- Structure located at relatively higher resistivity values at depth

Figure 80 Combined Geophysical Interpretation LF004

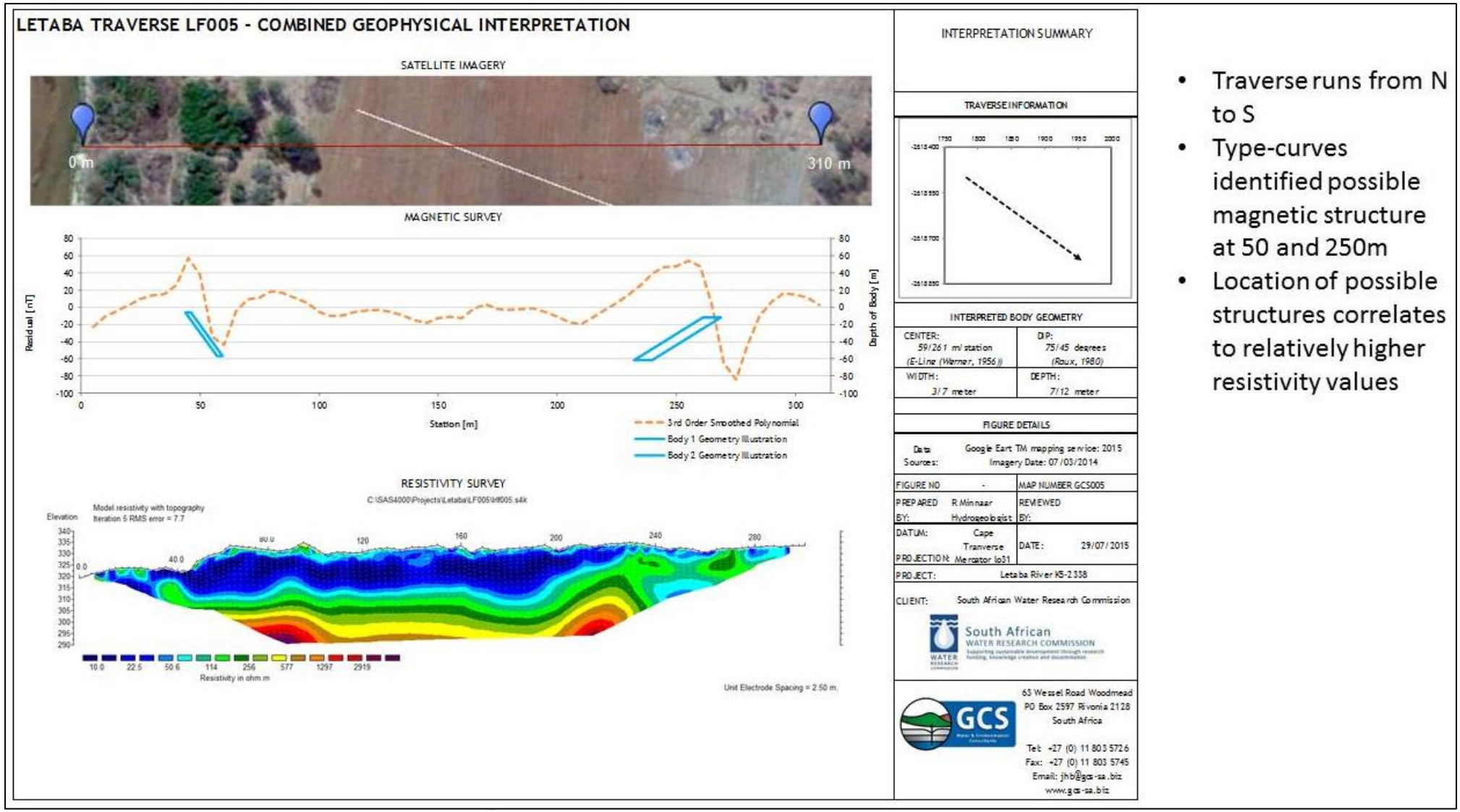

- Traverse runs from N to S
- Type-curves identified possible magnetic structure at 50 and 250m
- Location of possible structures correlates to relatively higher resistivity values

Figure 81 Combined Geophysical Interpretation LF005

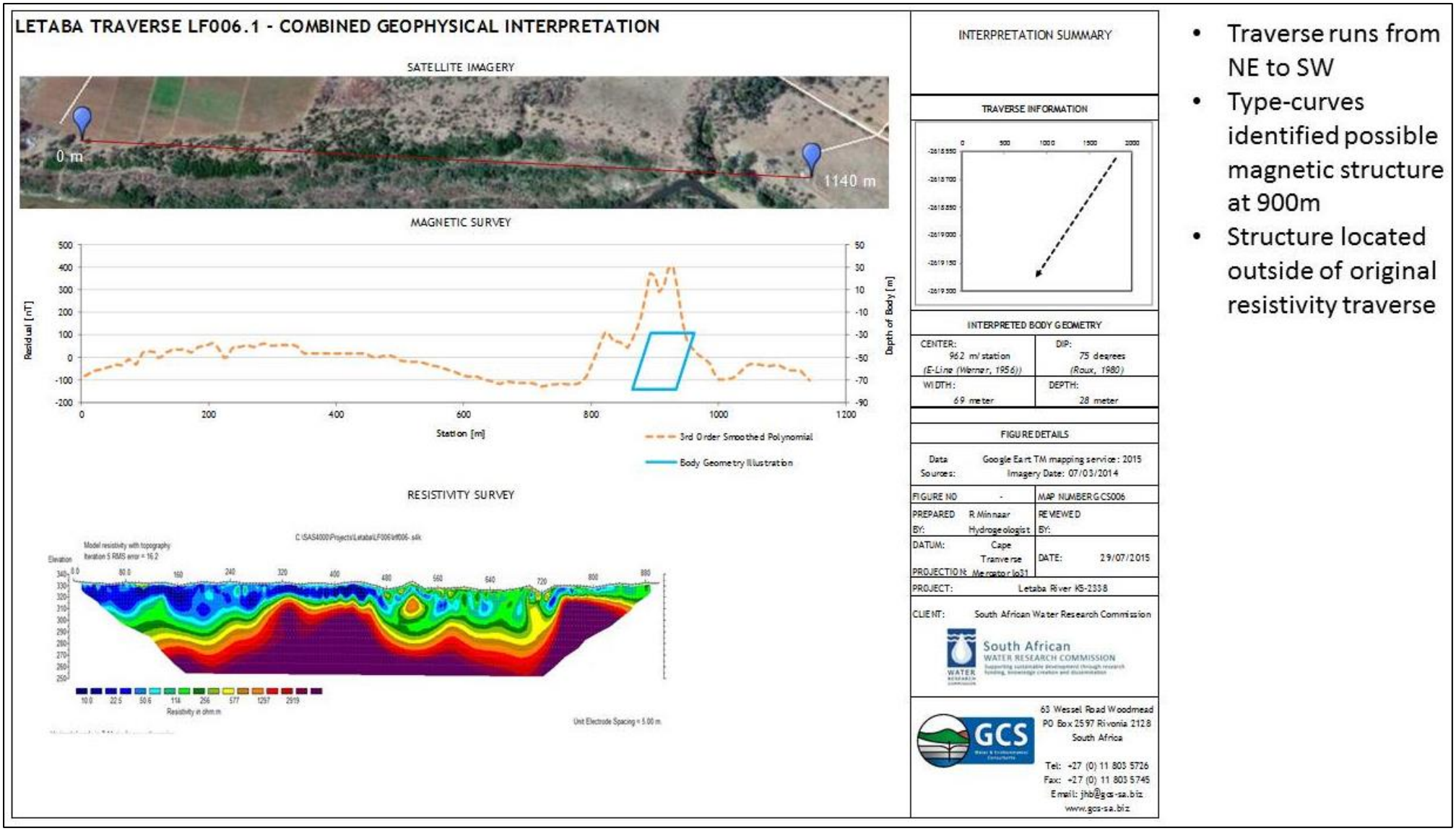

- Traverse runs from NE to SW
- Type-curves identified possible magnetic structure at 900m
- Structure located outside of original resistivity traverse

Figure 82 Combined Geophysical Interpretation LF006.1

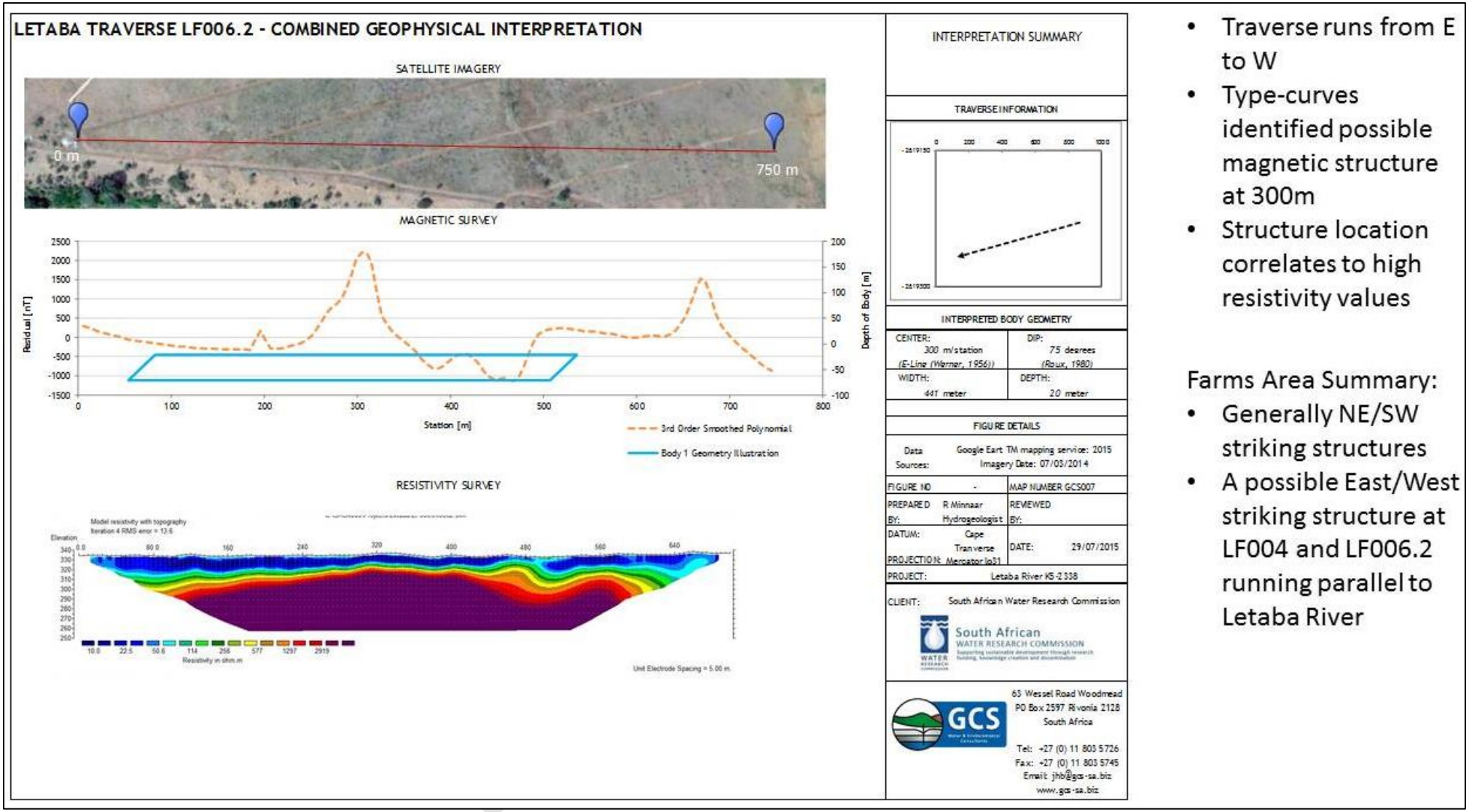

- Traverse runs from E to W
- Type-curves identified possible magnetic structure at 300m
- Structure location correlates to high resistivity values

Farms Area Summary:

- Generally NE/SW striking structures
- A possible East/West striking structure at LF004 and LF006.2 running parallel to Letaba River

Figure 83 Combined Geophysical Interpretation LF006.2

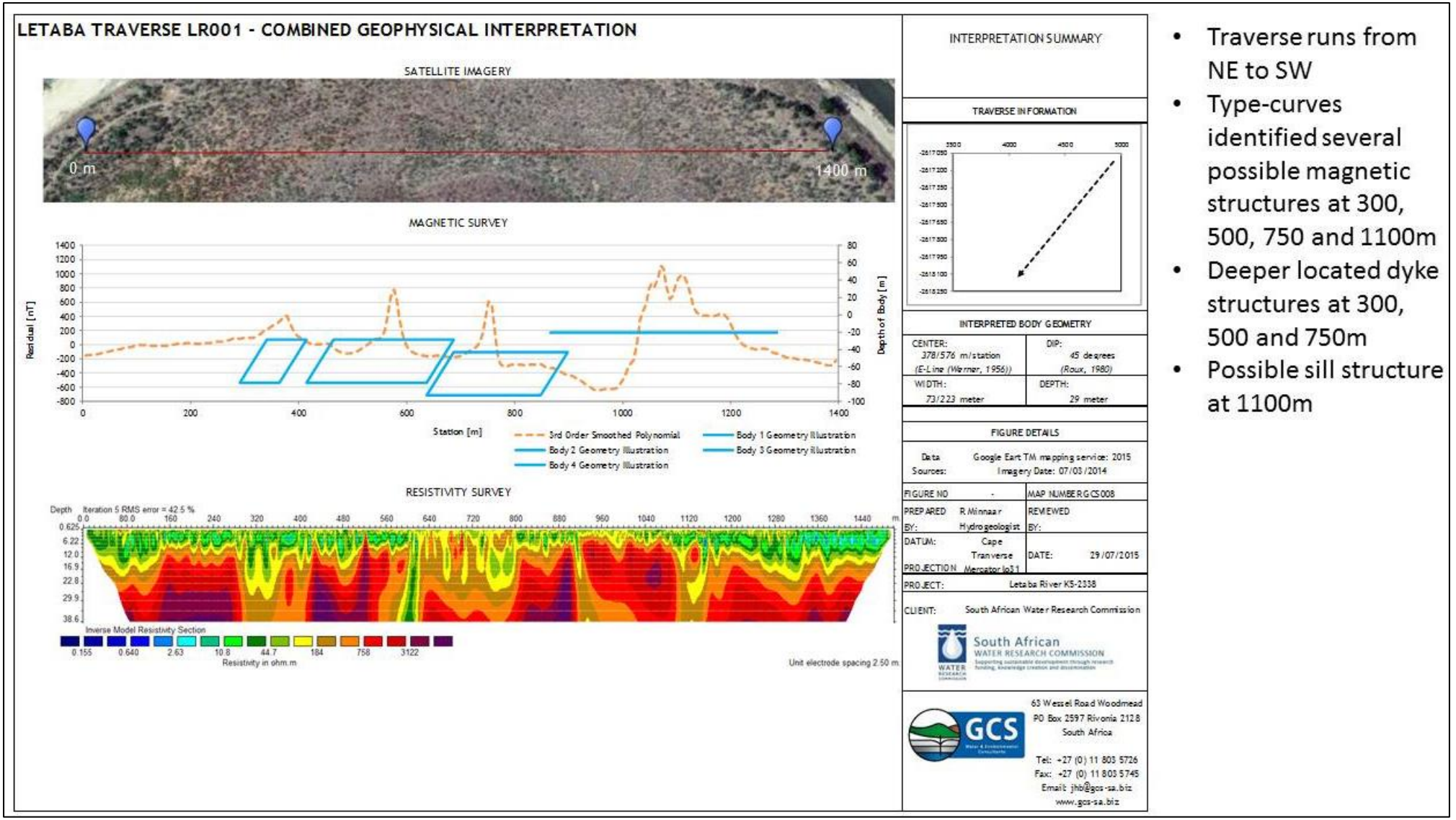

- Traverse runs from NE to SW
- Type-curves identified several possible magnetic structures at 300, 500, 750 and 1100m
- Deeper located dyke structures at 300, 500 and 750m
- Possible sill structure at 1100m

Figure 84 Combined Geophysical Interpretation LR001

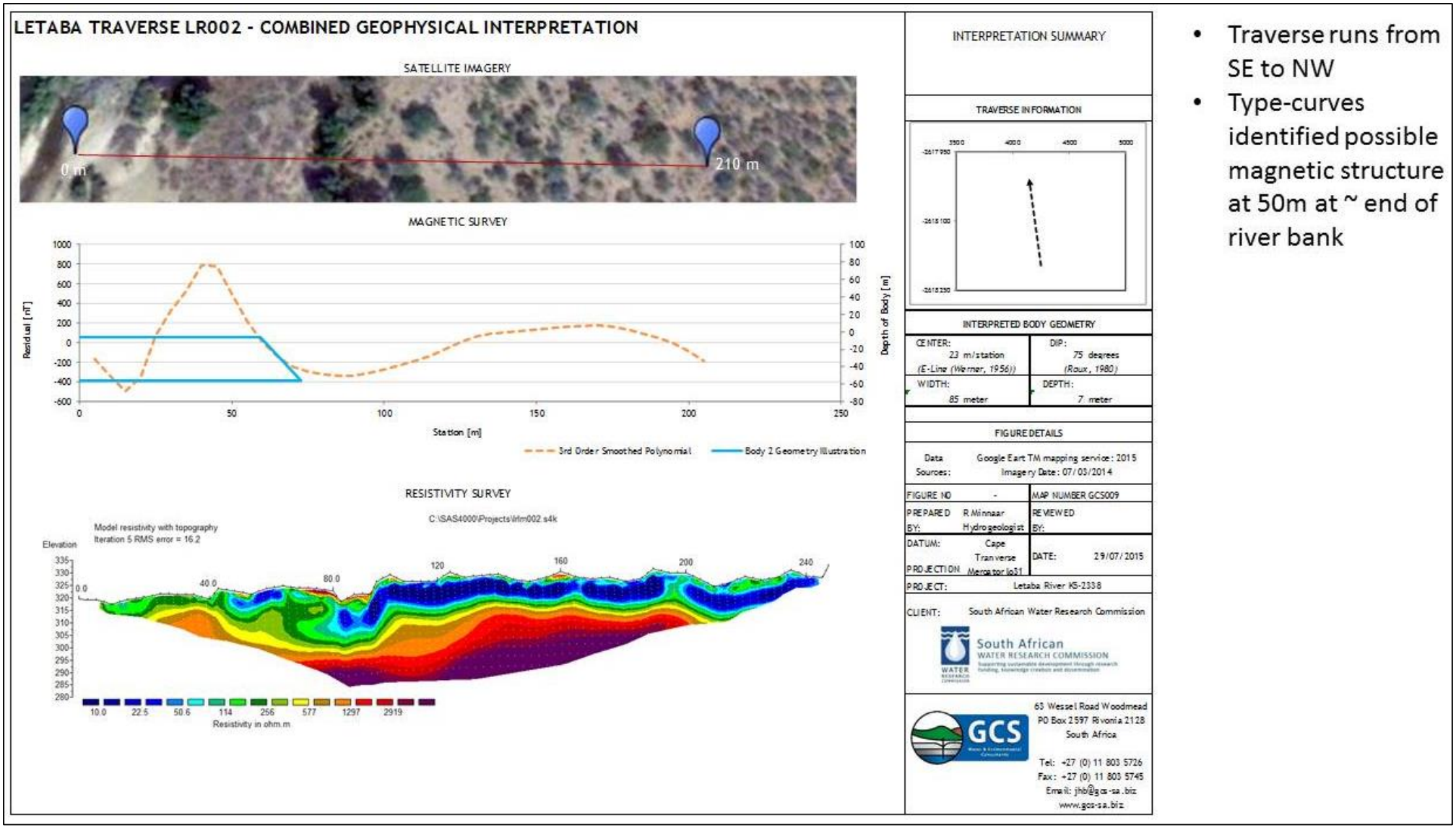

- Traverse runs from SE to NW
- Type-curves identified possible magnetic structure at 50m at ~ end of river bank

Figure 85 Combined Geophysical Interpretation LR002

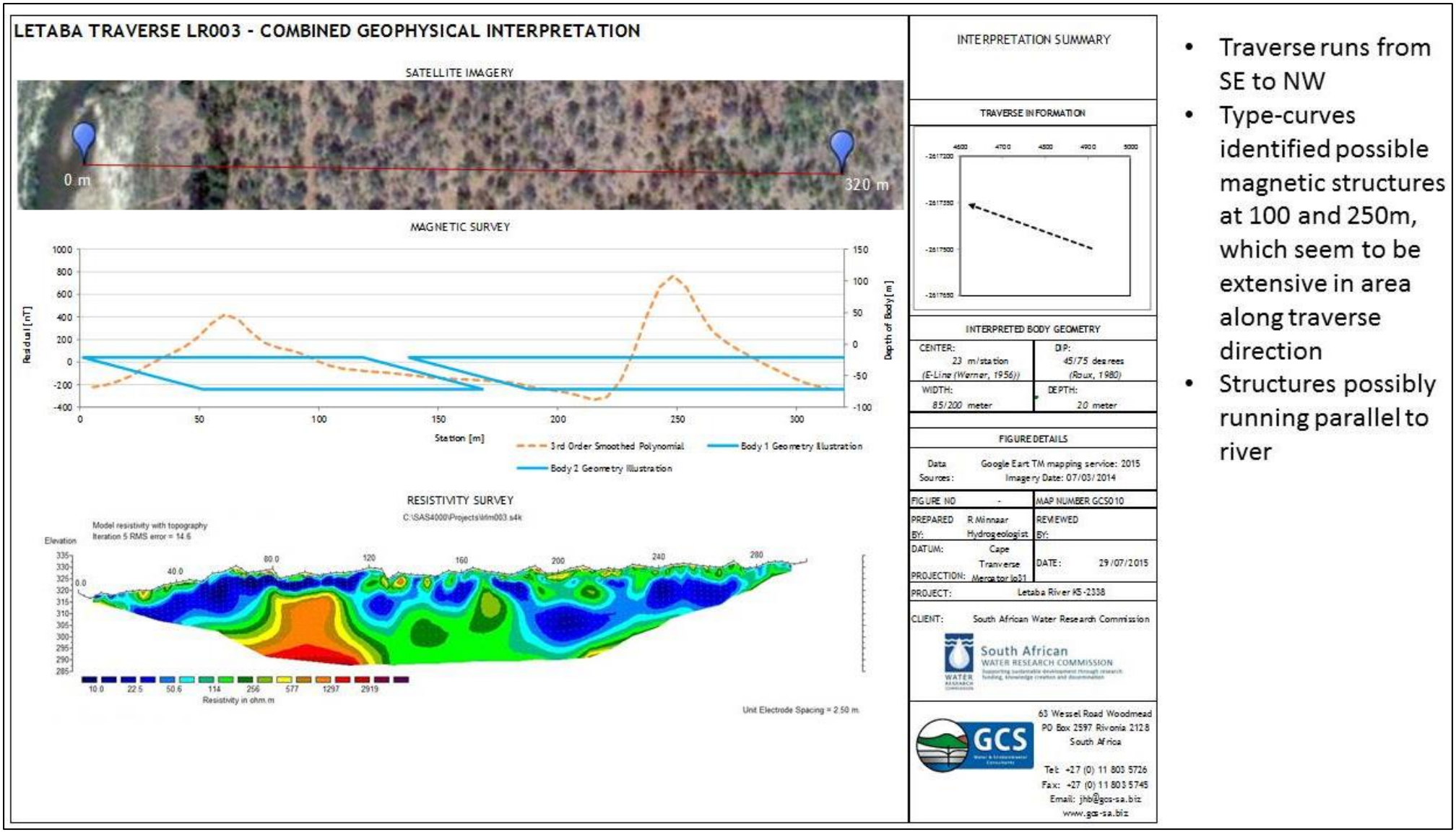

- Traverse runs from SE to NW
- Type-curves identified possible magnetic structures at 100 and 250m, which seem to be extensive in area along traverse direction
- Structures possibly running parallel to river

Figure 86 Combined Geophysical Interpretation LR003

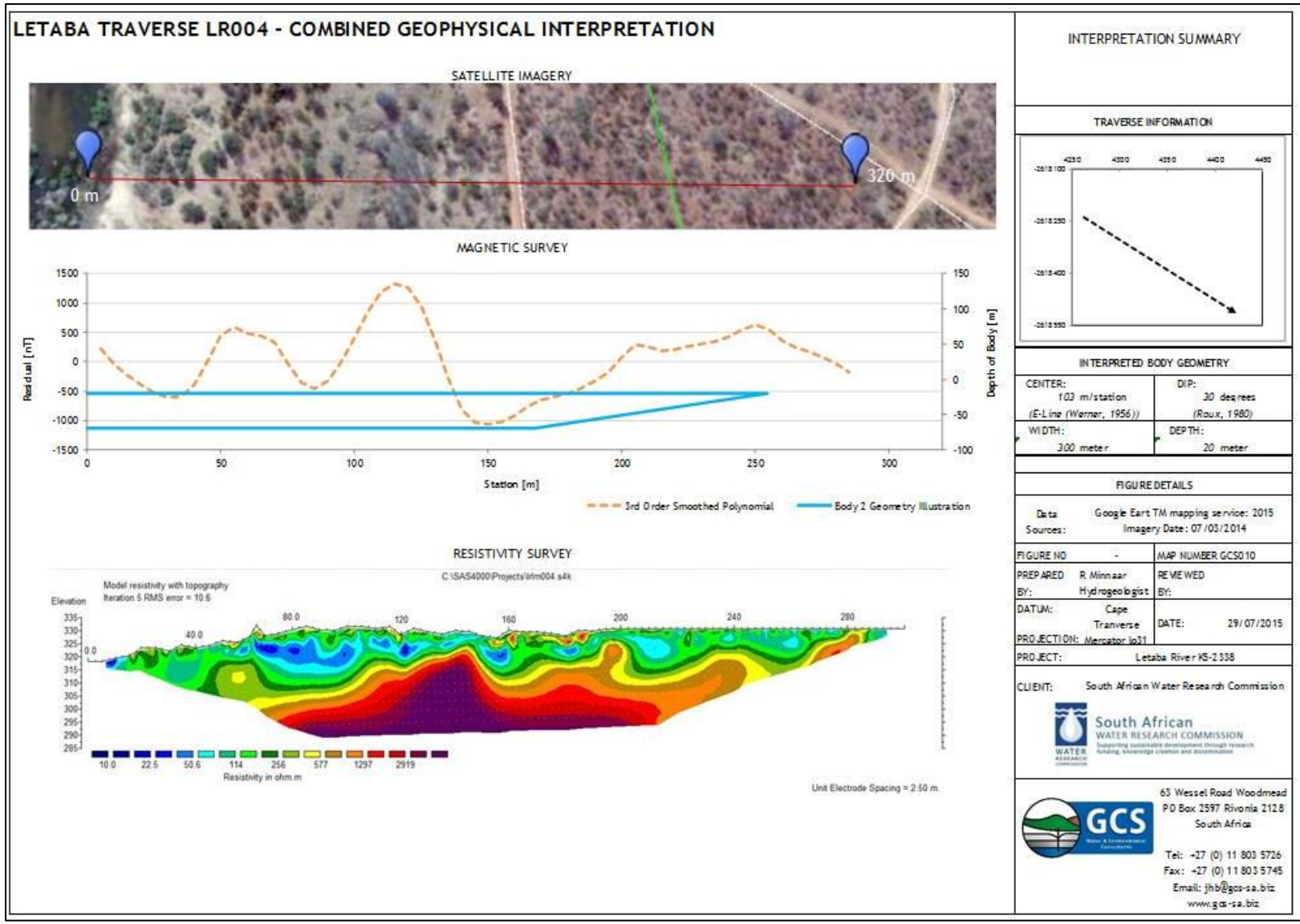

- Traverse runs from NW to SE
- Type-curves identified possible magnetic structure at 100m
- Structure location correlates to high resistivity values
- Structure possibly running parallel to river and plunging towards the river

Figure 87 Combined Geophysical Interpretation LR004

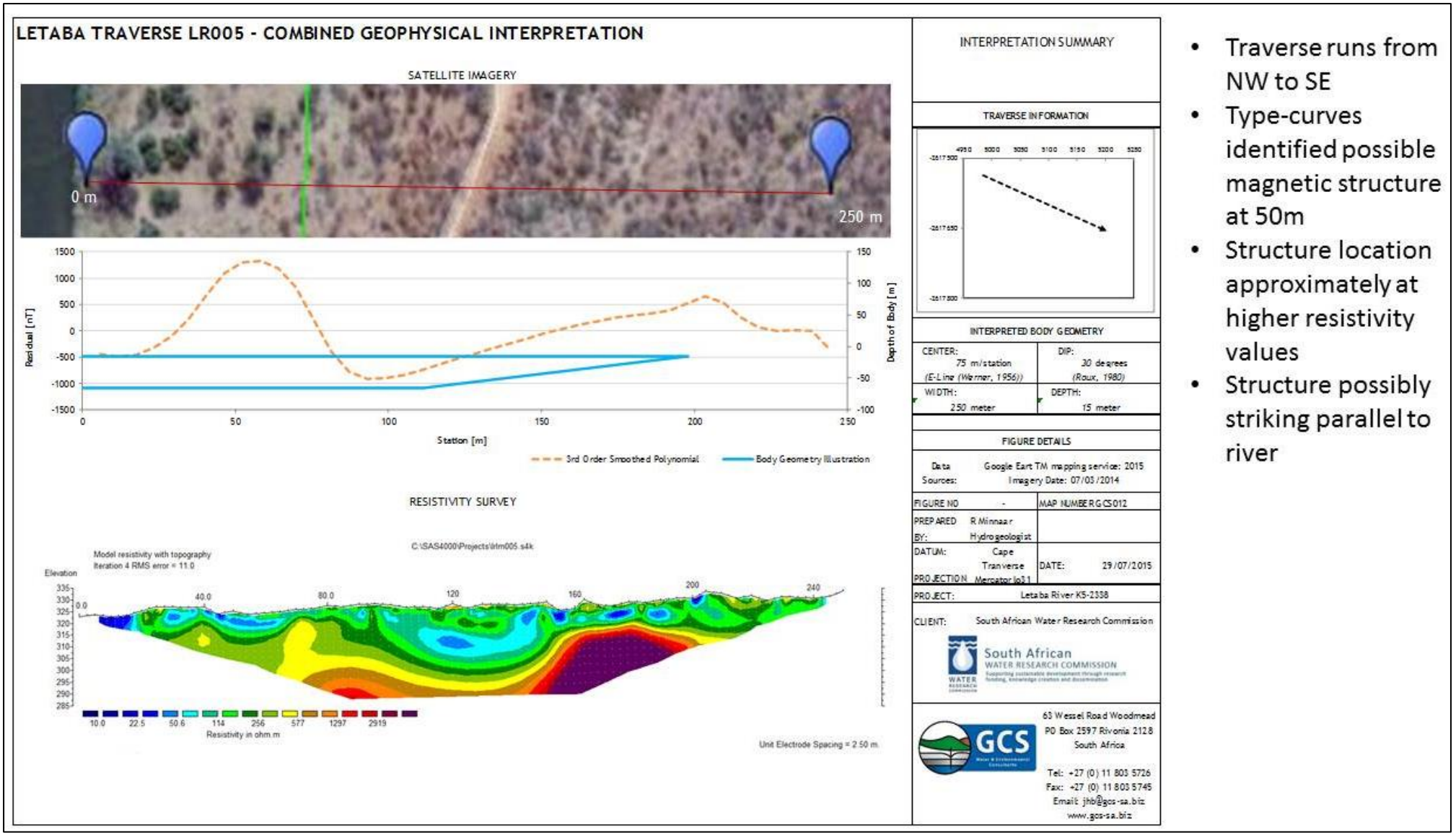

- Traverse runs from NW to SE
- Type-curves identified possible magnetic structure at 50m
- Structure location approximately at higher resistivity values
- Structure possibly striking parallel to river

Figure 88 Combined Geophysical Interpretation LR005

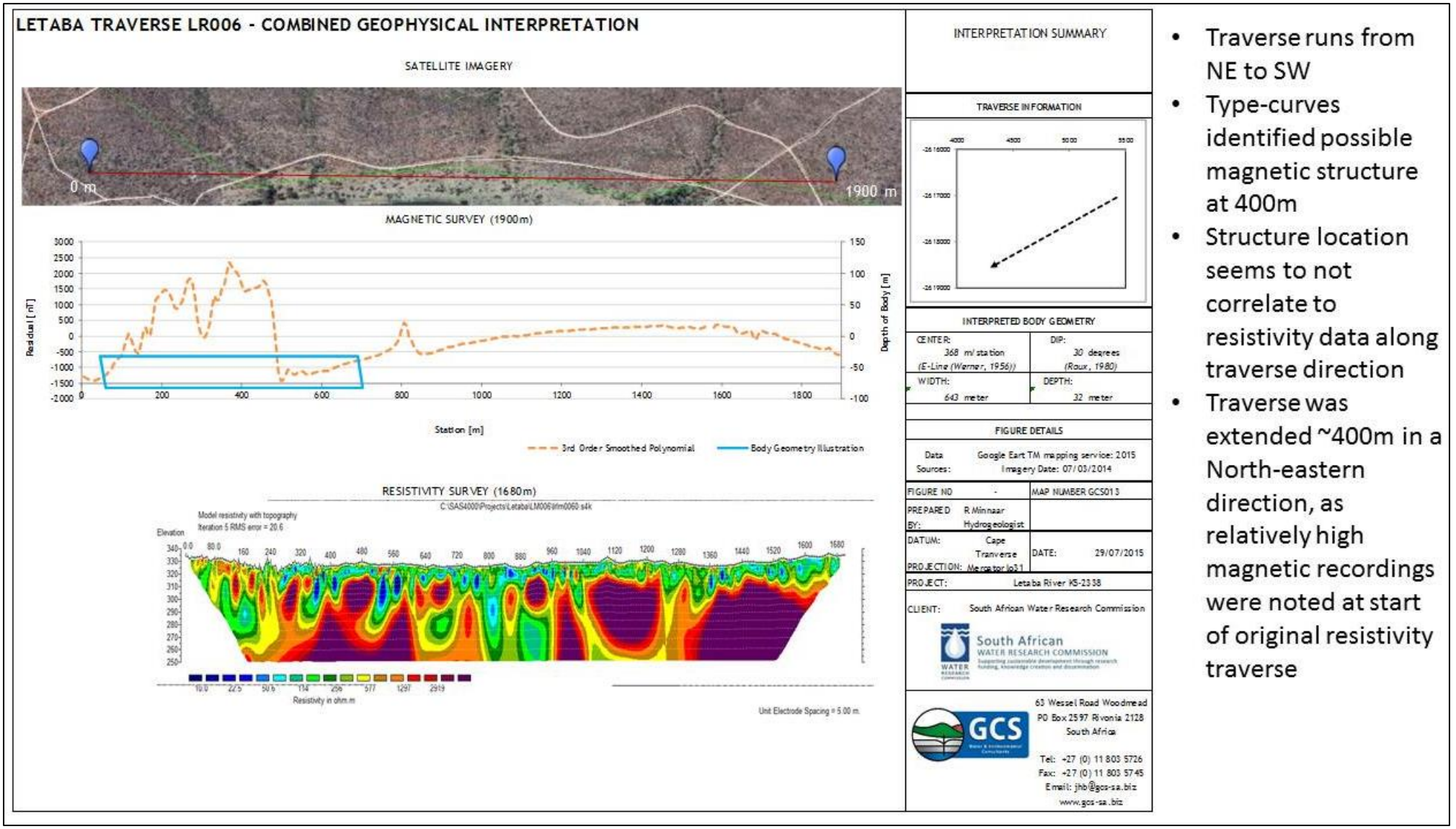

- Traverse runs from NE to SW
- Type-curves identified possible magnetic structure at 400m
- Structure location seems to not correlate to resistivity data along traverse direction
- Traverse was extended ~400m in a North-eastern direction, as relatively high magnetic recordings were noted at start of original resistivity traverse

Figure 89 Combined Geophysical Interpretation LR006